UNIVERSIDAD DE CHILE
FACULTAD DE CIENCIAS FÍSICAS Y MATEMÁTICAS
DEPARTAMENTO DE FÍSICA

# NEW QUANTUM TECHNOLOGIES: BATTERIES WITH QUBITS AND ELECTROMAGNETIC RESONATORS

TESIS PARA OPTAR AL GRADO DE
MAGÍSTER EN CIENCIAS, MENCIÓN FÍSICA

JAVIER ALEJANDRO CARRASCO ÁVILA

PROFESOR GUÍA:
FELIPE BARRA DE LA GUARDA
PROFESOR CO-GUÍA:
JERÓNIMO MAZE RÍOS

MIEMBROS DE LA COMISIÓN:
CARLA HERMANN AVIGLIANO
PABLO SOLANO

SANTIAGO DE CHILE
2021

ABSTRACT OF THE THESIS TO OPT
FOR THE DEGREE OF MASTER IN SCIENCE, MENTION IN PHYSICS
BY: JAVIER ALEJANDRO CARRASCO ÁVILA
DATE: 2021
THESIS ADVISOR: FELIPE BARRA DE LA GUARDA
THESIS CO-ADVISOR: JERÓNIMO MAZE RÍOS

# NEW QUANTUM TECHNOLOGIES: BATTERIES WITH QUBITS AND ELECTROMAGNETIC RESONATORS

In this thesis, an emerging quantum technology is studied as an open quantum system: the quantum battery (QB). This new technology has recently emerged as a promising tool for the thermodynamic control at the quantum scale [1–6]. A quantum battery is a quantum mechanical system that behaves as an efficient energy storage device. Its realization is motivated by the fact that genuine quantum effects such as entanglement or squeezing can typically boost the performances of classical protocols, e.g., by speeding up the underlying dynamics [7, 8]. These systems have been mostly studied neglecting the dissipation due to the interaction with the environment surrounding them. In this thesis, the main focus is to push forward the knowledge frontier in this regard, incorporating dissipation into the QB system. In order to do so, numerical simulations were performed to study if the collective effects that have been previously reported in QBs [9], still hold under dissipation. In particular, the system studied is made out of $N$ non-mutually interacting two-level systems (qubits) charged via a single electromagnetic field mode in a resonator. This configuration is compared to $N$ copies of a resonator with one qubit. The former is a collective QB while the latter is a parallel QB. The results show that the performance of parallel and collective QBs (for instance, the power) decreases under dissipation as expected. Nevertheless, the ratio between the power of the collective over the parallel QB increases with dissipation meaning that the deterioration in performance is smaller for the collective QB. More remarkably, it is found that the loss in performance due to dissipation can be reduced by scaling up the QB, which means equally increasing the injected energy and number of qubits. In many systems this is easier to do than decreasing dissipation. For example, nitrogen-vacancy centers in diamond (NV centers), which can be prepared to behave as spin qubits, may be in groups of hundreds in a sample of diamond [10]. This characteristic, together with its large values of decoherence time (time before losing the quantum phase) and longitudinal relaxation time (time before reaching thermal equilibrium) at room temperature [11], are the motivation to analyze, in this thesis, the feasibility of making QBs with NV centers. As a result of this analysis, it is concluded that for the type of QBs studied in this thesis, the technology is not yet good enough to realize a so called charger-based QB. Nonetheless, a general experimental restriction has been deduced, and the possibility of using NV centers for stable adiabatic QBs (not the focus of this thesis) has been identified as promising future work. The collective enhancements and performances were also studied in regard of charging energy, ergotropy (maximum amount of extractable energy with unitary operations), and transfer rate. For the first two, similar results as for the charging power are obtained. For the transfer rate, instead, it is found that its collective enhancement decreases and its performance increases as the dissipation rate increases. Last but not least, in the writing of this thesis, an effort to introduce new common nomenclature in the area of QBs has been done, as the literature is not completely consistent with the terms used up to now.

RESUMEN DE LA TESIS PARA OPTAR
AL GRADO DE MAGÍSTER EN CIENCIAS, MENCIÓN FÍSICA
POR: JAVIER ALEJANDRO CARRASCO ÁVILA
FECHA: 2021
PROF. GUÍA: FELIPE BARRA DE LA GUARDA
PROF. CO-GUÍA: JERÓNIMO MAZE RÍOS

# NEW QUANTUM TECHNOLOGIES: BATTERIES WITH QUBITS AND ELECTROMAGNETIC RESONATORS

En esta tesis, una tecnología cuántica emergente es estudiada como un sistema cuántico abierto: la batería cuántica (QB). Esta ha emergido recientemente como una herramienta prometedora para el control termodinámico a la escala cuántica [1–6]. Una QB es un sistema cuántico que se comporta como un dispositivo eficiente de almacenamiento de energía. Está motivada por el hecho de que efectos cuánticos genuinos tales como entrelazamiento o compresión pueden aumentar el rendimiento de protocolos clásicos, por ejemplo, acelerando la dinámica subyacente [7, 8]. Estos sistemas han sido estudiados en su mayoría despreciando la disipación debida a la interacción con el entorno que los rodea. En esta tesis, el foco principal es avanzar en esta frontera de conocimiento, incorporando disipación. Para hacerlo, simulaciones numéricas fueron realizadas para estudiar si los efectos colectivos que han sido reportados previamente en QBs [9] aún se mantienen bajo disipación. En particular, el sistema estudiado está hecho de $N$ sistemas de dos niveles (cúbit) que no interactúan mutuamente, cargados por medio de un modo de campo electromagnético en un resonador. Esta configuración es comparada con $N$ copias de un resonador con un cúbit. El primero es una QB colectiva y el último es una QB paralela. Los resultados muestran que el rendimiento en potencia de QBs paralelas y colectivas decrece bajo disipación como es esperado. Sin embargo, la razón entre las potencias de la QB colectiva sobre la QB paralela incrementa con la disipación, significando que la deterioración en rendimiento es menor para la QB colectiva. Por otro lado, se observa que la pérdida en rendimiento debido a la disipación se puede reducir escalando la QB, lo que significa aumentar igualmente la energía inyectada y el número de cúbits. En muchos sistemas esto es más fácil de hacer que disminuir la disipación. Por ejemplo, los centros nitrógeno-vacancia en diamante (centros NV), que pueden ser preparados como cúbits de espín, pueden estar en grupos de cientos en una muestra de diamante [10]. Esta característica, junto con sus grandes valores de tiempo de decoherencia (tiempo antes de perder la fase cuántica) y tiempo de relajación longitudinal (tiempo antes de alcanzar equilibrio térmico) a temperatura ambiente [11], son la motivación para analizar, en esta tesis, la factibilidad de fabricar QBs con centros NV. Como un resultado de este análisis, se concluye que para el tipo de QBs estudiadas en esta tesis, la tecnología aún no es lo suficientemente buena para construir una, así llamada, QB basada en cargador. Sin embargo, una restricción experimental general ha sido deducida y la posibilidad de usar centros NV para QBs adiabáticas estables (no el foco de esta tesis) ha sido identificado como trabajo futuro prometedor. Las mejoras colectivas y rendimientos también fueron estudiados en términos de energía, ergotropía (máxima cantidad de energía extraíble con operaciones unitarias) y tasa de transferencia. Para los primeros dos, resultados similares a los para potencia son obtenidos. Para la tasa de transferencia, en cambio, se obtiene que su mejora colectiva decrece y su rendimiento crece a medida que la tasa de disipación incrementa. Por último, en esta tesis, se ha introducido nueva nomenclatura común en el área de QBs, debido a que la literatura no es completamente consistente con los términos usados hasta ahora.

*A mis padres, por su apoyo infinito que me impulsó a seguir mi propio camino.*

# Agradecimientos

El camino que he recorrido para desarrollar esta tesis no habría sido un viaje tan ameno de no ser por grandes personas que me han acompañado en estos años. Tanto familia como amistades y colegas, todos han significado mucho para mí y es mi placer dejar registrados aquí mis agradecimientos.

Primero que todo, agradezco a mis profesores guía y co-guía, Felipe y Jerónimo, respectivamente, por su alta dedicación y, principalmente, por haber mostrado gran empatía, comprensión y simpatía, desde incluso antes de comenzar mi trabajo de tesis. Además, a Carla, quien fue mi profesora de óptica cuántica, enseñando con una gigantezca motivación poco vista en la universidad y un fuerte enfoque en el real aprendizaje por sobre lo demás, saliendo del esquema que dicta la norma. Pero, por sobre todo, agradezco a Carla por su apoyo incondicional desde el comienzo, desde que fui su alumno hasta la finalización de mi tesis, tanto en mis buenos momentos como en los difíciles.

Por supuesto, agradezco a todos mis amigos de la universidad, con quienes no sólo he disfrutado buenos momentos; de diversión, relajación, juegos, viajes, etc.; sino que también he podido conversar sobre asuntos científicos de física e ingeniería en diversas especialidades, lo que ha sido grato, motivante y, además, ayudado a la generación de nuevas ideas. Mención especial para Samuel, Kevin, Martín, Néstor, Richard, Albert y Diego Gallardo, todos "unas máquinas" en lo que se dedican y con quienes ha sido muy grato e interesante compartir. También gracias a Paloma, por haber sido siempre una gran amiga en todos los momentos, altos y bajos a lo largo de esta gran travesía. Pero, por sobre todo, agradezco a "Los Bellos"; i.e. a Óscar, Fernanda, Cristóbal, Diego, Mauricio, Catalina, Alfredo, Alonso, Nicolás, Vicente "*vegan*" y Vicente; sin quienes el estrés de la universidad no habría sido posible sobrellevar, porque sólo es posible cumplir con un gran desafío si va acompañado de momentos de desestrés, y con ellos no sólo he podido "pasarla bien", sino que también me han dado un hogar dentro de la universidad y más allá. En especial, gracias a quienes me apoyaron durante los momentos más difíciles.

Finalmente quiero agradecer a mi familia, que ha sido un pilar fundamental durante todos mis estudios y mi trabajo. A mis hermanos Andrés y Nathaly con quienes siempre puedo contar, relajarme y disfrutar; así como a mis padres que me han apoyado en absolutamente todo y con gran fuerza, sin lo cual, jamás habría podido seguir mi propio camino para descubrir mi pasión por la física y por la ingeniería.

# Contents

# Introduction

The possibility of using quantum resources for technological purposes is currently an active research field, in which quantum batteries (QBs) have emerged as promising tools for the thermodynamic control at the quantum scale [1–6]. A quantum battery is a quantum mechanical system that behaves as an efficient energy storage device. Its realization is motivated by the fact that genuine quantum effects such as entanglement or squeezing can typically boost the performances of classical protocols, e.g., by speeding up the underlying dynamics [7, 8]. Enhancements provided by quantum correlations in the charging (or discharging) process of a QB has been previously discussed in [12–15]. More recently, possible realizable models have been explored, including spin-chains and qubits interacting with electromagnetic fields [9, 16–21].

Up to now, research efforts have been mostly focused on understanding QBs as closed systems, isolated from the environment. The dissipation of real QBs has only recently been considered [22–28]. Hence, an important question to answer is how dissipation harms the performance of a QB. Understanding collective enhancements in the presence of dissipation is crucial to experimentally realize QBs.

In this thesis, the aforementioned question is addressed by analyzing the case of $N$ non-mutually interacting two-level systems (qubits) charged via a single electromagnetic field mode in a resonator. This system is described by the Tavis-Cummings model [29, 30], which is known to provide an effective description of experimentally feasible many-body systems in circuit and cavity QED [31–34]. This configuration is compared to $N$ copies of a resonator with one qubit. The former is a collective QB while the latter is a parallel QB.

Additionally, the feasibility of using nitrogen-vacancy centers in diamond (NV centers) as spin qubits in the Tavis-Cummings QBs, is studied. The main motivations for using NV centers is the experimental capability of grouping up hundreds of them (ideal for studying the collective behaviors) with one diamond sample [10], as well as the long dissipation times they possess at room temperature.

Therefore, the general and specific problems to solve in this thesis are:

1. **General problem**: Lack of knowledge in the behavior of QBs when dissipation is not neglected, which also results in a lack of experimental realizations of QBs to serve as proofs of concept and beyond.
2. **Specific problem**: The collective behavior of Tavis-Cummings QBs is not known when the system is under dissipation.

Hence, the work reported in this thesis attempts to help in the solution of this problems by the

1. **Specific solution**: simulating Tavis-Cummings QBs under dissipation to analyse the changes in the collective behavior that are relevant for QBs, while analysing the feasibility of fabricating these QBs with NV centers.

Therefore, the hypothesis is that, *through the results obtained from implementing the specific solution, a deeper knowledge on the experimental limitations and collective behavior of QBs will be obtained.*

### Outline of the thesis

In order to understand the results of this thesis, a background knowledge in open quantum systems, quantum optics, and NV centers is required. Therefore, chapter 1 is about the fundamental concepts of each of these subjects. It starts with a brief description of closed quantum systems in order to contrast them with the description of open quantum systems. Later on, a section about the quantum description of light and its interaction with spin qubits is developed. There is a deep emphasis in the quantization of the electromagnetic field, since it was re-derived from zero with the knowledge of various textbooks, but without completely following any of them. The main reason for this was to avoid large jumps in the steps in order to assure comprehension and readability for a larger audience. Also, because it is relevant for the thesis to understand the quantization inside a resonator or cavity, as opposed to the quantization in free-space, which is not completely explained in the textbooks used. By the end of chapter 1, the NV centers are introduced with detail in order to understand in what consists its spin qubit, and relevant data for the analyses to be done about implementing QBs with NV centers.

In chapter 2, quantum batteries are introduced from zero, using novel nomenclature to help distinguish between different types of QBs that, in the literature are sometimes referred to with the same name. Also the dynamical figures of merit of the QBs are introduced, as well as a novel figure of merit called **collective enhancement**. After the introduction of Tavis-Cummings QBs, by the end of chapter 2, an analysis of experimental limitations is done, obtaining a general restriction for Tavis-Cummings QBs, and applying it to the case of NV centers with the data introduced in chapter 2.

In chapter 3, the results from the numerical simulations are presented and analyzed deeply, utilizing the new figure of merit (collective enhancement). Finally, the conclusions summarize all the main results of the thesis.

*The work and results reported in this thesis about the collective enhancements (i.e. mainly chapter 3) have been published as a preprint manuscript in arXiv titled "Collective enhancement in dissipative quantum batteries" [35].*

# Chapter 1

# Fundamental concepts

The fundamental theoretical concepts to understand quantum batteries and the results developed in this thesis are explained in this chapter. First of all, quantum batteries are quantum systems and hence it is important to understand their dynamical evolution. This is the objective of sections 1.1 and 1.2, allowing to respectively describe the temporal evolution of a quantum battery isolated from, and immersed in a much bigger quantum environment acting as energy reservoir. Secondly, the quantum batteries studied in this thesis consist in quantum light interacting with matter qubits (two-level quantum systems corresponding to either magnetic or electric dipoles). Hence, the quantum description of light is needed, which is presented in section 1.3 together with its interaction with atoms and spins as qubits. Finally, to understand possible implementations of the quantum batteries studied, nitrogen-vacancy centers in diamond have been chosen as the main matter qubits of interest for this thesis. Therefore, understanding what they are and under which conditions they exhibit qubit behavior, along with their experimental limitations, is necessary and it is the objective of section 1.4.

## 1.1 Closed quantum systems

A closed quantum system (e.g. a quantum battery) is described by its Hamiltonian $\mathcal{H}$, an operator acting on a Hilbert space $\mathscr{H}$, which dictates the time evolution of its state, usually represented by its density operator $\rho \in \mathcal{S}(\mathscr{H})$, where $\mathcal{S}(\mathscr{H})$ is the set of states of $\mathscr{H}$. In the Schrödinger picture, the dynamic evolution of this quantum state is given by the **Liouville-von Neumann equation** [36]

$$\frac{\mathrm{d}\rho}{\mathrm{d}t} = -\frac{\mathrm{i}}{\hbar}[\mathcal{H}, \rho], \tag{1.1}$$

where $\hbar$ is the reduced Planck's constant. The solution to equation (1.1) from time $t_0$ to $t > t_0$ is given by

$$\rho(t) = \mathcal{U}(t, t_0)\rho(t_0)\mathcal{U}^\dagger(t, t_0) \tag{1.2}$$

in terms of the operator [36]

$$\mathcal{U}(t,t_0) = \mathcal{T}_{\leftarrow} \mathrm{e}^{-\frac{\mathrm{i}}{\hbar}\int_{t_0}^{t}\mathcal{H}(\tau)\mathrm{d}\tau}, \tag{1.3}$$

where $\mathcal{T}_{\leftarrow}$ is the chronological time-ordering operator, which orders products of time-dependent operators such that their time-arguments increase from right to left as indicated by the arrow.

In particular, if $\partial_t \mathcal{H} = 0$, i.e. no explicit time-dependency is shown in the Hamiltonian, which means that the system is energy-conservative (no extraction nor injection of energy is happening), then the unitary operator (1.3) simplifies to

$$\mathcal{U}(t,t_0) = \mathrm{e}^{-\mathrm{i}\frac{\mathcal{H}}{\hbar}(t-t_0)}, \tag{1.4}$$

yielding

$$\rho(t) = \mathrm{e}^{-\mathrm{i}\frac{\mathcal{H}}{\hbar}(t-t_0)}\rho(t_0)\mathrm{e}^{\mathrm{i}\frac{\mathcal{H}}{\hbar}(t-t_0)}. \tag{1.5}$$

Equivalently, it is possible to define the Liouville super-operator

$$\mathcal{L}\cdot = -\frac{\mathrm{i}}{\hbar}[\mathcal{H}, \cdot\,], \tag{1.6}$$

and write the Liouville-von Neumann equation (1.1) as

$$\frac{\mathrm{d}\rho}{\mathrm{d}t} = \mathcal{L}\rho, \tag{1.7}$$

with the formal solution [36]

$$\rho(t) = \mathcal{T}_{\leftarrow} \mathrm{e}^{\int_{t_0}^{t}\mathcal{L}(\tau)\mathrm{d}\tau}\rho(t_0), \tag{1.8}$$

which, for energy-conservative systems, simplifies to

$$\rho(t) = \mathrm{e}^{\mathcal{L}(t-t_0)}\rho(t_0). \tag{1.9}$$

This form of expression, using $\mathcal{L}$, serves to extend the solution of closed quantum systems to open quantum systems by adding the needed details explained in the next section.

## 1.2 Open quantum systems

An open quantum system S is just a part of a bigger closed universe-system U containing an environment E that interacts with S. Hence, U is described by the Hamiltonian

$$\mathcal{H}_{\mathrm{U}} = \mathcal{H}_{\mathrm{S}} + \mathcal{H}_{\mathrm{E}} + \mathcal{H}_{\mathrm{S-E}}, \tag{1.10}$$

where $\mathcal{H}_{\mathrm{S}}$ is the self-Hamiltonian of the open system S, $\mathcal{H}_{\mathrm{E}}$ is the free Hamiltonian of the environment E, and $\mathcal{H}_{\mathrm{S-E}}$ is the Hamiltonian describing the interaction between S and E. The environment $E$ is a much bigger system than $S$.

Each one of the systems, S, E, and U=S+E, have its own quantum state, $\rho_{\mathrm{S}} \in \mathcal{S}(\mathscr{H}_{\mathrm{S}})$, $\rho_{\mathrm{E}} \in \mathcal{S}(\mathscr{H}_{\mathrm{E}})$, and $\rho_{\mathrm{U}} \in \mathcal{S}(\mathscr{H}_{\mathrm{U}} = \mathscr{H}_{\mathrm{S}} \otimes \mathscr{H}_{\mathrm{E}})$, respectively. Clearly, as U is a closed system, its dynamics is determined through equation (1.7) with $\mathcal{H} = \mathcal{H}_{\mathrm{U}}$. Nevertheless, solving the evolution for the entire universe-system is unfeasible as it would require firstly to know the exact form of $\mathcal{H}_{\mathrm{E}}$ with all its internal structure, and secondly to consider a too complex and big Hamiltonian to solve either analytically or numerically. Furthermore, as the system of interest to study is S, too much untraceable and irrelevant information is contained in the solution for $\rho_{\mathrm{U}}(t)$.

Therefore, an equation for solely $\rho_{\mathrm{S}}(t) \equiv \mathrm{Tr}_E\{\rho_U(t)\}$, where all degrees of freedom corresponding to E have been traced out, is ideal. To achieve this, many assumptions on the systems and their interaction must be taken into account. Depending on the strength, $\lambda$, in $\mathcal{H}_{\mathrm{S-E}}$ there are two main regimes that are studied separately: the **weak coupling limit**, if $\lambda$ is much smaller than the strength of the rest of $\mathcal{H}_{\mathrm{U}}$; and the **strong coupling limit**, if not [36, 37]. This thesis is concerned with the weak-coupling limit, valid for the systems studied. Although, in order to understand the dynamical evolution in this regime, the more general framework of **Lindblad dynamics** is required.

### 1.2.1 Lindblad dynamics

The reduced state $\rho_{\mathrm{S}}(t)$ is said to evolve through Lindblad dynamics if it is given by the **Lindblad master equation** [36, 37]

$$\frac{\mathrm{d}\rho_{\mathrm{S}}}{\mathrm{d}t} = \mathcal{L}\rho_{\mathrm{S}}, \tag{1.11}$$

where the Lindblad super-operator $\mathcal{L}$ is given by

$$\mathcal{L}\,\cdot\, = -\frac{\mathrm{i}}{\hbar}[\mathcal{H}_{\mathrm{L}},\,\cdot\,] + \mathfrak{D}(\,\cdot\,), \tag{1.12}$$

$$\mathfrak{D}(\,\cdot\,) \equiv \sum_{k}^{N^2-1} \gamma_k \left[ L_k \,\cdot\, L_k^\dagger - \frac{1}{2}\Big\{ L_k^\dagger L_k,\,\cdot\, \Big\} \right], \tag{1.13}$$

where $L_k$ are called **Lindblad operators**, $\mathfrak{D}$ is called the **dissipator**, $N = \dim(\mathscr{H}_{\mathrm{S}})$, and $\gamma_k$ are the **relaxation** or **dissipation rates** for the different decay modes $k$ of the open system S. In this thesis, $\mathcal{H}_{\mathrm{L}}$ is referred to as the **Lindblad Hamiltonian**, which in general is different than $\mathcal{H}_{\mathrm{S}}$. The dimensionless Lindblad operators $L_k$ are operators on $\mathscr{H}_{\mathrm{S}}$ that couple S, through the different dissipation channels (decay modes) $k$, to E. The products $\sqrt{\gamma_k}L_k$ are called collapse or jump operators and they can undergo unitary transformations leaving the generator $\mathcal{L}$ invariant. There is also another transformation that leaves $\mathcal{L}$ invariant, which is shown in appendix A [36, 37].

The solution to the Lindblad equation (1.11) is given by the non-unitary map [36, 37]

$$\mathcal{E}_{(t,t_0)} : \rho_{\mathrm{S}}(t_0) \mapsto \mathcal{E}_{(t,t_0)}\rho_{\mathrm{S}}(0) \equiv \rho_{\mathrm{S}}(t) \tag{1.14}$$

expressed

$$\mathcal{E}_{(t,t_0)} = \mathcal{T}_{\leftarrow} \mathrm{e}^{\int_{t_0}^{t} \mathcal{L}(\tau)\mathrm{d}\tau}, \tag{1.15}$$

which, in the case of $\partial_t \mathcal{H}_{\mathrm{L}} = 0$ and $\partial_t L_k = 0$, simplifies to

$$\mathcal{E}_{(t,t_0)} = \mathrm{e}^{\mathcal{L}(t-t_0)}. \tag{1.16}$$

Hence, the solution of the Lindblad equation seems identical to the solution (1.8) of the Liouville-von Neumann equation, just remembering the change of $\mathcal{L}$. Nevertheless, there is the important difference that the map $\mathcal{E}_{(t,t_0)}$ is not unitary. This is an essential, very significant, characteristic of open quantum systems, typically leading to **decoherence**, i.e. the loss of well defined quantum superposition states [36]. Indeed, decoherence is a form of dissipation that does not involve energy loss and, hence, comes from a specific form of $L_k$ accompanied by a dissipation rate $\gamma_k$.

#### Limitations

The given Lindblad equation an its solution given by the map $\mathcal{E}_{(t,t_0)}$ are valid within the fulfillment of some conditions. The dynamical map $\mathcal{E}_{(t,t_0)}$ must be a completely positive trace-preserving (CPTP[1]) Markovian linear map, where:

- **CPTP** means that the evolution keeps the state positive despite of its interaction with the environment and always with trace one. Therefore, noticing that the self-adjoint property is also hold, this means that the state is kept as a quantum state.
- **Markovian** means that it can be decomposed in any arbitrary number of CPTP linear maps over subsequent time intervals. Hence, it gives a notion of time-continuity during the evolution without backflow from the environment.

Rigorous mathematical definitions of these properties are given in appendix A [36, 37].

### 1.2.2 Weak coupling limit

Within the weak coupling limit,

$$\mathcal{H}_{\mathrm{L}} \equiv \mathcal{H}_{\mathrm{S}} + \mathcal{H}_{\mathrm{LS}}, \tag{1.17}$$

where $\mathcal{H}_{\mathrm{LS}}$ is called the **Lamb-shift Hamiltonian**, and it commutes with $\mathcal{H}_{\mathrm{S}}$. Therefore, $\mathcal{H}_{\mathrm{LS}}$ only produces a shift in the energy levels of S due to its coupling to the environment E, leaving all dissipative effects contained in the dissipator $\mathfrak{D}$.

There are many ways to obtain the Lindblad master equation related to the microscopic structure of the systems studied. One possible recipe within the weak coupling limit, valid for $\partial_t \mathcal{H}_{\mathrm{U}} = 0$, i.e. when there are no external fields, is given in appendix B. The Lindblad master equations for the systems studied in this thesis are given in section 1.3.

Comparing equations (1.11) and (1.7), it is clear that the Lindblad equation contains the Liouville-von Neumann equation as the specific case where $\mathcal{H}_{\mathrm{LS}} = 0$ and $\mathfrak{D} = 0$. The

[1] Although one could argue that this, rather than a limitation, is a requirement for real systems. And any non-CPTP map would only represent an approximation to real dynamics.

first equality has sense as the Lamb-shift occurs due to the coupling to the environment. Furthermore, the latter equality is simply achieved by considering null dissipation rates, i.e. $\gamma_k = 0$, with the natural meaning that no dissipation is happening. Therefore, one gets equation (1.7) as the natural simplification of equation (1.11) when there is no dissipation, i.e. S is a closed quantum system. This also justifies using the same symbol for the Liouville and the Lindblad super-operators.

#### Limitations

For the evolution to be a CPTP Markovian linear map, i.e. for the Lindblad equation to be valid, the following approximations are required in the weak coupling limit [36]:

- **Born approximation**: the systems S and E are coupled weakly enough in order to neglect the effect of S over E and, therefore, $\rho_{\mathrm{U}}(t) \approx \rho_{\mathrm{S}}(t) \otimes \rho_{\mathrm{E}}(t_0)$.
- **Markov approximation**: the time-scale of decay for the environment $\tau_{\mathrm{E}}$ is much shorter than the smallest time-scale of the open system dynamics $\tau_{\mathrm{S}} \gg \tau_{\mathrm{E}}$. This approximation is often deemed a "short-memory environment" as it requires that environmental correlation functions decay on a time-scale fast compared to those of S.
- **Secular approximation**: the elements in the master equation corresponding to transition frequencies $\Delta\nu_{k,l} \equiv |\nu_k - \nu_l|$ are $\Delta\nu_{k,l} \ll 1/\tau_{\mathrm{S}}$, i.e. all fast rotating terms in the interaction picture can be neglected. This is also called *rotating wave approximation*.

## 1.3 Quantum light and matter

### 1.3.1 Quantum electromagnetic waves

#### Separating radiation and static fields

From classical electrodynamics, it is known that light is a propagating wave of electromagnetic field. This result is extracted from Maxwell's equations,

$$\begin{aligned} \boldsymbol{\nabla} \times \mathbf{E} &= -\frac{\partial \mathbf{B}}{\partial t}, & \boldsymbol{\nabla} \times \mathbf{B} &= \mu_o \epsilon_0 \frac{\partial \mathbf{E}}{\partial t} + \mu_0 \mathbf{J}, \\ \boldsymbol{\nabla} \cdot \mathbf{E} &= \frac{\rho}{\epsilon_0}, & \boldsymbol{\nabla} \cdot \mathbf{B} &= 0, \end{aligned} \tag{1.18}$$

where $\mathbf{E}$ and $\mathbf{B}$ are the total electric and magnetic fields, respectively; $\rho$ and $\mathbf{J}$ are the charge and current densities, respectively; $\epsilon_0$ and $\mu_0$ are the permittivity and permeability of free space, respectively.

Although, Maxwell's equations not only describe electromagnetic waves, but also static fields attached to the existence of charges in space. The latter fields are not electromagnetic radiation and, therefore, not light. Hence, before quantizing light, a separation of these two

types of electromagnetic fields is needed. The standard approach is used in this thesis, using Coulomb's gauge $\boldsymbol{\nabla} \cdot \mathbf{A} = 0$ for the vector potential, $\mathbf{A}$, defined by $\mathbf{B} \equiv \boldsymbol{\nabla} \times \mathbf{A}$.

Within this gauge and considering the wave vector $\mathbf{k}$ dual to the position $\mathbf{r}$ under spatial Fourier transform, the vector potential fulfills $\mathbf{A} \perp \mathbf{k}$ and the two degrees of freedom corresponding to electromagnetic fields of radiation are given by the two orthogonal components of $\mathbf{A}$, namely $\mathbf{A}_1$ and $\mathbf{A}_2$, which are $\perp \mathbf{k}$. These two vectors, spanning the plane $\perp \mathbf{k}$, define the two well known directions of polarization $\hat{\mathbf{e}}_{1,2} \equiv \mathbf{A}_{1,2}/\|\mathbf{A}_{1,2}\|$ fulfilling $\hat{\mathbf{e}}_1 \perp \hat{\mathbf{e}}_2$. Furthermore, within Coulomb's gauge, the electromagnetic fields of radiation are related to $\mathbf{A}$ by

$$\mathbf{B} \equiv \boldsymbol{\nabla} \times \mathbf{A}, \tag{1.19}$$

$$\mathbf{E}_\perp = -\frac{\partial}{\partial t}\mathbf{A}, \tag{1.20}$$

where $\mathbf{E}_\perp \equiv [\mathbf{E} \cdot \hat{\mathbf{e}}_1]\,\hat{\mathbf{e}}_1 + [\mathbf{E} \cdot \hat{\mathbf{e}}_2]\,\hat{\mathbf{e}}_2$, and the static electric field $\mathbf{E}_\parallel \equiv [\mathbf{E} \cdot (\mathbf{k}/\|\mathbf{k}\|)]\,(\mathbf{k}/\|\mathbf{k}\|)$ belonging to charges is given by

$$\mathbf{E}_\parallel = -\boldsymbol{\nabla} U, \tag{1.21}$$

$$U = \frac{1}{4\pi\epsilon_0} \int \mathrm{d}^3 r' \frac{\rho(\mathbf{r}', t)}{\|\mathbf{r} - \mathbf{r}'\|}, \tag{1.22}$$

where $U(\mathbf{r}, t)$ is the known scalar potential.

Hence, the Maxwell's equations of radiation are

$$\boldsymbol{\nabla} \times \mathbf{E}_\perp = -\frac{\partial \mathbf{B}}{\partial t}, \qquad \boldsymbol{\nabla} \times \mathbf{B} = \mu_o \epsilon_0 \frac{\partial \mathbf{E}_\perp}{\partial t} + \mu_0 \mathbf{J}_\perp, \tag{1.23}$$

where only components $\perp \mathbf{k}$ have been left, and $\mathbf{J}_\perp \equiv [\mathbf{J} \cdot \hat{\mathbf{e}}_1]\,\hat{\mathbf{e}}_1 + [\mathbf{J} \cdot \hat{\mathbf{e}}_2]\,\hat{\mathbf{e}}_2$ gives rise to radiation coming from accelerated charges moving in the direction $\hat{\mathbf{k}} \equiv \mathbf{k}/\|\mathbf{k}\|$. Although, to focus on radiation itself, independent of its source, $\mathbf{J}_\perp = \mathbf{0}$ is set. This happens, for example, in free space. Additionally, applying equations (1.19, 1.20), the radiation equations (1.23) reduce to

$$\nabla^2 \mathbf{A} - \frac{1}{c^2}\frac{\partial^2 \mathbf{A}}{\partial t^2} = \mathbf{0}, \tag{1.24}$$

which is a homogeneous wave equation for waves propagating at the speed of light in vacuum, $c \equiv 1/\sqrt{\mu_0 \epsilon_0}$.

Therefore, within Coulomb's gauge and absence of radiation sources, all radiation information in Maxwell's equation is given by $\mathbf{A}$, which can also be shown to be gauge invariant by simply noticing that $\mathbf{E}_\perp$ is gauge invariant and using equation (1.20). A formal proof of this is given in appendix C. Hence, gauge independent dynamics of light can be obtained by simply using $\mathbf{A}$ under Coulomb's gauge. Because of these reasons, within this choice of gauge, the vector potential $\mathbf{A}$ is called the **radiation field**.

**Fields as a collection of harmonic oscillators**

The radiation equation (1.24) can be recast in the dual $\mathbf{k}$-space by applying the 3D spatial Fourier transform, obtaining

$$\frac{\partial^2 \tilde{\mathbf{A}}}{\partial t^2} + c^2 k^2 \tilde{\mathbf{A}} = \mathbf{0}, \tag{1.25}$$

where $\tilde{\mathbf{A}}(\mathbf{k}, t) \equiv \int_{-\infty}^{+\infty} \mathbf{A}(\mathbf{r}, t) \mathrm{e}^{-\mathrm{i}\mathbf{k}\cdot\mathbf{r}} \, \mathrm{d}^3\mathbf{r}$ is the spatial Fourier transform of the radiation field in rectangular coordinates, and $k = \|\mathbf{k}\|$. Furthermore, projecting onto the polarization direction $\hat{\mathbf{e}} \in \{\hat{\mathbf{e}}_1, \hat{\mathbf{e}}_2\}$, scalar harmonic oscillator equations

$$\frac{\partial^2 \tilde{A}_e}{\partial t^2} + c^2 k^2 \tilde{A}_e = 0, \tag{1.26}$$

are obtained, where $\tilde{A}_e \equiv \tilde{\mathbf{A}} \cdot \hat{\mathbf{e}}$. These harmonic oscillators oscillate at angular frequency $\omega_k = ck$ and have solutions

$$\tilde{A}_e(\mathbf{k}, t) = \tilde{\alpha}_{e,\omega_k} \mathrm{e}^{-\mathrm{i}\omega_k t} + \tilde{\beta}_{e,\omega_k} \mathrm{e}^{\mathrm{i}\omega_k t}, \tag{1.27}$$

over which, the inverse-Fourier transform is applied to recover the radiation field components,

$$A_e(\mathbf{r}, t) = \frac{1}{(2\pi)^3} \int_{-\infty}^{+\infty} \mathrm{d}^3\mathbf{k} \left( \tilde{\alpha}_{e,\omega_k} \mathrm{e}^{-\mathrm{i}\omega_k t} + \tilde{\beta}_{e,\omega_k} \mathrm{e}^{\mathrm{i}\omega_k t} \right) \mathrm{e}^{\mathrm{i}\mathbf{k}\cdot\mathbf{r}} \tag{1.28}$$

$$= \frac{1}{(2\pi)^3} \int_{0}^{+\infty} \mathrm{d}^3\mathbf{k} \left\{ \left( \tilde{\alpha}_{e,\omega_k} \mathrm{e}^{-\mathrm{i}\omega_k t} + \tilde{\beta}_{e,\omega_k} \mathrm{e}^{\mathrm{i}\omega_k t} \right) \mathrm{e}^{\mathrm{i}\mathbf{k}\cdot\mathbf{r}} + \mathrm{c.c.} \right\}, \tag{1.29}$$

where the integration limits hold for all three rectangular coordinates, and the second equality comes from $\mathbf{A} \in \mathbb{R}^3 \Rightarrow \tilde{\mathbf{A}}(\mathbf{k}, t) = \tilde{\mathbf{A}}^*(-\mathbf{k}, t) \Rightarrow \tilde{A}_e(\mathbf{k}, t) = \tilde{A}_e^*(-\mathbf{k}, t)$, and $k = \|\pm\mathbf{k}\|$.

In equation (1.29), it is clear that terms $\propto \tilde{\alpha}_{e,\omega_k}$ and $\propto \tilde{\beta}_{e,\omega_k}$ correspond to waves propagating along the $\hat{\mathbf{k}}$ and $-\hat{\mathbf{k}}$ directions, respectively. Therefore, if no boundary conditions are set, i.e. plane waves in both $\pm\mathbf{k}$ directions are independent complete solutions, the study might be separated for only waves propagating along $\hat{\mathbf{k}}$ by setting the condition $\tilde{\beta}_{e,\omega_k} = 0$. Nonetheless, to contain standing wave solutions that appear from boundary conditions, $\tilde{\beta}_{e,\omega_k}$ will be left as a yet to determine integration constant.

Recalling that $\mathbf{A} = A_{e_1}\hat{\mathbf{e}}_1 + A_{e_2}\hat{\mathbf{e}}_2$, the complete solution is given by

$$\mathbf{A}(\mathbf{r}, t) = \sum_{e=e_1,e_2} \frac{\hat{\mathbf{e}}}{(2\pi)^3} \int_{0}^{\infty} \mathrm{d}^3\mathbf{k} \left( \tilde{\alpha}_{e,\omega_k} \mathrm{e}^{\mathrm{i}(\mathbf{k}\cdot\mathbf{r} - \omega_k t)} + \tilde{\beta}_{e,\omega_k} \mathrm{e}^{\mathrm{i}(\mathbf{k}\cdot\mathbf{r} + \omega_k t)} + \mathrm{c.c.} \right), \tag{1.30}$$

where the relative differences between $\tilde{\alpha}_{e_1,\omega_k}(\tilde{\beta}_{e_1,\omega_k})$ and $\tilde{\alpha}_{e_2,\omega_k}(\tilde{\beta}_{e_2,\omega_k})$ define different polarizations.

Hence, replacing the expression (1.30) into equations (1.19, 1.20), the electromagnetic fields of radiation are obtained,

$$\mathbf{E}_\perp(\mathbf{r}, t) = \mathrm{i} \sum_{e=e_1,e_2} \frac{1}{(2\pi)^3} \int_{0}^{\infty} \mathrm{d}^3\mathbf{k} \, \omega_k \hat{\mathbf{e}} \left( \tilde{\alpha}_{e,\omega_k} \mathrm{e}^{\mathrm{i}(\mathbf{k}\cdot\mathbf{r} - \omega_k t)} - \tilde{\beta}_{e,\omega_k} \mathrm{e}^{\mathrm{i}(\mathbf{k}\cdot\mathbf{r} + \omega_k t)} - \mathrm{c.c.} \right), \tag{1.31}$$

$$\mathbf{B}(\mathbf{r}, t) = \mathrm{i} \sum_{e=e_1,e_2} \frac{1}{(2\pi)^3} \int_{0}^{\infty} \mathrm{d}^3\mathbf{k} \, (\mathbf{k} \times \hat{\mathbf{e}}) \left( \tilde{\alpha}_{e,\omega_k} \mathrm{e}^{\mathrm{i}(\mathbf{k}\cdot\mathbf{r} - \omega_k t)} + \tilde{\beta}_{e,\omega_k} \mathrm{e}^{\mathrm{i}(\mathbf{k}\cdot\mathbf{r} + \omega_k t)} - \mathrm{c.c.} \right), \tag{1.32}$$

which can be replaced in the electromagnetic radiation Hamiltonian,

$$\mathcal{H} = \frac{1}{2}\int_{\mathcal{V}} \mathrm{d}^3\mathbf{r}\left(\epsilon_0 \mathbf{E}_\perp^2 + \frac{1}{\mu_0}\mathbf{B}^2\right), \tag{1.33}$$

where $\mathcal{V}$ is the volume of integration, to obtain

$$\mathcal{H} = \frac{2\epsilon_0}{(2\pi)^3}\sum_{e=e_1,e_2}\int_0^\infty \mathrm{d}^3\mathbf{k}\,\omega_k^2\left(\tilde{\alpha}_{e,\omega_k}\tilde{\alpha}^*_{e,\omega_k} + \tilde{\beta}_{e,\omega_k}\tilde{\beta}^*_{e,\omega_k}\right). \tag{1.34}$$

The complex amplitudes $\tilde{\alpha}_{e,\omega_k}, \tilde{\beta}_{e,\omega_k}$ can be rewritten as

$$\begin{pmatrix}\tilde{\alpha}_{e,\omega_k}\\ \tilde{\beta}_{e,\omega_k}\end{pmatrix} \equiv \sqrt{\frac{\hbar(2\pi)^3}{2\epsilon_0\omega_k}}\begin{pmatrix}\alpha_{e,\omega_k}\\ \beta_{e,\omega_k}\end{pmatrix} \tag{1.35}$$

where $\alpha_{e,\omega_k}, \beta_{e,\omega_k}$ are just the amplitudes rescaled. Then, the electromagnetic fields of radiation and their Hamiltonian are rewritten as

$$\mathbf{E}_\perp(\mathbf{r},t) = \mathrm{i}\sum_{e=e_1,e_2}\int_0^\infty \mathrm{d}^3\mathbf{k}\,E_{\omega_k}\hat{\mathbf{e}}\left(\alpha_{e,\omega_k}\mathrm{e}^{\mathrm{i}(\mathbf{k}\cdot\mathbf{r}-\omega_k t)} - \beta_{e,\omega_k}\mathrm{e}^{\mathrm{i}(\mathbf{k}\cdot\mathbf{r}+\omega_k t)} - \mathrm{c.c.}\right), \tag{1.36}$$

$$\mathbf{B}(\mathbf{r},t) = \mathrm{i}\sum_{e=e_1,e_2}\int_0^\infty \mathrm{d}^3\mathbf{k}\,B_{\omega_k}(\hat{\mathbf{k}}\times\hat{\mathbf{e}})\left(\alpha_{e,\omega_k}\mathrm{e}^{\mathrm{i}(\mathbf{k}\cdot\mathbf{r}-\omega_k t)} + \beta_{e,\omega_k}\mathrm{e}^{\mathrm{i}(\mathbf{k}\cdot\mathbf{r}+\omega_k t)} - \mathrm{c.c.}\right), \tag{1.37}$$

$$\mathcal{H} = \sum_{e=e_1,e_2}\int_0^\infty \mathrm{d}^3\mathbf{k}\,\hbar\omega_k\left(\alpha_{e,\omega_k}\alpha^*_{e,\omega_k} + \beta_{e,\omega_k}\beta^*_{e,\omega_k}\right), \tag{1.38}$$

where

$$E_{\omega_k} \equiv \sqrt{\frac{\hbar\omega_k}{2\epsilon_0(2\pi)^3}}, \qquad B_{\omega_k} \equiv \frac{E_{\omega_k}}{c}. \tag{1.39}$$

**Quantization**

To easily quantize, the amplitudes $\alpha_{e,\omega_k}, \beta_{e,\omega_k} \in \mathbb{C}$ can be rewritten in terms of new variables $q^{\alpha(\beta)}_{e,\omega_k}, p^{\alpha(\beta)}_{e,\omega_k} \in \mathbb{R}$ as

$$\alpha_{e,\omega_k} = \frac{1}{\sqrt{2\hbar\omega_k}}\left(\omega_k q^\alpha_{e,\omega_k} + \mathrm{i}p^\alpha_{e,\omega_k}\right), \tag{1.40}$$

$$\beta_{e,\omega_k} = \frac{1}{\sqrt{2\hbar\omega_k}}\left(\omega_k q^\beta_{e,\omega_k} - \mathrm{i}p^\beta_{e,\omega_k}\right), \tag{1.41}$$

from which the Hamiltonian (1.38) is rewritten as

$$\mathcal{H} = \sum_{e=e_1,e_2}\int_0^\infty \mathrm{d}^3\mathbf{k}\,\frac{1}{2}\left\{(p^\alpha_{e,\omega_k})^2 + \omega_k^2(q^\alpha_{e,\omega_k})^2 + (p^\beta_{e,\omega_k})^2 + \omega_k^2(q^\beta_{e,\omega_k})^2\right\}, \tag{1.42}$$

where it is clear that the Hamiltonian corresponds to a continuous collection of non-interacting simple harmonic oscillators with canonical positions $q^{\alpha(\beta)}_{e,\omega_k}$ and momentums $p^{\alpha(\beta)}_{e,\omega_k}$ (for further detail, refer to [38]). From here, the quantization is trivially achieved by upgrading the canonical variables to operators satisfying the commutation relations dictated by the principles of quantum mechanics, i.e.

$$\left[q^{\alpha(\beta)}_{e,\omega_k}, q^{\alpha(\beta)}_{e',\omega_{k'}}\right] = \left[p^{\alpha(\beta)}_{e,\omega_k}, p^{\alpha(\beta)}_{e',\omega_{k'}}\right] = 0, \qquad \left[q^{\alpha(\beta)}_{e,\omega_k}, p^{\alpha(\beta)}_{e',\omega_{k'}}\right] = \mathrm{i}\hbar\delta_{e,e'}\delta_{k,k'}, \tag{1.43}$$

which is equivalent to upgrading the complex amplitudes $\alpha_{e,\omega_k}(\beta^*_{e,\omega_k})$ and $\alpha^*_{e,\omega_k}(\beta_{e,\omega_k})$ to annihilation and creation operators, $a_{e,\omega_k}(b_{e,\omega_k})$ and $a^\dagger_{e,\omega_k}(b^\dagger_{e,\omega_k})$, respectively, fulfilling the bosonic commutation relations

$$[a_{e,\omega_k}, a_{e',\omega_{k'}}] = [a^\dagger_{e,\omega_k}, a^\dagger_{e',\omega_{k'}}] = 0, \qquad [a_{e,\omega_k}, a^\dagger_{e',\omega_{k'}}] = \delta_{e,e'}\delta_{k,k'}, \tag{1.44}$$

$$[b_{e,\omega_k}, b_{e',\omega_{k'}}] = [b^\dagger_{e,\omega_k}, b^\dagger_{e',\omega_{k'}}] = 0, \qquad [b_{e,\omega_k}, b^\dagger_{e',\omega_{k'}}] = \delta_{e,e'}\delta_{k,k'}. \tag{1.45}$$

Hence, the quantized electromagnetic fields of radiation and their Hamiltonian, in the Heisenberg picture, are

$$\mathbf{E}_\perp(\mathbf{r},t) = \mathrm{i}\sum_{e=e_1,e_2}\int_0^\infty \mathrm{d}^3\mathbf{k}\, E_{\omega_k}\hat{\mathbf{e}}\left(a_{e,\omega_k}\mathrm{e}^{\mathrm{i}(\mathbf{k}\cdot\mathbf{r}-\omega_k t)} - b^\dagger_{e,\omega_k}\mathrm{e}^{\mathrm{i}(\mathbf{k}\cdot\mathbf{r}+\omega_k t)} - \mathrm{h.c.}\right), \tag{1.46}$$

$$\mathbf{B}(\mathbf{r},t) = \mathrm{i}\sum_{e=e_1,e_2}\int_0^\infty \mathrm{d}^3\mathbf{k}\, B_{\omega_k}(\hat{\mathbf{k}}\times\hat{\mathbf{e}})\left(a_{e,\omega_k}\mathrm{e}^{\mathrm{i}(\mathbf{k}\cdot\mathbf{r}-\omega_k t)} + b^\dagger_{e,\omega_k}\mathrm{e}^{\mathrm{i}(\mathbf{k}\cdot\mathbf{r}+\omega_k t)} - \mathrm{h.c.}\right), \tag{1.47}$$

$$\mathcal{H} = \sum_{e=e_1,e_2}\int_0^\infty \mathrm{d}^3\mathbf{k}\,\hbar\omega_k\left(a^\dagger_{e,\omega_k}a_{e,\omega_k} + b^\dagger_{e,\omega_k}b_{e,\omega_k} + 1\right), \tag{1.48}$$

which can be written in the Schrödinger picture by simply setting $t = 0$. The expression of the Hamiltonian was obtained by first symmetrizing the products of complex amplitudes and then upgrading to operators, i.e. $\alpha_{e,\omega_k}\alpha^*_{e,\omega_k} \mapsto \frac{1}{2}(\alpha_{e,\omega_k}\alpha^*_{e,\omega_k} + \alpha^*_{e,\omega_k}\alpha_{e,\omega_k})$ and $\beta_{e,\omega_k}\beta^*_{e,\omega_k} \mapsto \frac{1}{2}(\beta_{e,\omega_k}\beta^*_{e,\omega_k} + \beta^*_{e,\omega_k}\beta_{e,\omega_k})$.

### Fields inside a resonator

If the electromagnetic radiation is confined inside a resonator (e.g. a cavity), standing wave solutions emerge. Typical boundary conditions of this situation correspond to a parallelepiped geometry with $\mathbf{A} = 0$ in each face. This implies that, before quantization, $\tilde{A}_e = -\tilde{A}^*_e \Rightarrow \alpha_{e,\omega_k} = -\beta^*_{e,\omega_k}$. Hence, after quantization, $a = -b$, which has sense as a photon traveling in the $\hat{\mathbf{k}}$ direction only exists if the same photon is traveling in the $-\hat{\mathbf{k}}$ direction after reflection on the boundaries. Moreover, the border conditions used correspond to perfect metallic surfaces, for which a phase change in $\pi$ radiands after reflection is known to happen in classical electrodynamics. This phase change is captured in the minus sign relating $a$ to $b$.

Additionally, a discrete number of wave-vectors $\mathbf{k}$ is allowed by the boundary conditions. For the given resonator those are

$$\mathbf{k}_n \equiv \mathbf{k}_{(n_x,n_y,n_z)} \equiv k_{n_x}\hat{\mathbf{x}} + k_{n_y}\hat{\mathbf{y}} + k_{n_z}\hat{\mathbf{z}} = \frac{2\pi n_x}{L_x}\hat{\mathbf{x}} + \frac{2\pi n_y}{L_y}\hat{\mathbf{y}} + \frac{2\pi n_z}{L_z}\hat{\mathbf{z}}, \tag{1.49}$$

where $L_{x,y,z}$ are the dimensions of the parallelepiped cavity, and $n_{x,y,z} \in \mathbb{N}$. To account this effect correctly, a modes distribution

$$g(\mathbf{k}) = \frac{2\pi}{L_x}\frac{2\pi}{L_y}\frac{2\pi}{L_z}\sum_{n_x}\sum_{n_y}\sum_{n_z}\delta(k_x - k_{n_x})\delta(k_y - k_{n_y})\delta(k_z - k_{n_z}) \tag{1.50}$$

must be inserted inside the $\mathbf{k}$-integrals of the fields and the Hamiltonian.

Therefore, equations (1.46–1.47) can be recast in terms of standing wave modes as

$$\mathbf{E}_\perp(\mathbf{r},t) = \sum_{e=e_1,e_2}\sum_{\mathbf{k}=\mathbf{k}_n} E_{\omega_k}\hat{\mathbf{e}}\left(b^\dagger_{e,\omega_k}\mathrm{e}^{\mathrm{i}\omega_k t} + b_{e,\omega_k}\mathrm{e}^{-\mathrm{i}\omega_k t}\right)\sin(\mathbf{k}\cdot\mathbf{r}), \tag{1.51}$$

$$\mathbf{B}(\mathbf{r},t) = \sum_{e=e_1,e_2}\sum_{\mathbf{k}=\mathbf{k}_n} \mathrm{i}B_{\omega_k}(\hat{\mathbf{k}}\times\hat{\mathbf{e}})\left(b^\dagger_{e,\omega_k}\mathrm{e}^{\mathrm{i}\omega_k t} - b_{e,\omega_k}\mathrm{e}^{-\mathrm{i}\omega_k t}\right)\cos(\mathbf{k}\cdot\mathbf{r}), \tag{1.52}$$

$$\mathcal{H} = \sum_{e=e_1,e_2}\sum_{\mathbf{k}=\mathbf{k}_n}\hbar\omega_k\left(b^\dagger_{e,\omega_k}b_{e,\omega_k} + \frac{1}{2}\right), \tag{1.53}$$

where the transformations

$$\sqrt{\frac{2(2\pi)^3}{V}}E_{\omega_k} \mapsto E_{\omega_k}, \qquad \sqrt{\frac{2(2\pi)^3}{V}}B_{\omega_k} \mapsto B_{\omega_k}, \qquad \sqrt{\frac{2(2\pi)^3}{V}}\beta_{e,\omega_k} \mapsto \beta_{e,\omega_k} \tag{1.54}$$

have been done before quantization, i.e. the factors $(2\pi)^3$ have been changed by $V/2$, where $V \equiv L_xL_yL_z$ is the volume of the parallelepiped cavity.

### Quantum states of light

A single mode of linearly polarized electromagnetic radiation has a Hamiltonian

$$\mathcal{H} = \hbar\omega\left(b^\dagger b + \frac{1}{2}\right), \tag{1.55}$$

obtained from equation (1.53) by choosing a specific allowed pair $(e,\mathbf{k})$. This Hamiltonian has the same basis of the number operator $N = b^\dagger b$ known from the quantum simple harmonic oscillator. Hence, the eigenenergies are quantized in levels separated by $\hbar\omega$. This quanta of energy of electromagnetic radiation is called a photon.

Therefore, the base vector states of electromagnetic radiation are the **number states** $|n\rangle$, where $n$ is the number of photons. These are also called **Fock states**, and can be written as a density operator

$$\rho_n^{\mathrm{Fock}} \equiv |n\rangle\langle n|, \tag{1.56}$$

where the vacuum vector state $|0\rangle$ is included and is different than having no field, implying it is always present, unlike in classical electrodynamics. Hence, this is an important result from the quantum theory.

Other very important states are the **coherent states**, defined as the eigenkets, $|\beta\rangle$, of the annihilation operator, $b$, with associated eigenvalue $\beta \in \mathbb{C}$, i.e. $b|\beta\rangle = \beta|\beta\rangle$. These states

are important because allow to recover the classical electromagnetic fields and Hamiltonian of radiation as the expectation values of their quantum (operator) versions. In this sense, $\beta$ can be seen as the complex amplitude before quantization, which justifies using the same notation for both. The coherent states can be expanded in the Fock basis as

$$|\beta\rangle = \mathrm{e}^{-\frac{|\beta|^2}{2}} \sum_{m=0}^{\infty} \frac{\beta^m}{\sqrt{m!}} |m\rangle \,, \tag{1.57}$$

corresponding to a mean number of photons $\langle\beta|N|\beta\rangle = |\beta|^2$.

The third basic class of quantum sates of light is the one of the (Gibbs) **thermal states**

$$\rho^{\mathrm{th}} \equiv \frac{\mathrm{e}^{-\frac{\mathcal{H}}{k_{\mathrm{B}}T}}}{\mathrm{Tr}\left(\mathrm{e}^{-\frac{\mathcal{H}}{k_{\mathrm{B}}T}}\right)}, \tag{1.58}$$

where $T$ is the temperature, and $k_{\mathrm{B}}$ is the Boltzmann's constant. For a single mode of light, the thermal state can be expanded in the Fock basis as

$$\rho^{\mathrm{th}}_{\bar{n}} \equiv \frac{1}{1+\bar{n}} \sum_{m=0}^{\infty} \left(\frac{\bar{n}}{1+\bar{n}}\right)^m |m\rangle\langle m| \,, \tag{1.59}$$

where $\bar{n} = \mathrm{Tr}\left(N\rho^{\mathrm{th}}_{\bar{n}}\right)$ is the mean number of photons, related to the temperature by

$$\bar{n} = \frac{1}{\mathrm{e}^{\frac{\hbar\omega}{k_{\mathrm{B}}T}} - 1}, \tag{1.60}$$

known as the Bose-Einstein distribution in statistical mechanics (recall that photons are bosons, seen in the fulfillment of the commutation relations (1.44) and (1.45)).

Each of these states can be squeezed and displaced in the phase space by squeezing and displacing operators, respectively. The resulting states are also very interesting and have unique properties. Nevertheless, in this thesis, only the Fock, coherent, and thermal states are used and analyzed in detail to describe quantum batteries.

### 1.3.2 Atoms and spins

#### Spin and atomic qubits interacting with light

A single mode of linearly polarized light inside a 1-D resonator is described, in the Schrödinger picture, by the fields

$$\mathbf{E}_{\perp}(z) = E_{\omega}\hat{\mathbf{x}}\left(b^{\dagger} + b\right)\sin(k_z z), \tag{1.61}$$

$$\mathbf{B}(z) = \mathrm{i}B_{\omega}\hat{\mathbf{y}}\left(b^{\dagger} - b\right)\cos(k_z z), \tag{1.62}$$

and the free Hamiltonian (1.55). These have been obtained, again, from equation (1.53) by choosing a specific allowed pair $(e, \mathbf{k})$, and also considering a 1-dimensional volume $V = L$.

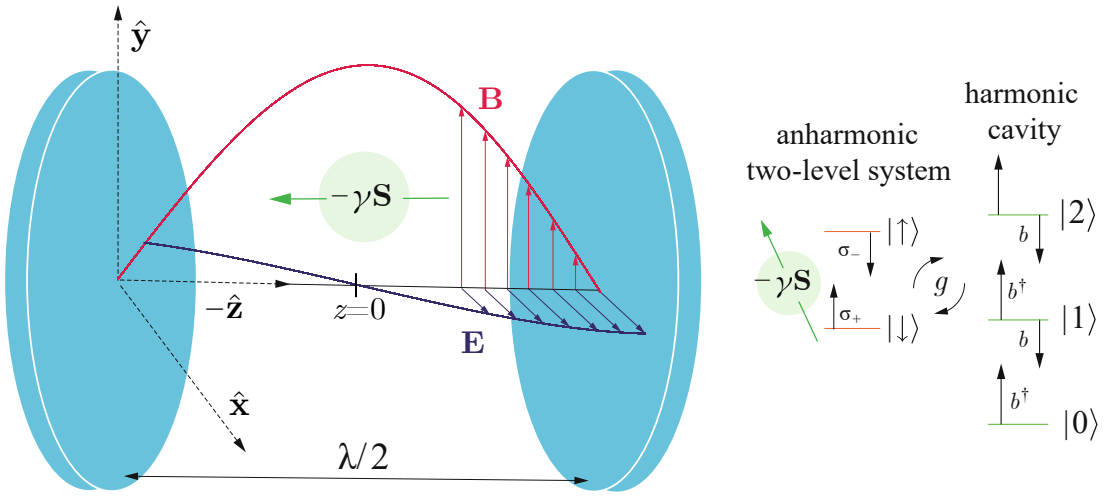


Figure 1.1: Spin qubit inside a single mode electromagnetic resonator for waves of wavelength $\lambda$. The right energy level diagrams represent the effect of the raising and lowering spin operators $\sigma_\pm$, as well as the effect of the creation and annihilation operators $b, b^\dagger$. Picture adapted from [39].

Without loss of generality, an electric field polarized in the $\hat{\mathbf{x}}$ direction has been chosen, representing modes confined in the $\hat{\mathbf{z}}$ propagation direction.

At the center of this resonator ($z = 0$), a spin qubit is placed (see Figure 1.1). Hence it interacts with the oscillating magnetic field $\mathbf{B}(z) = B_y\hat{\mathbf{y}}$ through the interaction Hamiltonian

$$\mathcal{H}_{\text{int}} = -\boldsymbol{\mu}\cdot\mathbf{B}, \tag{1.63}$$

where $\boldsymbol{\mu}$ is the magnetic dipole moment of the spin-$\frac{1}{2}$ system, given by

$$\boldsymbol{\mu} = -\gamma\mathbf{S}, \tag{1.64}$$

where $\gamma/(2\pi)$ is the gyromagnetic ratio of the spin system considered, and $\mathbf{S} \equiv S_x\hat{\mathbf{x}}+S_y\hat{\mathbf{y}}+S_z\hat{\mathbf{z}}$ is the spin-$\frac{1}{2}$ operator vector, i.e.

$$S_j \equiv \frac{\hbar}{2}\sigma_j, \quad \forall j = x, y, z \tag{1.65}$$

where $\sigma_j$ are the Pauli operators diagonalized among the $\hat{\mathbf{z}}$ direction, which in matrix representation are

$$\sigma_x = \begin{pmatrix} 0 & 1 \\ 1 & 0 \end{pmatrix}, \qquad \sigma_y = \begin{pmatrix} 0 & -\mathrm{i} \\ \mathrm{i} & 0 \end{pmatrix}, \qquad \sigma_z = \begin{pmatrix} 1 & 0 \\ 0 & -1 \end{pmatrix}. \tag{1.66}$$

Hence,

$$\mu_y \equiv \boldsymbol{\mu}\cdot\hat{\mathbf{y}} = -\gamma\frac{\hbar}{2}\sum_{i,j}\sigma_y^{ij}\,|j\rangle\langle i| \equiv -\gamma\sum_{i,j}M_y^{ij}\,|j\rangle\langle i|\,, \tag{1.67}$$

where $\sigma_y^{ij}$ is the $(i,j)-$matrix-element of $\sigma_y$, and $M_y^{ij} \equiv \frac{\hbar}{2}\sigma_y^{ij}$ is the corresponding transition matrix element of the magnetic dipole. The kets $|j\rangle \in \{|e\rangle \equiv \begin{pmatrix}1 & 0\end{pmatrix}^\intercal, |g\rangle \equiv \begin{pmatrix}0 & 1\end{pmatrix}^\intercal\}$ are the eigenvectors of $\sigma_y$, where $|e\rangle$ and $|g\rangle$ are the excited and ground states of the $z-$spin qubit, respectively.

Therefore, using equations (1.62) and (1.67) in (1.63) at $z = 0$ gives

$$\mathcal{H}_{\text{int}} = -\mathrm{i}\gamma B_\omega \sum_{i,j} M_y^{ij} \, |j\rangle\langle i| \otimes \left(b^\dagger - b\right), \tag{1.68}$$

which simplifies to

$$\mathcal{H}_{\text{int}} = -\hbar g \left(\sigma_+ - \sigma_-\right)\left(b^\dagger - b\right), \tag{1.69}$$

where $\sigma_+ \equiv |e\rangle\langle g|$ and $\sigma_- \equiv |g\rangle\langle e| = (\sigma_+)^\dagger$ are raising and lowering operators for the spin qubit, respectively; and

$$g \equiv \frac{\gamma B_\omega \left|M_y^{eg}\right|}{\hbar} = \frac{\gamma B_\omega}{2} \tag{1.70}$$

is the coupling constant. The tensor product has been omitted to simplify notation.

The secular terms $\sigma_+ b^\dagger$ and $\sigma_- b$ are neglected in the so called *rotating wave approximation*, valid for $g \ll \omega$ [39–44]. This is the same type of approximation explained at the end of section 1.2, in which rapidly oscillating terms are neglected, although this time the approximation is made on terms that come from the Hamiltonian instead of the dissipator. In this limit, the interaction Hamiltonian (1.69) reduces to

$$\mathcal{H}_{\text{int}} = \hbar g \left(\sigma_+ b + \sigma_- b^\dagger\right). \tag{1.71}$$

Hence, adding the free Hamiltonians of each subsystem, i.e. the light mode and the spin qubit, the complete Hamiltonian under the rotating wave approximation is

$$\mathcal{H}_{\text{JC}} = \hbar\omega b^\dagger b + \frac{\hbar}{2}\omega_q \sigma_z + \hbar g \left(\sigma_+ b + \sigma_- b^\dagger\right), \tag{1.72}$$

known as **Jaynes-Cummings Hamiltonian**, where $\omega_q$ is the angular frequency of the qubit, i.e. $\hbar\omega_q$ is the energy separation between its two eigenenergies. The constant factor $\frac{1}{2}$ of the Hamiltonian (1.55) has been eliminated by simply performing an energy shift of $\frac{\hbar\omega}{2}$ to the reference energy used, which does not change the dynamics.

If the electric field is linearly polarized in $\mp\hat{\mathbf{y}}$ instead of $\hat{\mathbf{x}}$, the interaction Hamiltonian (1.71) is changed to

$$\mathcal{H}'_{\text{int}} = \pm\mathrm{i}\hbar g \left(\sigma_+ b - \sigma_- b^\dagger\right), \tag{1.73}$$

where $g$ has not been changed, because $\left|M_y^{eg}\right| = \left|M_y^{ge}\right| = |M_x^{eg}| = |M_x^{ge}| = \frac{\hbar}{2}$.

Nevertheless, $\mathcal{H}_{\text{int}}$ and $\mathcal{H}'_{\text{int}}$ reproduce the same dynamics as there is a unitary transformation between the two Hamiltonians. This proof is left in appendix D. Furthermore, if instead

of a spin qubit interacting with the oscillating magnetic field, the study is done over an atom interacting as an electric dipole with the oscillating electric field, the Hamiltonian (1.71) is also obtained if the coupling constant is changed to $g = -E_\omega \mathbf{P}^{eg} \cdot \hat{\mathbf{j}}/\hbar$ [40, 41], where $\mathbf{P}^{eg} \cdot \hat{\mathbf{j}} = q \langle e|\mathbf{r}|g\rangle \cdot \hat{\mathbf{j}}$ is the $g \to e$ transition matrix element of the electric dipole along the polarization direction of the electric field, $\hat{\mathbf{j}}$, and $-q$ is the electric charge of the electron. Therefore, the Jaynes-Cummings Hamiltonian can be used without loss of generality to represent the quantum dynamics of a spin or atomic qubit interacting with a single linearly polarized light mode.

When there are $N$ qubits, instead of a single one, the Jaynes-Cummings Hamiltonian (1.72) is changed to the **Tavis-Cummings Hamiltonian**,

$$\mathcal{H}_{\mathrm{TC}} = \hbar\omega b^\dagger b + \frac{\hbar}{2}\sum_{i=1}^{N}\omega_q^i\sigma_z^i + \hbar\sum_{i=1}^{N} g^i(\sigma_+^i b + \sigma_-^i b^\dagger), \tag{1.74}$$

where the index $i$ indicates the $i-$th qubit. If the qubits are identical, $\omega_q^i = \omega_q$. Additionally, if they are spread within a spherical volume of a diameter much smaller than the wavelength of the light mode, i.e. they can all be considered to be at $z = 0$, then $g^i = g$. In this case $\mathcal{H}_{\mathrm{TC}}$ simplifies to

$$\mathcal{H}'_{\mathrm{TC}} = \hbar\omega b^\dagger b + \frac{\hbar}{2}\omega_q\sum_{i=1}^{N}\sigma_z^i + \hbar g\sum_{i=1}^{N}(\sigma_+^i b + \sigma_-^i b^\dagger), \tag{1.75}$$

which can be recast as

$$\mathcal{H}'_{\mathrm{TC}} = \hbar\omega b^\dagger b + \hbar\omega_q J_z + \hbar\Omega(J_+ b + J_- b^\dagger), \tag{1.76}$$

where $\Omega = \sqrt{N}g$ is the collective coupling factor, and $J_z, J_\pm$ are dimensionless (divided by $\hbar$) collective spin$-\frac{N}{2}$ operators given by

$$J_z = \frac{1}{2}\sum_{i=1}^{N}\sigma_z^i, \qquad J_\pm = \frac{1}{\sqrt{N}}\sum_{i=1}^{N}\sigma_\pm^i. \tag{1.77}$$

where $J_\pm$ has been normalized by $\sqrt{N}$. In this way, $N$ qubit excitations correspond to 1 excitation of the complete ensemble normalized. Hence, noticing that the coupling factor of this ensemble of qubits, $\Omega$, is enhanced by a factor $\sqrt{N}$ compared to the single-qubit coupling factor, $g$, it is clear that the collective system of qubits evolves with an interaction dynamics at a rate $\sqrt{N}$ faster than for single qubits. For the initial conditions of interest for this thesis (excepting thermal states), this was checked in [9]. For more details and other initial conditions refer to [43].

The resonator can be classically driven by injecting a stream of classical coherent light of angular frequency $\omega_d$. In this case, the **driving Hamiltonian**

$$\mathcal{H}_{\mathrm{d}} = \hbar F_d\left(\mathrm{e}^{-\mathrm{i}\omega_d t}b^\dagger + \mathrm{e}^{\mathrm{i}\omega_d t}b\right), \tag{1.78}$$

must be added to the Tavis-Cummings Hamiltonian. The term $F_d$ is the driving amplitude, i.e. the amplitude of the classical light injected, which can also present time-dependence. Hence, using $\mathcal{H}'_{\mathrm{TC}}$, the total Hamiltonian is

$$\mathcal{H}'_{\mathrm{DTC}} = \hbar\omega b^\dagger b + \hbar\omega_q J_z + \hbar\Omega(J_+ b + J_- b^\dagger) + \hbar F_d\left(\mathrm{e}^{-\mathrm{i}\omega_d t}b^\dagger + \mathrm{e}^{\mathrm{i}\omega_d t}b\right), \tag{1.79}$$

where DTC stands for "driven Tavis-Cummings". For a single mode resonator, if the driving field is injected through semi-transparent walls, the only allowed driving angular frequency is $\omega_d = \omega$ [43], which is usually the case of interest.

The Hamiltonian $\mathcal{H}'_{\text{DTC}}$ is the one that describes the quantum batteries studied in this thesis, whether driving is considered ($F_d \neq 0$) or not ($F_d = 0$). Hence, to study the quantum batteries in dissipative conditions (coupled to an environment), the specific possible dissipation mechanisms for the qubits and the resonator's electromagnetic field must be understood.

When adding dissipation to the system with free Hamiltonian $\mathcal{H}'_{\text{DTC}}$, if the system is weakly coupled to the environment, the dynamics is described by the Lindblad master equation (1.11). The typical mechanisms of dissipation considered here are three [42]:

- The resonator light mode is coupled to a thermal bath of photons, i.e. an environment composed of infinite light modes in thermal state at a given temperature $T$. The resulting dissipation effects over the resonator mode are given by a dissipator $\mathfrak{D}_{\text{r}}$ and a null Lamb-shift Hamiltonian.
- The qubits are coupled to the same thermal bath of photons that couple with the resonator light mode. Nevertheless, the coupling factors are different, resulting in different relaxation rates. The resulting dissipation effects over the qubits are given by a dissipator $\mathfrak{D}_{\text{q1}}$ and a non-null Lamb-shift Hamiltonian.
- The qubits are coupled to other sources of dissipation. The specific dissipation mechanisms here depend on the specific system used as qubit. Nevertheless, a general phenomenological dissipator can be used to account for the decoherence effects produced due to these interactions. The resulting dissipation effects over the qubits are given by a dissipator $\mathfrak{D}_{\text{q2}}$ and a null Lamb-shift Hamiltonian.

In general, the dissipator can not be separated in many dissipators each representing the dissipation mechanisms of the separated subsystems. However, for the driven Tavis-Cummings model with Hamiltonian $\mathcal{H}'_{\text{DTC}}$ it is possible to separate the total dissipator $\mathfrak{D}$ as [42]

$$\mathfrak{D} = \mathfrak{D}_{\text{r}} + \mathfrak{D}_{\text{q1}} + \mathfrak{D}_{\text{q2}}, \tag{1.80}$$

which is useful because each dissipation mechanism occurs at a different relaxation rate, which allows to consider only the dissipators acting in the time-scale of interest. For example, often the relaxation rates of the qubits are much smaller than the ones of the resonator light mode, allowing to consider $\mathfrak{D} \approx \mathfrak{D}_{\text{r}}$ for short enough time-scales, which are the ones studied along the current thesis.

The dissipator $\mathfrak{D}_{\text{r}}$ of equation (1.80) is explicitly given by [42]

$$\mathfrak{D}_{\text{r}}(\rho) = \kappa(n_{\text{th}} + 1)\left[2a\rho a^\dagger - \left\{a^\dagger a, \rho\right\}\right] + \kappa n_{\text{th}}\left[2a^\dagger \rho a - \left\{aa^\dagger, \rho\right\}\right], \tag{1.81}$$

where $n_{\text{th}}$ is the mean number of thermal photons in the environment, related to the temperature of the bath through the equation (1.60), and $2\kappa = \gamma_{\text{r},0}$ is the relaxation rate of $\mathfrak{D}_{\text{r}}$ at zero temperature.

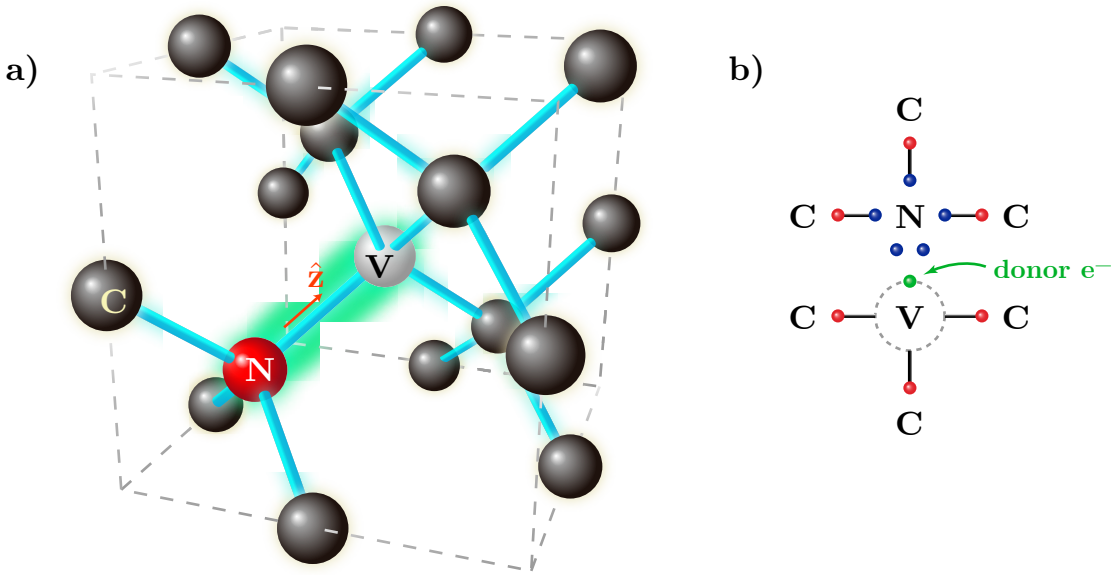


Figure 1.2: **(a)** Structure of the NV center in the diamond lattice, highlighting the NV axis along the $\hat{\mathbf{z}}$ direction. **(b)** Diagram showing the electrons of the $NV^-$. Five (blue) correspond to the valence orbital of N, and one (green) donor electron coming from the diamond lattice was trapped in the vacancy. Also, the picture shows the (red) electrons from the valence orbitals of the nearby carbons that would normally (without the defect) complete the bonds.

## 1.4 Nitrogen-Vacancy centers in diamond

### 1.4.1 Structure

The nitrogen-vacancy center in diamond or **NV center**, for short, is a defect in the diamond lattice produced by the replacement of a carbon atom with a nitrogen atom and an adjacent missing carbon atom (the *vacancy*). This is depicted in Figure 1.2.a, where the so called *NV axis* is identified as the axis along the $\hat{\mathbf{z}}$ direction. The NV center of practical interest for quantum technologies is the negatively charged one ($NV^-$) in which a donor electron from the lattice is trapped by the center [11], as depicted in Figure 1.2.b. Therefore, along this thesis, whenever talking about the NV center, it is implicitly referred to the $NV^-$, unless explicitly stated otherwise.

The $NV^-$ consists of the nitrogen nucleus and six electrons ($e^-$), five from the valence orbital of the nitrogen, and one donor electron from the lattice. These electrons must occupy the available energy levels from the neighbouring bonds, some of which are dangling due to the vacancy. Symmetry arguments based on the trigonal structure of the lattice are required to notice that, effectively, only two of the six electrons are free to move between the energy levels available by the dangling bonds [11]. Hence, these two electrons behave as a spin-1 system. On the other hand, the nitrogen atom can be a nitrogen-14 ($^{14}N$) or nitrogen-15 ($^{15}N$) [11], meaning that the nuclear spin can be a spin-1 or spin-$\frac{1}{2}$ system, respectively.

Besides the energy levels described before, the $NV^-$ also shows optical transitions, located

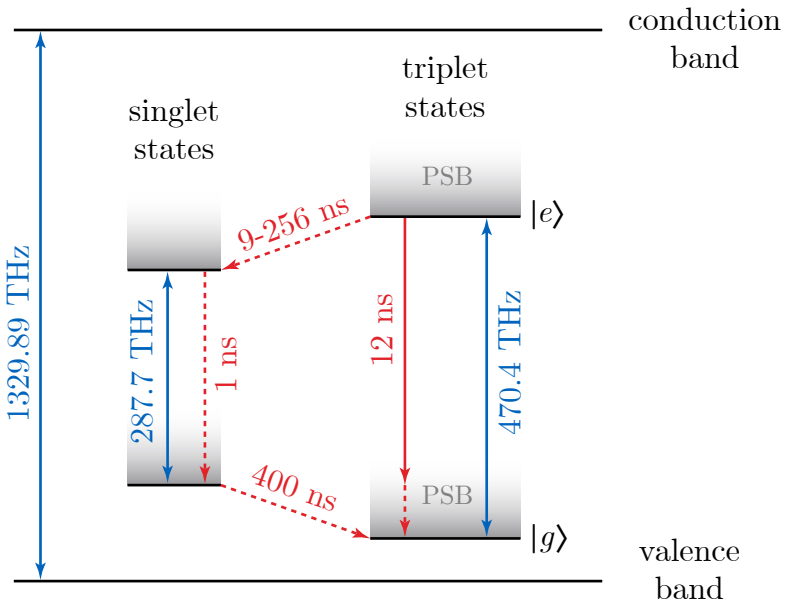


Figure 1.3: Optical energy levels of the $NV^-$. The frequency separations between energy levels are shown in blue, and lifetime transitions in red. The 12 ns decay from $|e\rangle$ to $|g\rangle$ usually occurs to an excited state of the phonon sideband (PSB) of $|g\rangle$, indicated by the continuous arrow finishing higher than the base level of $|g\rangle$. Values from [10, 45].

between the conduction and valence bands of the diamond crystal [10, 11]. As a first approximation, there is a ground state $|g\rangle$, and an optical excited state $|e\rangle$, where the term *optical* is used to remark that the frequency separation between the two levels corresponds to visible light in the electromagnetic spectrum. These are the two main eigenstates, which are triplets due to the spin-1 system formed by the $NV^-$ electrons. There are also two singlet states, but they are not relevant for the current thesis. These energy levels explained are depicted in Figure 1.3, where each energy level is shown as a continuous of levels (fading from black to white in the picture), due to phonons that appear when the interaction with the lattice vibration modes is taken into account [11, 45].

The application of the $NV^-$ of interest for the current thesis is building an effective two-level quantum system that interacts with microwaves. To do so, it is enough to use the ground state $|g\rangle$, as is shown in the next subsections. Nonetheless, the protocols used to initialize such qubit in its ground state, require of the optical transitions [10, 11].

### 1.4.2 The $NV^-$ Hamiltonian

The complete expression of the effective Hamiltonian that describes the ground state triplet of the $NV^-$, neglecting the interaction with nearby carbon nuclear spins, is given by

$$\mathcal{H}_{\text{NV}} = \mathcal{H}^c_{\text{NV}} + V_{\text{NV}} \tag{1.82}$$

where $\mathcal{H}^c_{\text{NV}}$ is the **canonical spin-Hamiltonian of trigonal defects**, and $V_{\text{NV}}$ is the potential that accounts for interactions with external fields. In detail, the former is given

by [11]

$$\frac{\mathcal{H}^c_{\rm NV}}{h} = D_{\rm gs}\left[S_z^2 - \frac{S(S+1)}{3}\right] + A^{\parallel}_{\rm gs} S_z I_z + A^{\perp}_{\rm gs}\left[S_x I_x + S_y I_y\right] + P_{\rm gs}\left[I_z^2 + \frac{I(I+1)}{3}\right], \quad (1.83)$$

where $S_j$ ($I_j$), $\forall j = x, y, z$, are the dimensionless spin operators of the $NV^-$ electrons (nitrogen nucleus) with total spin number $S = 1$ ($I = 1, \frac{1}{2}$; for $^{14}$N and $^{15}$N, respectively). $D_{\rm gs}, A^{\parallel}_{\rm gs}, A^{\perp}_{\rm gs}$, and $P_{\rm gs}$ are constant factors that account for the strength of each interaction in the Hamiltonian $\mathcal{H}^c_{\rm NV}$, where the subindex "gs" is there to remember that they correspond to the optical ground state of the $NV^-$. $D_{\rm gs}$ is the **fine structure splitting**[2]due only to spin-spin interaction between the $NV^-$ electrons, neglecting spin-orbit interactions, which is experimentally justified [11]. $A^{\parallel(\perp)}_{\rm gs}$ is the **axial (non-axial) magnetic hyperfine parameter**, and $P_{\rm gs}$ is the **nuclear electric quadrupole parameter**. The latter is non-zero only for $^{14}$N. All these factors ($D_{\rm gs}, A^{\parallel}_{\rm gs}, A^{\perp}_{\rm gs}$, and $P_{\rm gs}$) vary very slowly with the temperature. Therefore, measured values (see Tables 1.1 and 1.2) are used for each range of temperatures in which the $NV^-$ is to be studied.

| Temperature (K) | $D_{\rm gs}$ (GHz) |
|---|---|
| 4–7 | 2.88 |
| 300 | 2.87 |

Table 1.1: Fine structure splitting parameter for different temperatures. Despite of a very wide variation in temperature, $D_{\rm gs}$ changes very little. Data from [11].

| Isotope | $A^{\parallel}_{\rm gs}$ (MHz) | $A^{\perp}_{\rm gs}$ (MHz) | $P_{\rm gs}$ (MHz) |
|---|---|---|---|
| $^{14}$N | -2.16 | 2.7 | -4.94 |
| $^{15}$N | 3.0 | 3.6 | — |

Table 1.2: Factors that set the interaction strength of terms involving the nitrogen nuclear spin. The nitrogen-15 has no nuclear electric quadrupole parameter. The temperature variation of these parameters is negligible and, hence, not reported. Data from [11].

| $\gamma_{\rm e}$ (MHz/G) | $g^{\parallel}_{\rm gs}$ | $g^{\perp}_{\rm gs}$ | $d^{\parallel}_{\rm gs}$ (Hz cm/V) | $d^{\perp}_{\rm gs}$ (Hz cm/V) |
|---|---|---|---|---|
| 2.8 | 2.0029 | 2.0029 | 17 | 0.35 |

Table 1.3: Factors accounting for the interaction strength between the free Hamiltonian of the $NV^-$ and external fields. Data from [11, 46, 47].

[2]Also called **zero field splitting** [10].

| Isotope | $\gamma_{\mathrm{N}}$ (kHz/G) |
|---|---|
| $^{14}$N | 0.3 |
| $^{15}$N | -0.432 |

Table 1.4: Gyromagnetic ratio of the nitrogen nuclear spin. Data from [46, 48, 49]

The potential $V_{\mathrm{NV}}$ of equation (1.82) in general includes interactions with an external magnetic field $\mathbf{B} = B_x\hat{\mathbf{x}} + B_y\hat{\mathbf{y}} + B_z\hat{\mathbf{z}}$, an external electric field $\mathbf{E} = E_x\hat{\mathbf{x}} + E_y\hat{\mathbf{y}} + E_z\hat{\mathbf{z}}$, and an external strain field $\boldsymbol{\delta} = \delta_x\hat{\mathbf{x}} + \delta_y\hat{\mathbf{y}} + \delta_z\hat{\mathbf{z}}$. Hence $V_{\mathrm{NV}}$ is in general given by [11]

$$V_{\mathrm{NV}} = V_{\mathrm{NV}}^{\mathrm{magnetic}} + V_{\mathrm{NV}}^{\mathrm{electric}} + V_{\mathrm{NV}}^{\mathrm{strain}}, \tag{1.84}$$

$$\frac{1}{h}V_{\mathrm{NV}}^{\mathrm{magnetic}} = \mu_{\mathrm{B}} g_{\mathrm{gs}}^{\parallel} S_z B_z + \mu_{\mathrm{B}} g_{\mathrm{gs}}^{\perp}(S_x B_x + S_y B_y) + \mu_{\mathrm{N}} g_{\mathrm{N}} \mathbf{I}\cdot\mathbf{B}, \tag{1.85}$$

$$\frac{1}{h}V_{\mathrm{NV}}^{\mathrm{electric}} = d_{\mathrm{gs}}^{\parallel} E_z \left(S_z^2 - \frac{S(S+1)}{3}\right) + d_{\mathrm{gs}}^{\perp}\left\{E_x(S_y^2 - S_x^2) + E_y(S_xS_y + S_yS_x)\right\}, \tag{1.86}$$

$$\frac{1}{h}V_{\mathrm{NV}}^{\mathrm{strain}} = d_{\mathrm{gs}}^{\parallel} \delta_z \left(S_z^2 - \frac{S(S+1)}{3}\right) + d_{\mathrm{gs}}^{\perp}\left\{\delta_x(S_y^2 - S_x^2) + \delta_y(S_xS_y + S_yS_x)\right\}, \tag{1.87}$$

where $\mu_{\mathrm{B}}$ is Bohr's magneton, $\mu_{\mathrm{N}}$ is the nuclear magneton of the nitrogen, $g_{\mathrm{gs}}^{\parallel(\perp)}$ is the axial (non-axial) component of the ground state electronic $g$-factor tensor, $g_{\mathrm{N}}$ is the isotropic nuclear $g$-factor of the nitrogen, and $d_{\mathrm{gs}}^{\parallel(\perp)}$ is the axial (non-axial) component of the ground state electric dipole moment. Experimental measurements of these quantities are shown in Tables 1.3 and 1.4, where the gyromagnetic ratios of the electron, $\gamma_{\mathrm{e}} \equiv g_{\mathrm{e}}\mu_{\mathrm{B}}$, and the nitrogen nucleus, $\gamma_{\mathrm{N}} \equiv g_{\mathrm{N}}\mu_{\mathrm{N}}$, are also shown.

### 1.4.3 Constructing a spin qubit with the NV$^-$

The most common way to construct a qubit from the NV$^-$ Hamiltonian is by applying solely an external static (classic) magnetic field $\mathbf{B}^{\mathrm{stat}} = B_z^{\mathrm{stat}}\hat{\mathbf{z}}$ over the NV center. Hence, $V_{\mathrm{NV}} = V_{\mathrm{NV}}^{\mathrm{magnetic}}$. Furthermore, since $\gamma_{\mathrm{N}} \ll \gamma_{\mathrm{e}}$, the interaction between the nitrogen's nuclear spin and $B_z^{\mathrm{stat}}$ can usually be neglected in $V_{\mathrm{NV}}^{\mathrm{magnetic}}$. Similarly, by noticing that $D_{\mathrm{gs}} \gg A_{\mathrm{gs}}^{\parallel}, A_{\mathrm{gs}}^{\perp}, P_{\mathrm{gs}}$, the spin-spin interactions involving the nitrogen's nuclear spin can also be neglected. Therefore, the total NV Hamiltonian is reduced to

$$\frac{\mathcal{H}'_{\mathrm{NV}}}{h} = D_{\mathrm{gs}}\left[S_z^2 - \frac{2}{3}\right] + \gamma_{\mathrm{e}} S_z B_z^{\mathrm{stat}}, \tag{1.88}$$

where $g_{\mathrm{gs}}^{\parallel} \approx g_{\mathrm{gs}}^{\perp} \approx g_{\mathrm{e}}$ has been applied (see Table 1.3). The resultant Hamiltonian $\mathcal{H}'_{\mathrm{NV}}$ was obtained by neglecting all nitrogen's nuclear terms, which means ignoring the hyperfine structure of the NV center. This is a good approximation as long as there is no addition of terms that modifies the dynamics of interest into one that evolves at a rate of the order of magnitude of the neglected terms, namely, at MHz for $A_{\mathrm{gs}}^{\parallel}, A_{\mathrm{gs}}^{\perp}$, and $P_{\mathrm{gs}}$; or kHz for $\gamma_{\mathrm{N}}$.

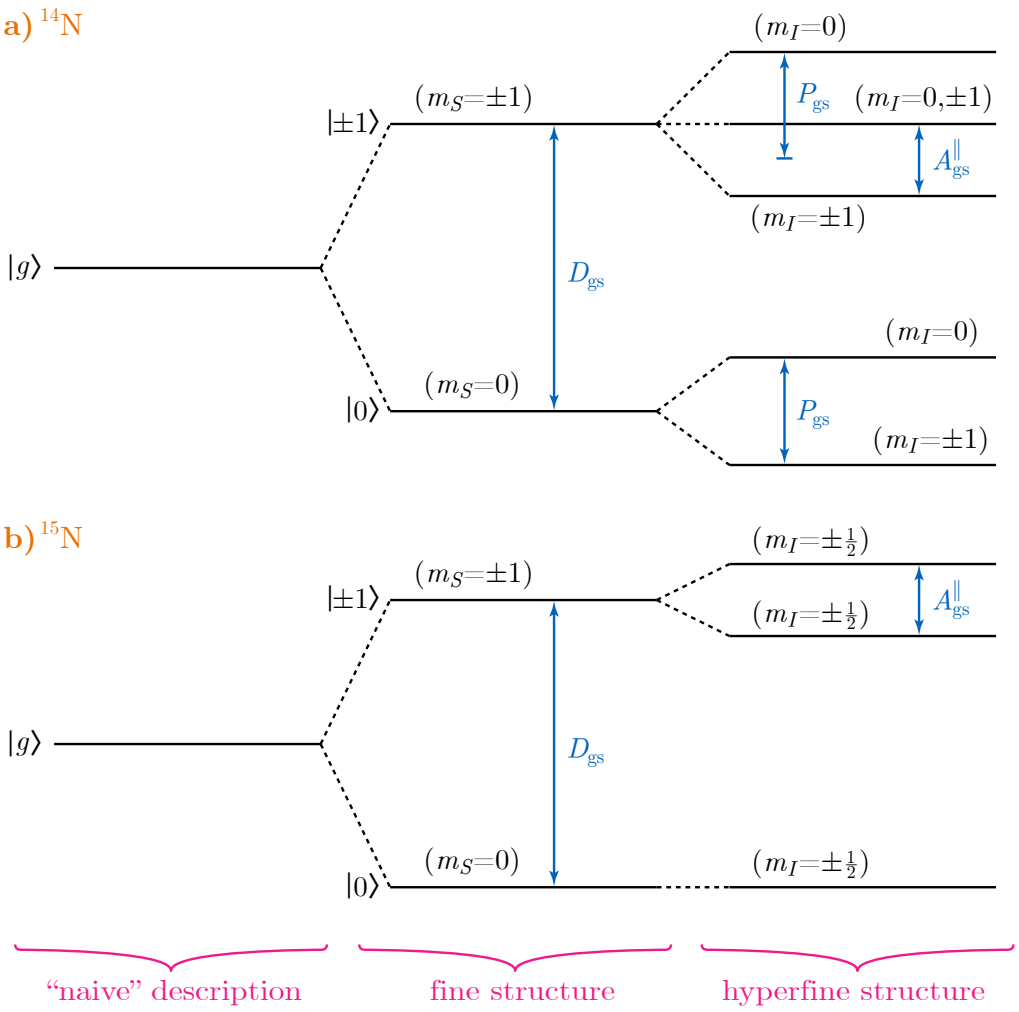


Figure 1.4: Details of the optical ground state of the $NV^-$ for **(a)** $^{14}$N, and **(b)** $^{15}$N. The fine structure takes into consideration the spin-1 structure of the $NV^-$ electrons. The hyperfine structure also considers the spin structure of the nitrogen nucleus, together with the spin-spin interaction between the $NV^-$ electrons and the nitrogen nucleus. The dimensionless spin eigenvalues of the $NV^-$ electrons (nitrogen nucleus) are denoted by $m_S$ ($m_I$). Diagrams based on [11].

The effect of $B_z^{\rm stat}$ on equation (1.88) is splitting the eigenenergy associated to $|\pm1\rangle$ through the *Zeeman effect*, as depicted in Figure 1.5. If $B_z^{\rm stat}$ is large enough, the eigenenergy with spin projection $m_S = 1$ can be neglected. Hence, by selecting the two lowest energy levels[3]as an effective two-level system, a qubit Hamiltonian is finally constructed,

$$\mathcal{H}^q_{\rm NV} = h(D_{\rm gs} - \gamma_{\rm e} B_z^{\rm stat})\frac{1}{2}\sigma_z, \tag{1.89}$$

where $\hbar\omega_q = h(D_{\rm gs} - \gamma_{\rm e} B_z^{\rm stat})$ is the qubit energy separation, i.e. the separation between the

[3]This is just one of the alternatives. More generally, the eigenstate that will not be driven by the microwave is neglected. Hence, the two other eigenstates form the qubit of practical interest.

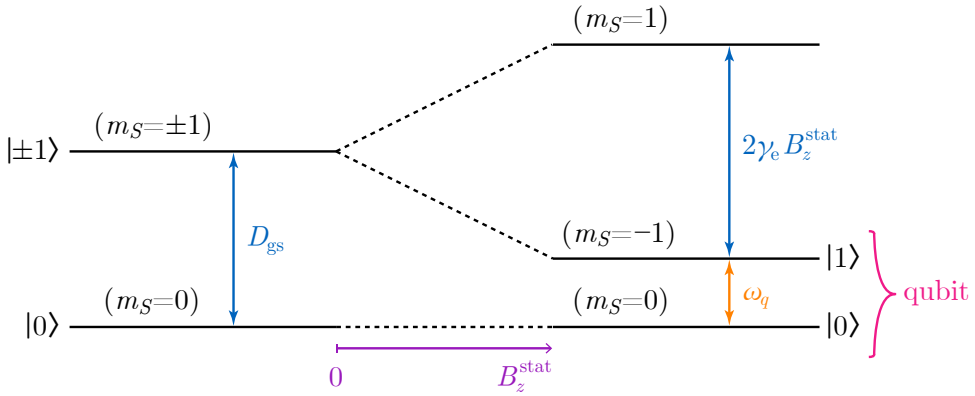


Figure 1.5: Construction of a qubit from the hyperfine structure of the optical ground state of the $NV^-$. By turning on an static (classic) magnetic field $B_z^{\text{stat}}\hat{\mathbf{z}}$, the degenerated $|\pm1\rangle$ vector state starts splitting, through the Zeeman effect. For large enough $B_z^{\text{stat}}$, the highest energy level can be ignored, defining the qubit by the subsystem with eigenkets $|0\rangle$ and $|1\rangle$.

two eigenenergy levels of the qubit. Hence, equation (1.89) can be recast as

$$\mathcal{H}_{\text{NV}}^q = \frac{\hbar}{2}\omega_q\sigma_z, \tag{1.90}$$

which is the general form of describing the free Hamiltonian of a spin-$\frac{1}{2}$ qubit.

This $NV^-$ qubit has been experimentally realized many times. It is characterized by having a large **longitudinal relaxation time** $T_1 \approx 3-10$ ms [11,50,51], and large **dephasing times** $T_2^* \approx 1.7-3.7$ $\mu$s [11,46] and $T_2 \approx 32-600$ $\mu$s [11], at room temperature (300 K). Large variations are due to different types of NV samples [10,11]. These times are the inverse of dissipation rates due to interaction with the environment. The longitudinal relaxation time is the mean time the spin qubit reaches thermal equilibrium. The dephasing time, instead, is a decoherence time, and corresponds to the average time the spin qubit can maintain its quantum phase. The difference between $T_2$ and $T_2^*$ is that the former is valid for a single NV qubit (or an ideal homogeneous sample), while the latter is valid for an ensemble of NV qubits with different local conditions [11].

### 1.4.4 $NV^-$ spin qubit inside a resonator

If the NV center described, in its optical ground state, by $\mathcal{H}_{\text{NV}}^q$ is placed at the center of a single-mode electromagnetic resonator, the interaction with the quantum electromagnetic wave must be taken into consideration. In particular, if the quantum fields are the ones of equations (1.61) and (1.62), which are linearly polarized as $\mathbf{E} = E_x\hat{\mathbf{x}}$ and $\mathbf{B} = B_y\hat{\mathbf{y}}$, then the additional interaction Hamiltonian is

$$\mathcal{H}_{\text{int}} = \frac{h}{2}\gamma_e(\sigma_y B_y), \tag{1.91}$$

where equations (1.85) and (1.86) have been used together with neglecting the third energy level of the NV's ground state (recall the conditions valid for $\mathcal{H}_{\text{NV}}^q$ to faithfully represent $\mathcal{H}_{\text{NV}}$),

as well as the interaction with the electric field. The latter approximation is valid because the interaction with the electric field is orders of magnitude smaller than the interaction with the magnetic field. Indeed, the magnitudes of the electromagnetic field are $B_\omega$ and $E_\omega = cB_\omega$, where $\omega$ is the resonator frequency and $c \approx 2.998 \cdot 10^8$ m/s is the speed of light in vacuum (for simplicity, to avoid additional quantum interactions with the dielectric media, vacuum is considered inside the resonator, which also implies that the phase speed of the radiation is $c$), and hence, using Table 1.3, it is possible to obtain the scaling orders of the magnetic and electric interactions, namely

$$\mathcal{O}(\gamma_\mathrm{e} B_\omega) = \mathcal{O}(B_\omega) \times 10^6 \text{ Hz/G} \tag{1.92}$$

$$\mathcal{O}(d_\mathrm{gs}^\perp E_\omega) = \mathcal{O}(B_\omega) \times 10^8 \text{ m/s} \times \text{Hz cm/V} = \mathcal{O}(B_\omega) \times 10^2 \text{ Hz/G}, \tag{1.93}$$

which yields

$$\frac{\mathcal{O}(\gamma_\mathrm{e} B_\omega)}{\mathcal{O}(d_\mathrm{gs}^\perp E_\omega)} = 10^4 \tag{1.94}$$

$$\Rightarrow \mathcal{O}(\gamma_\mathrm{e} B_\omega) \gg \mathcal{O}(d_\mathrm{gs}^\perp E_\omega), \tag{1.95}$$

justifying that the interaction with the electric field of the radiation can be neglected. The second equality of equation (1.93) was obtained by applying 1 cm/V $= 10^{-6}$ s/(G m).

The interaction Hamiltonian of equation (1.91) is the same one of equation (1.63). Hence, the dynamics is described by the Jaynes-Cummings Hamiltonian (1.72) with coupling constant

$$g = \gamma_\mathrm{e} B_\omega \pi, \tag{1.96}$$

directly obtained from equation (1.70)[4].

The extension towards many qubits inside a resonator then follows as described in subsection 1.3.2. Nonetheless, it is experimentally difficult to get a sample of NV spin qubits with all of them having the same qubit energy separation, because each NV center has its own different $z$-axis[5], meaning that the static field $\mathbf{B}^\mathrm{stat}$ will be projected with a different magnitude over the different NV axes. This phenomena is known as **inhomogeneous broadening** of the NV centers. Therefore, in most scenarios, under the rotating wave approximation, the Hamiltonian (1.76) is just a first approximation to the real Hamiltonian (1.74).

[4]The factor $\pi$ appears because $\gamma_\mathrm{e}$ is in units of frequency, while $\gamma$ in equation (1.70) is in units of angular frequency.

[5]There are four possible orientations for the $z$-axis in diamond due to its trigonal structure depicted in Figure 1.2.a.

# Chapter 2

# Quantum batteries

## 2.1 A new quantum technology

A quantum technology is defined as a technology that uses fundamental quantum properties of a system to obtain an advantage in performance over the corresponding analogous technology that does not exploit those quantum properties. Examples of quantum technologies are:

- Quantum computers, which use quantum entanglement and superposition to achieve speedups in numerical computations that, in principle, seem impossible for nowadays classical computers.
- Quantum communications, where quantum state teleportation, entanglement and superposition are used to either have unbreakable internet security keys, relying on physics principles rather than algorithmic complexity, or build a full quantum channel able to share quantum information rather than classical information.
- Quantum sensing, where the sensibility and nature of quantum interactions are used to improve precision of parametric measurements (e.g. time, temperature, or any non-quantum observable) beyond what is possible with classical systems.

Similarly, a recent new quantum technology has been discovered and is being studied: **quantum batteries** (QBs). This concept has emerged as a promising tool for the thermodynamic control at quantum scales [1–6]. A QB is a quantum mechanical system that behaves as an efficient energy storage device. Its realization is motivated by the fact that genuine quantum effects, such as entanglement or squeezing, can typically boost the performances of classical protocols, e.g., by speeding up the underlying dynamics [7, 8]. Enhancements provided by quantum correlations in the charging (or discharging) process of a QB has been discussed in general terms in [12–15]. More recently, possible realizable models have been explored, including spin-chains and qubits interacting with electromagnetic fields [9, 16–21].

## 2.2 Definition

### 2.2.1 Holder-only quantum batteries

The main part of any QB is a quantum system able to store energy. This quantum system is named **holder** throughout this thesis. If the QB consists of solely the holder, it is a **holder-only QB**. Nonetheless, to completely define a QB, a protocol that details how to charge, discharge and keep the energy stored in the holder is required.

A holder-only QB consists of the holder with associated free Hamiltonian $\mathcal{H}_h$ on which an external classical time-dependent field is applied, adding a Hamiltonian $V(t)$, to charge and discharge the holder. Hence, the total Hamiltonian of this QB is given by

$$\mathcal{H}'_\lambda = \mathcal{H}_h + \lambda V(t), \tag{2.1}$$

where the parameter $\lambda$ can be 0 or 1 and defines in which stage is the QB: $\lambda = 1$ for the charging and discharging stages, and $\lambda = 0$ for the storage stage. When $\lambda = 1$, the charging or discharging process occurs through a unitary operation

$$\mathcal{U}_t = \mathcal{T}_{\leftarrow} \mathrm{e}^{-\frac{\mathrm{i}}{\hbar}\int_{t_0}^{t} \mathcal{H}'_\lambda(\tau)\mathrm{d}\tau}, \tag{2.2}$$

where $t_0$ is the initial time of the corresponding process. This charging-storage-discharging protocol, together with the hamiltonian $\mathcal{H}'_\lambda$, fully describes a holder-only QB (depicted in Fig. 2.1). This protocol works as long as the stage switching, i.e. the change of value of $\lambda$, occurs in a timescale much smaller than the one of the Hamiltonian dynamics.

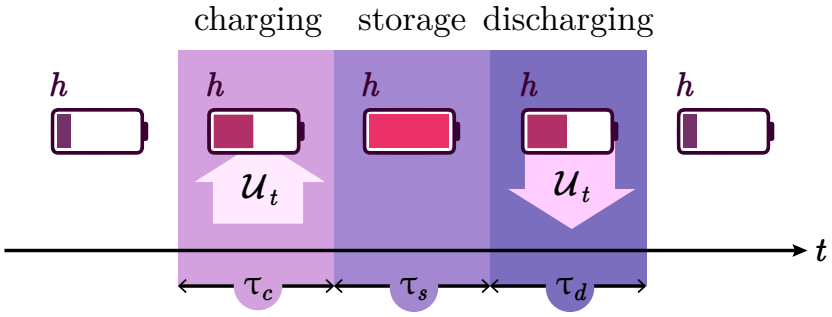


Figure 2.1: A generic holder-only QB consisting of a holder "$h$" in its three operation stages: charging, storage, and discharging. The holder, initially empty, obtains energy through a unitary operation $\mathcal{U}_t$ active for a time $\tau_c$. The energy transferred to the holder is stored for a time $\tau_s$ until it is desired to use the energy. Afterwards, the holder is discharged through the unitary operation $\mathcal{U}_t$ active for a time $\tau_d$. This thesis focuses on time scales for which the holder dissipation is negligible.

### 2.2.2 Charger-based quantum batteries

This thesis focuses on charger-based QBs, but holder-only QBs have been explained before because many texts of the current literature don't make the effort to distinguish between them, and sometimes calling "quantum battery" to just the holder.

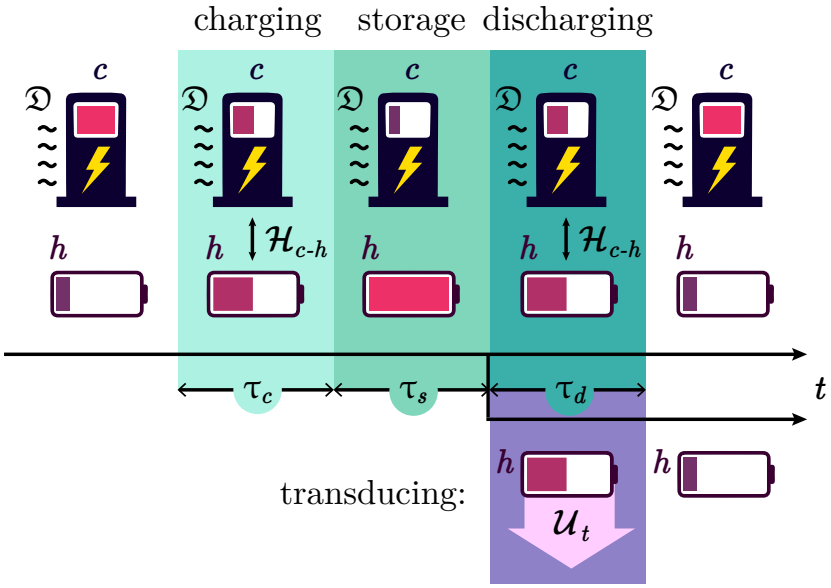


Figure 2.2: A generic charger-based QB consisting of a charger "$c$" and a holder "$h$" in its three operation stages: charging, storage, and discharging. The holder, initially empty, obtains energy from the charger interacting a time $\tau_c$ with the Hamiltonian $\mathcal{H}_{c-h}$. The energy transferred to the holder is stored for a time $\tau_s$ until it is desired to use the energy. To discharge the holder in a time $\tau_d$ it is possible to proceed in transducing mode (bottom) with external classical fields over the holder through a unitary operation $\mathcal{U}_t$, or in normal mode (top) through the charger where the dissipation channels might be used to finally extract the energy. This thesis focuses on time scales for which the charger dissipation ($\mathfrak{D}$) is relevant, but holder dissipation is negligible.

A general definition of **charged-based QBs**, i.e. QBs where the holder is assisted by an additional quantum system, is not fully given in the current literature, and solving it is the goal of this section.

A general charger-based QB consists of two subsystems: an energy "holder" that stores energy for long times, and an energy "**charger**" that acts as transducer of energy to deliver external input energy into the holder. The charger can also be used as a discharging path for the holder, unless the battery is designed to be directly discharged from the holder via external classical fields. This thesis defines the former discharging mode as "**normal**", and the latter as "**transducing**". Furthermore, it is identified that the battery can be charged up either from initial conditions or through external classical driving. In the former charging case (ICC), the charger is prepared in an energetic state and then left to interact with the holder allowing energy transfer, while in the latter (DC) the charger starts empty in energy and it simply acts as the path to directly transfer the external input energy into the holder.

In the ICC case, the charger-based QB system is effectively described by the Hamiltonian $\mathcal{H}_\lambda$, an operator in the total Hilbert space $\mathscr{H}_c \otimes \mathscr{H}_h$ that is given by

$$\mathcal{H}_\lambda = \mathcal{H}_c + \mathcal{H}_h + \lambda \mathcal{H}_{c-h}, \tag{2.3}$$

where $\mathcal{H}_{c,h}$ (acting on $\mathscr{H}_{c,h}$) are the free Hamiltonians of the charger and holder, respectively,

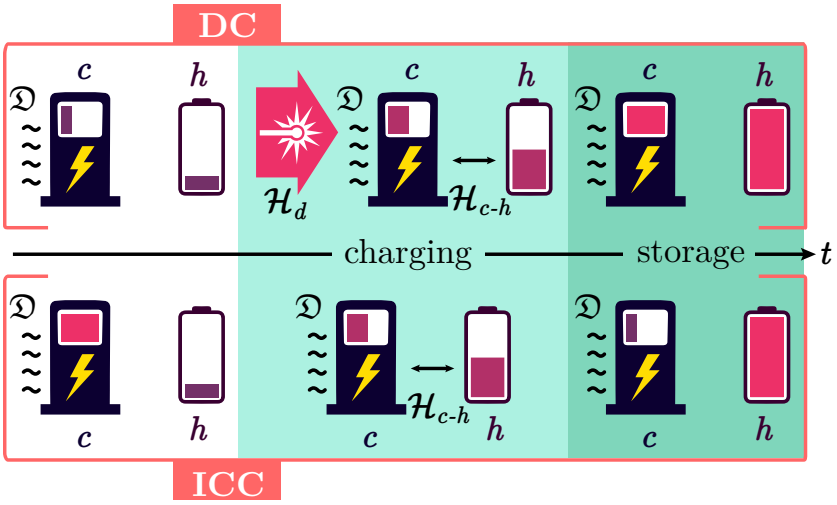


Figure 2.3: The two ways of charging up the holder: driven charging (DC) and initial conditions charging (ICC). In DC the charger and holder are initially empty and the energy is supplied from an external classical driving onto the charger via the Hamiltonian $\mathcal{H}_d(t)$. In ICC instead, the charger starts from a prepared energetic initial condition that then allows the energy transfer to the holder. The states shown in the storage stage, correspond to only the times just after the end of the charging process. For longer storage times, the charger is empty in both DC and ICC.

interacting via the Hamiltonian $\mathcal{H}_{c-h}$ (acting on $\mathscr{H}_c \otimes \mathscr{H}_h$). The parameter $\lambda$ can be 0 or 1 and defines in which stage is the QB: $\lambda = 1$ for the charging and normal discharging stages, and $\lambda = 0$ for the storage and transducing discharging stages. For this QB protocol to work, the switching time between stages must be much smaller than the characteristic time of the dynamical evolution of the battery in each separate stage. Fulfilling this condition, the Hamiltonian $\mathcal{H}_\lambda$ is correctly considered time-independent in each separate stage. The previously defined QB model is pictured in Fig. 2.2.

In the DC case, the Hamiltonian of the charger-based QB system is

$$\mathcal{H}_{\lambda,\xi}(t) = \mathcal{H}_\lambda + \xi\mathcal{H}_d(t), \tag{2.4}$$

where $\mathcal{H}_d(t)$ (acting on $\mathscr{H}_c$) is the driving Hamiltonian, active only in the charging stage, which is expressed by the binary value of the parameter $\xi \in \{0, 1\}$: $\xi = 1$ in the charging stage, and $\xi = 0$ otherwise. The difference between the ICC and DC cases is depicted in Fig. 2.3. The protocol explained for the DC case also works as long as the switching between stages (now determined by the change of both, $\lambda$ and $\xi$) occurs in a much shorter timescale than the one of the Hamiltonian dynamics at each separate stage. Nonetheless, unlike the other QBs described, for DC charger-based QBs the charging stage is governed by a time-dependent Hamiltonian because $\frac{\partial\mathcal{H}_d(t)}{\partial t} \neq 0$.

This thesis focuses on ICC charger-based QBs. Hence, the QB Hamiltonian used is $\mathcal{H}_\lambda$ defined by equation (2.3). The dynamical evolution is then given by the Lindblad master equation (1.11) using $\mathcal{H}_\lambda$ as the system Hamiltonian $\mathcal{H}_S$ and where the dissipator $\mathfrak{D}$ is in general a combination of dissipators acting on the holder and the charger, both separately and jointly. But, in this thesis, it is argued that a QB has practical sense only if the dissipation

rates of the holder, $\gamma_h^i$, are much smaller than the ones of the charger, $\gamma_c^j$, i.e. $\gamma_h^i \ll \gamma_c^j$ for all dissipation channels $i, j$. In particular, $\gamma_h^{\max} \equiv \max_i\{\gamma_h^i\} \ll \min_j\{\gamma_c^j\} \equiv \gamma_c^{\min}$. Hence, if the frequency holder-charger coupling factor is $g \gg \gamma_h^{\max}$ but comparable to $\gamma_c^{\min}$, during charging and discharging stages it is sufficient to consider only the charger dissipator $\mathfrak{D}_c$ in the master equation, allowing to set $\mathfrak{D} \approx \mathfrak{D}_c$ as depicted in Fig. 2.2. During the storage stage, holder dissipators might be added, but the situation of storage times $\tau_s \ll 2\pi/\gamma_h^{\max}$ where holder dissipation is negligible is still interesting as battery since $\tau_s \gg 2\pi/\gamma_c^{\min}$ is still allowed, meaning that the QB could achieve an energy storage beyond what would be possible with just the charger.

## 2.3 Parallel and collective versions

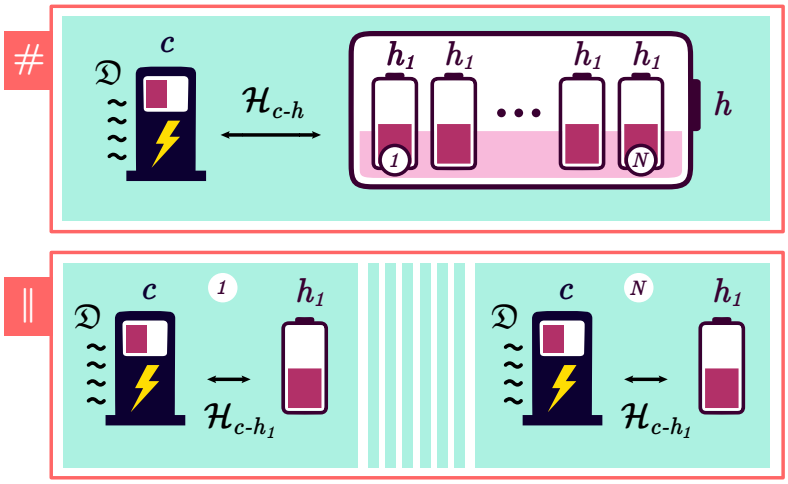


Figure 2.4: Collective (#) and parallel (‖) versions of a QB of size $N$. The collective QB has one charger "$c$" with $E_c$ initial energy and one holder "$h$" consisting in $N$ units cells "$h_1$". The parallel QB has $N$ copies of "$c$" with $E_h/N$ initial energy, each interacting with a different unit cell "$h_1$" as holder. Hence, the ‖ QB is just $N$ copies of the $N$-times down-scaled # QB.

If the holder of a QB consists in $N$ copies of a subsystem, i.e. $N$ holder unit cells, we can compare its performance versus $N$ copies of the QB with only one holder unit cell. These represent two versions of a QB that have the same maximum storable energy. The former is the **collective version** (#) as it has $N$ holder unit cells interacting with the same charger, while the latter is the **parallel version** (‖) as it has $N$ independent copies of one charger with one holder unit cell (see Fig. 2.4).

## 2.4 Dynamical Figures of merit

In this thesis, the most relevant dynamical quantities for a charger-based QB are selected and identified as its **dynamical figures of merit**, $f$. These are defined in such a way that,

the larger is $f$, the better the QB performance in that regard. Therefore, ideally all figures of merit $f$ would be as large as possible in a QB.

How much energy can be transferred and stored into the holder is clearly a very relevant quantity for the QB, to be maximized if possible. The transfer of energy from charger to holder, or viceversa, takes some time $\tau$ to be ideally minimized. Depending on the application of the QB, the power during the charging and discharging stages is more relevant than the transferred energy, and it is also to be maximized if possible. Finally, if the charger-based QB is to be discharged in transducing mode, i.e. by an external classical field directly acting on the holder, the maximum amount of extractable energy through unitary operations (ergotropy [52]) is more relevant than the amount of stored energy in the holder.

Thus, the following are defined as dynamical figures of merit:

- Charger (holder) energy, $E_{c(h)}$.
- Charger (holder) transfer rates, $\Omega_{c(h)} \equiv 2\pi/\tau$.
- Charger (holder) power, $P_{c(h)} = E_{c(h)}\Omega_{c(h)}$.
- Holder ergotropy, $\mathcal{E}_h$.

**Ergotropy**

The ergotropy is the maximum amount of extractable energy through unitary operations, for a given quantum state. Hence, it is given by [1]

$$\mathcal{E}[\rho] \equiv \mathrm{tr}(\rho\mathcal{H}) - \min_{\mathcal{U}\in\mathscr{U}}\{\mathrm{tr}\big(\mathcal{U}\rho\mathcal{U}^\dagger\mathcal{H}\big)\}, \tag{2.5}$$

where $\rho$ is the state of the system just before applying the unitary operation, $\mathcal{H}$ is the free Hamiltonian of the system, and $\mathscr{U}$ is the space of allowed unitary operators $\mathcal{U}$.

If $\mathcal{H}$ is non-degenerate, a simple formula for computing $\mathcal{E}$ can be obtained. Indeed, the state $\rho$ and (non-degenerate) Hamiltonian $\mathcal{H}$ of a system can be written orderly as

$$\rho = \sum_k r_k \left|r_k\right\rangle\!\left\langle r_k\right|, \ r_k \geq r_{k+1}, \tag{2.6}$$

$$\mathcal{H} = \sum_k \varepsilon_k \left|\varepsilon_k\right\rangle\!\left\langle \varepsilon_k\right|, \ \varepsilon_k < \varepsilon_{k+1}, \tag{2.7}$$

where $r_k, \varepsilon_k$ are the eigenvalues and $\left|r_k\right\rangle, \left|\varepsilon_k\right\rangle$ the eigenkets of the state and Hamiltonian, respectively. Then the ergotropy of $\rho$ can be calculated by [52]

$$\mathcal{E}[\rho] = \sum_{jk} r_j\varepsilon_k(\left|\langle r_j|\varepsilon_k\rangle\right|^2 - \delta_{jk}), \tag{2.8}$$

where $\delta_{jk}$ is the Kronecker delta.

## 2.5 Quantum advantage

In holder-only QBs, parallel and collective versions are also defined, but in this case, as there is no charger, they differ in if the holder units cells interact (collective version) or not (parallel version) with each other [1].

This type of QB allows different procedures for charging up the holder, represented by different drivings $V(t)$ in equation (2.1). In order to fairly compare different procedures, an energy constrain is needed. A possible constrain is $\|\mathcal{H}_h\|_{\text{op}} = E_{\max}$ for a given maximum energy $E_{\max} > 0$, where $\|\mathcal{H}_h\|_{\text{op}}$ equals the largest eigenvalue of $\mathcal{H}_h$. Under this constrain, a maximum amount of charging power, $P_{\text{op}}^{\parallel *}$, is obtained for the parallel version of the QB. This maximum is the solution to the power optimization problem over all possible drivings. The "*" symbol is used on $P$ to remember that the constrain $\|\mathcal{H}_h\|_{\text{op}} = E_{\max}$ has been set.

In order to compare a specific procedure (whether in collective or parallel version) with the optimal parallel procedure, and determine which charges up the holder faster, a ratio called **quantum advantage** is defined by [1]

$$\frac{P^*}{P_{\text{op}}^{\parallel *}} = \frac{1/\tau^*}{1/\tau^{\parallel *}}, \tag{2.9}$$

where $P^*$ is the power of the procedure in study, and the equality holds due to the chosen constrain, meaning that both procedures charge up the holder in the same amount of energy.

This concept of quantum advantage is, ideally, to be extended to open holder-only QBs, where the holder suffers from dissipation, but the optimization problem becomes harder. Furthermore, it would be ideal to extend this concept to open charger-based QBs, in which only charger dissipation is relevant during the charging stage, but again the optimization problem becomes too complex to be practical in most scenarios. Hence, inspired by the quantum advantage, a new figure of merit is defined for charger-based QBs in the next section.

## 2.6 Collective enhancement

When the parallel and collective versions of an isolated charger-based QB are compared, the latter shows an increase in the transfer rate due to correlations [12–15]. This motivates the definition of the transfer rate collective enhancement (similar to the quantum advantage of equation (2.9)) $\Gamma_{1/\bar{\tau}} = (1/\bar{\tau}^{\#})/(1/\bar{\tau}^{\parallel}) \equiv \bar{\Omega}^{\#}/\bar{\Omega}^{\parallel}$ where $\bar{\tau}^{\#}$ and $\bar{\tau}^{\parallel}$ are the interaction times ($\tau$) needed to charge or discharge the QB up to its first dynamical maximum in the collective and parallel versions, respectively. $\Gamma_{1/\bar{\tau}}$ quantifies how much larger is the transfer rate $\bar{\Omega} \equiv 2\pi/\bar{\tau}$ for the collective version compared to parallel one. If $\Gamma_{1/\bar{\tau}} > 1$, the collective QB has a larger transfer rate than the parallel QB, meaning that $\bar{\Omega}$ is enhanced in the collective version of the QB.

This thesis extends the previous concept to all interesting dynamical figures of merit $f$ of a QB that quantify its performance (larger $f$, better battery), by defining novel figures of

merit: the **collective enhancements**

$$\Gamma_{\bar{f}} \equiv \frac{\bar{f}^{\#}}{\bar{f}^{\|}}. \tag{2.10}$$

If $\Gamma_{\bar{f}} > 1$, $f$ is enhanced in the collective version. Therefore, $\Gamma_{\bar{f}}$ is identified as a very important quantity, a new figure of merit, of charger-based QBs in their collective version.

For isolated QBs, $\Gamma_{1/\bar{\tau}} > 1$ and $\Gamma_{\bar{E}_h} < 1$, where the bar represents the event of first maximum transferred energy into the holder during the charging stage. In this thesis, it is shown that the former inequality also holds for non-isolated QBs, while the latter changes in the simulated systems.

## 2.7 Tavis-Cummings quantum batteries

This thesis focuses on a QB model in which the charger is a single electromagnetic field mode in a resonator coupled to an array of $N$ non-mutually interacting identical spin qubits that act as the holder [9]. Under the rotating wave approximation, the microscopic Hamiltonian is that of the Tavis-Cummings model given by equation (1.79) for the driven QB case, and given by equation (1.76) if the QB is charged by a prepared initial condition of charger. Focusing on the latter, the QB hamiltonian $\mathcal{H}_\lambda$ is constituted by: $\mathcal{H}_c = \hbar\omega_c a^\dagger a, \mathcal{H}_h = \hbar\omega_h \sum_{i=1}^{N} \sigma_i^+ \sigma_i^-, \mathcal{H}_{c-h} = \hbar g \sum_{i=1}^{N} (a\sigma_i^+ + a^\dagger \sigma_i^-)$, where $a$ ($a^\dagger$) is a bosonic annihilation (creation) operator, $\sigma_i^\pm$ are raising ($+$) or lowering ($-$) spin operators for the $i$-th qubit, $\omega_{c,h}$ are the characteristic frequencies of the resonator and the qubits, respectively, and $g$ is the coupling strength. The charger dissipator is given by equation (1.81), $\mathfrak{D}_c[\cdot] = \kappa(n_{\text{th}} + 1)(2a \cdot a^\dagger - a^\dagger a \cdot - \cdot a^\dagger a) + \kappa n_{\text{th}}(2a^\dagger \cdot a - aa^\dagger \cdot - \cdot aa^\dagger)$, where $2\kappa$ is the charger dissipation rate at zero temperature. This type of QB is called **Tavis-Cummings quantum battery**.

In this physical system, transitioning between battery stages means to change between negligible ($\lambda = 0$) and non-negligible ($\lambda = 1$) holder-charger interaction, which can be achieved by external fields that modify $\omega_{c,h}$ to transition between far-from-resonant ($\lambda = 0$) and resonant ($\lambda = 1$) dynamics. Hence, $\omega_c = \omega_h$ during charging and normal discharging stages.

Simulations of the Tavis-Cummings QB have been performed for this thesis using $g = 10^{-3}\omega_c$ to be consistent with the rotating wave approximation. Also, $n_{\text{th}} = 0$ is used in order to study solely the dissipation from the charger avoiding the re-population effects of a nonzero temperature. The cases of driven charging and $n_{\text{th}} > 0$ are beyond the scope of this thesis and they are left as future work.

## 2.8 Dissipation

Up to now, research efforts have been mostly focused on understanding QBs as closed systems, isolated from the environment. The dissipation of real QBs has only recently been considered [22–28].

In [22], DC charger-based QBs were studied in 3 simple systems: qubit-qubit interaction, electromagnetic single mode cavity-cavity interaction, and the Jaynes-Cummings model; considering dissipation at very low temperatures. Hence, there is energy flow from the driving (coherent channel of energy) and, if $T \neq 0$, from the thermal bath (incoherent channel of energy) into the QB. The interplay between both was analyzed, concluding differently depending on the system. In the *thermal protocol* ($F_d = 0$ and $T > 0$), the ergotropy was shown to be always zero in the three systems, while in the *mixed regime* ($F_d > 0$ and $T > 0$) for the particular case of the Jaynes-Cummings model, the time at which energy and ergotropy are maximal was shown to decrease monotonically with the driving field $F_d$.

In [23], a special protocol to extract work from a holder-only QB in a (Gibbs) thermal state was designed. To do so, the protocol requires and engineered thermal bath made out of copies of the QB system, which allows the QB to reach an *active equilibrium Gibbs state*, instead of a passive one, which in short, means that it has non-zero ergotropy, allowing work extraction.

In [24], the *aging* of DC Tavis-Cummings QBs was studied, analyzing their performance after many cycles of charging and discharging while considering the individual decays of the spin qubits as dissipation (dissipator $\mathfrak{D}_{q2}$ of equation (1.80), but incomplete as no *dephasing* dissipator is included). It was concluded that, because of the slow, individual decay processes during energy storage, the battery "ages" and can store less energy in subsequent charging processes, although a limit-cycle charging capacity is reached, depending on the duration of the storage and discharging intervals.

In [25], a novel holder-only QB is proposed, build as a special open quantum network with a symmetry that topologically prevents energy loss during the storage stage.

In [26], the dissipative dynamics of a holder-only QB made out of a single qubit was studied. Decoherence and pure dephasing mechanisms were considered by separate as the dissipator, showing better performance in the former case as a higher amount of energy can be charged up, which is also more stable during the storage stage.

In [27], optimal quantum control theory and quantum thermodynamics are combined to build a protocol that corrects decoherence during the storage stage of a QB. The protocol consists in nonselective, frequent, projective measurements that keep the open QB in its highest ergotropy state.

In [28], a holder-only QB is charged and discharged via interactions with local bosonic reservoirs, while Markovian or non-Markovian dephasing noises are also considered. Counter to intuition, some results showed that the dephasing noise helped to obtain better battery performances in ergotropy and transfer rate, specially for the non-Markovian case.

All previously listed studies attempt to help towards answering the question of how harming dissipation is for the performance of a QB. But, as the difficult task it is, each study tackles a different aspect, usually studying specific cases. Contributing to this task, the work of this thesis extends the study previously done in [9] and [4] for closed charger-based QBs, by incorporating charger dissipation. Most importantly, in [9], an advantage in charging power when comparing the collective and parallel versions of a Tavis-Cummings QB is reported. In this

thesis, the main question to answer is if this advantage still holds, or not, under dissipation, while also studying other figures of merit. Hence, the work of the current thesis means a step forward in understanding collective enhancements in the presence of dissipation, which is crucial to experimentally realize QBs. This is achieved by performing lengthy simulations with QuTiP [53], a Python library for simulation of quantum systems, whose results are shown and analyzed in chapter 3.

## 2.9 Feasibility of experimental realizations

There are many experimentally feasible many-body systems in circuit and cavity QED [31–34], described by the Tavis-Cummings model. Nonetheless, the charger-based QBs described require additional restrictions to properly work with the formalism explained. Firstly, there must be a mechanism to easily transition from resonant to far-from-resonance dynamics, and viceversa, on the same qubits-resonator system. Secondly, these transitions must be performed quickly enough to allow the study of each battery stage separately with time-independent Hamiltonians. Finally, for the QB to be useful, the dissipation rate of the resonator must be much larger than the one of the qubits. The latter condition is usually fulfilled, as the qubits used often correspond to matter qubits, with natural dissipation rates much larger than photon systems. The other two conditions, though, must be studied with further detail.

### 2.9.1 Condition of fast enough stage switching

The time $\tau_Y$ in which the switching between battery stages must be performed should be much smaller than the charging time $\tau_c$, i.e.

$$\tau_Y \ll \tau_c, \tag{2.11}$$

which is in general very hard to achieve.

In more detail, the change in *detuning* (difference between resonator and qubit frequencies) must be $\delta = 0 \longrightarrow\sim 10g$ to fulfill the condition of far-from-resonance, $\delta \gg g$. The factor of 10 is justified numerically with simulations not shown here, in which a detuning of $\delta = 10g$ was enough far of resonant to be able to neglect the qubit-resonator interaction. In order to achieve such change, the external control field $Y$ (the one that determines $\delta$, as for example, a magnetic field $B_z^{\text{stat}}$ in the case of $NV^-$) must be changed in $\Delta Y = 0 \longrightarrow 10g/\gamma_Y$, where $\gamma_Y$ is named in this thesis as the *gyro-field* factor (an attempt to generalize the concept of the gyromagnetic factor). Moreover, from [9] and the simulations to be shown in chapter 3, the charging time can be approximated by[1]

$$\tau_c \sim \frac{\tau_c|_{N=1}}{\sqrt{N}} \leq \tau_c|_{N=1} \approx \frac{2\pi}{4g}, \tag{2.12}$$

[1]Depending on the initial conditions, this will be a better or worse approximation.

where $\tau_c|_{N=1}$ is the charging time of the case with 1 qubit. Therefore, the condition (2.11) is recast

$$\tau_Y \ll \frac{2\pi}{4g\sqrt{N}}. \tag{2.13}$$

Then, setting a realizable rate of change $R_{\Delta Y} \equiv \Delta Y/\tau_Y$ of the control field, a condition for $g$ is obtained,

$$\frac{40}{\gamma_Y R_{\Delta Y}} \left(\frac{g}{2\pi}\right)^2 \ll \frac{1}{\sqrt{N}}, \tag{2.14}$$

which sets an unwanted upper bound for $g$. It is undesired for the QB because lower $g$ means slower *Rabi-like* oscillations [40, 43], and therefore, slower battery charging and discharging. Also, smaller values of $g$ means that more detailed energy-level structures of the system approximated as a qubit must be taken into consideration to actually realize a qubit, which might become a huge problem. For example, the hyperfine structure of the $NV^-$ might not be possible to neglect, as was done at the end of chapter 1. Therefore, the upper bound set by (2.14) should, ideally, be the highest possible, which is achieved with large values of $\gamma_Y$ and $R_{\Delta Y}$.

## 2.10 Using NV centers for quantum batteries

The NV centers in diamond and Rydberg atoms have large decoherence times even at room temperature [10, 11, 45–47, 50, 51, 54]. Instead, other possible implementations, as superconducting qubits, require very low cryogenic temperatures and have even smaller decoherence times. Therefore, to overpass the limitation of temperature, Rydberg atoms might be the answer for a proof of concept, although it would be hard to accomplish a technologically practical QB with at least $\sim 10^4$ of them. Hence, the candidate of NV centers is to be analyzed here, since they can come in large numbers in diamond samples [10].

For NV spin qubits, $Y$ can be a magnetic field $B_z^{\text{stat}}$ that changes the qubit frequency via Zeeman effect, as explained in chapter 1. Recalling the value of the NV gyromagnetic ratio $\gamma_e$ (see Table 1.3), the gyro-field factor in this case is $\gamma_B = \gamma_e = 2.8$ MHz/G. Finally, a realistic possible change of magnetic field is of around 100 G in 300 $\mu$s, corresponding to $R_{\Delta B} \approx 0.3$ G/$\mu$s. Then the condition (2.14) is fulfilled, for $N = 1, ..., 10^4$, if

$$\frac{g}{2\pi} \leq \frac{g_{\max}}{2\pi} \sim 1 \text{ kHz}, \tag{2.15}$$

where 1 order of magnitude of difference has been considered sufficient for the "$\ll$" inequality (2.14) to hold. Unfortunately, these values of $g$ are so small that not even the hyperfine structure of the NV center is enough to correctly define a qubit, making it a too hard to realize alternative for a charger-based QB, at least with current technology than only permits $R_{\Delta B} \approx 0.3$. Larger values of $R_{\Delta B} \approx 0.3$ in some future might allow to rethink the use of NV centers for this application.

Nonetheless, the long longitudinal relaxation time of the $NV^-$, plus the ability to have hundreds of them together, all at room temperature, makes it a good candidate to realize other

type of QBs not explained in this thesis, since they are more recent and focus on maximizing ergotropy, rather than the charging power. These are the **stable adiabatic quantum batteries** (SA-QBs), which have been recently studied by [5, 6, 21], and it is an approach in which the evolution doesn't rely on being fully coherent. Therefore, encouragement toward studying how to implement SA-QBs with NV centers, is recommended as a conclusion of this analysis.

# Chapter 3

# Collective enhancement in dissipative Tavis-Cummings quantum batteries

## 3.1 Main simulation results

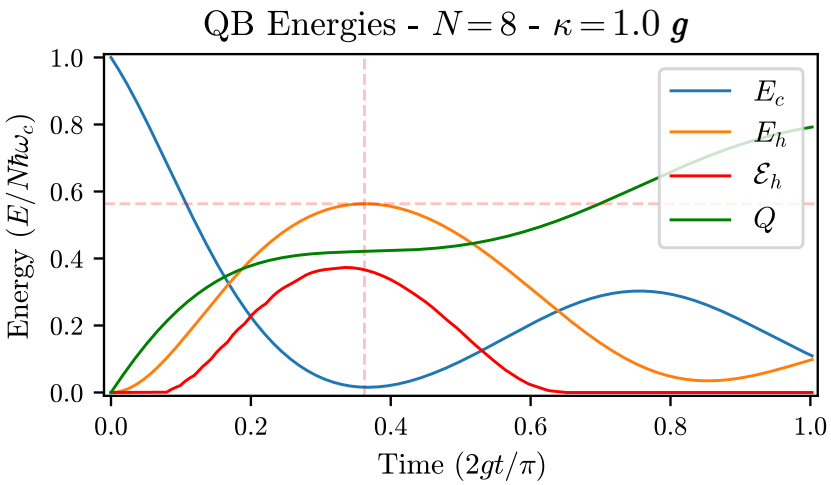


Figure 3.1: Mean energy $E_h$ and ergotropy $\mathcal{E}_h$ charged on the holder (array of $N$ qubits) when charging from an initial Fock light state. The mean energy $E_c$ of the charger (resonator) and heat $Q$ from the QB are also shown. The dynamics seen correspond to *Rabi-like* oscillations, transferring energy from the charger to the holder. The holder oscillations for different $N$ and $\kappa$ are given in the next section. The segmented red lines are crossing at the first maximum of $E_h$, defining the time at which all performances are analyzed.

The matter of study in this chapter is the robustness of the collective enhancements when dissipation is taken into account in the Tavis-Cummings QB. Three cases are studied: Fock, coherent, and thermal states as initial condition of the resonator. All three with mean number of photons $\mathrm{Tr}\{a^\dagger a\,\mathrm{Tr}_h\{\rho(0)\}\} = N$. In all cases, the qubits are initially in their ground state. The figures of merit analyzed are the holder (charger) energy $E_{h(c)}$, transfer rate $\Omega_{h(c)} \equiv 2\pi/\tau_{h(c)}$, power $P_{h(c)} \equiv E_{h(c)}/\tau_{h(c)}$, and ergotropy $\mathcal{E}_{h(c)}$ during the charging stage.

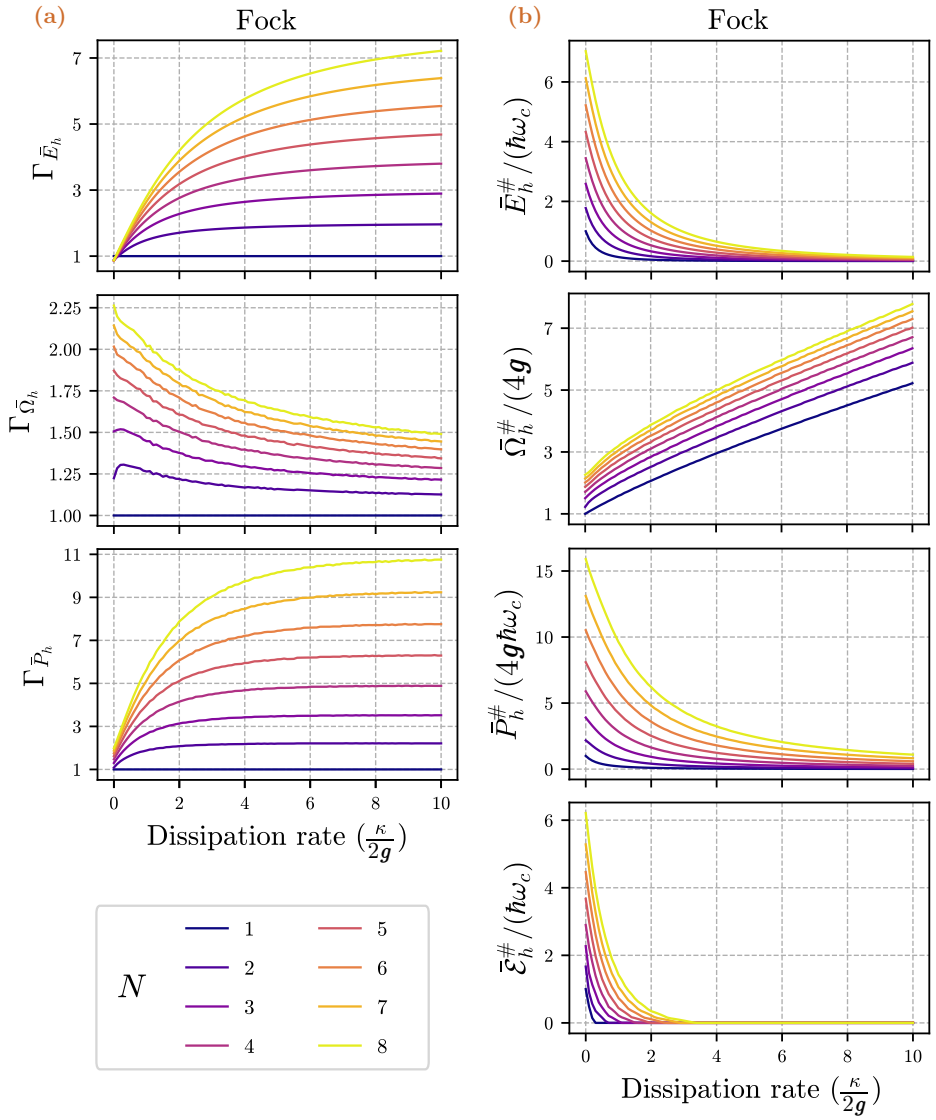


Figure 3.2: Collective (a) enhancements $\Gamma_{\bar{f}}$ and (b) performances for the first maximum charge when charging from Fock initial conditions for energy, transfer rate, power, and ergotropy. The results for coherent and thermal initial conditions are given in the next section.

Figure 3.1 depicts these energies and the heat from the QB, $Q(t) \equiv -\int_0^t \mathrm{Tr}\{\mathcal{H}(t')\mathfrak{D}[\rho(t')]\}\mathrm{d}t'$, over time. Frequencies are shown in terms of the Rabi frequency of the Fock case when $N = 1$ and $\kappa = 0$, given by $\Omega_R \equiv 2g$. Figure 3.2 shows the collective enhancements $\Gamma_{\bar{f}}$ and performances $\bar{f}$ for the Fock case for different values of $\kappa$ and $N$. The other two cases produce very similar results and are hence included in the next section. Nonetheless, the key differences between them are visualized in Figure 3.3 for the respective collective and parallel QBs.

Naturally, larger dissipation rates produce faster loss of energy available to charge up the holder resulting in a decrease of $\bar{E}_h^{\#}$ as well as $\bar{\mathcal{E}}_h^{\#}$ (see Figure 3.2). On the other hand, larger $\kappa$ also means that the first maximum transferred energy into the holder, although smaller, is reached sooner, and therefore the transfer rate performance increases (see Figure 3.2). Hence, as the decrease of $\bar{E}_h^{\#}$ shows to be higher than the increase of $\bar{\Omega}_h^{\#}$, the charging power $\bar{P}_h^{\#}$ ends

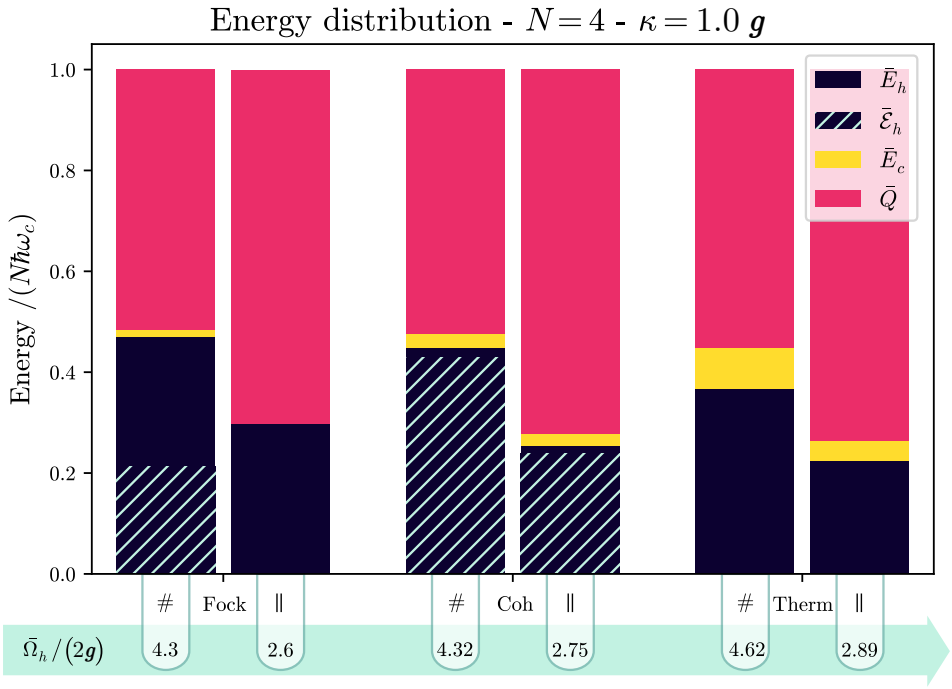


Figure 3.3: Distribution of the total energy over the QB. Collective (#) and parallel (||) are compared for the three cases of initial conditions simulated.

up decreasing. These results are plotted for different $N$ in Figure 3.2.b, which shows that the curves move upwards when $N$ increases, meaning that a reduction in performance due to dissipation may be restored by scaling up the QB. For $\kappa = 0$ this behavior was obtained in [9], and our results for $\kappa > 0$ can here be thought as an extrapolation of those results. Although, caution must be taken with the statement about restoring the performance, because the separation between curves of consecutive values of $N$ seems to get smaller in each increment for a fixed $\kappa$, and even more as $\kappa$ is also increased. However, for values of $\kappa$ around $4g$ or smaller, it is argued that there is no need to fabricate a resonator with the highest possible quality factor as long as there is compensation by scaling up the QB. This can be of practical advantage for realizing a QB with systems where adding more qubits and photonic energy is feasible, as in the case of NV centers, which come as natural defects in diamond crystals [10].

The increase of the performances with $N$ is explained (for $\kappa = 0$) by the collective behavior of the qubits producing a larger effective Rabi frequency, allowing for a faster population of the excited eigenenergies, as discussed from equations (1.76) and (1.77) in chapter 1. This upgrade of the performances is better quantified as collective enhancement in Figure 3.2.a, where it is clear that the collective QB version is better than the parallel one ($\Gamma_{\bar{f}} > 1$), except for the energies at $\kappa \approx 0$ where $\Gamma_{\bar{E}_h} \leq 1$. This exception is important because it shows that a simple extrapolation of the collective enhancement in energy obtained at $\kappa = 0$ would give the wrong result as if the parallel battery was to perform better. Moreover, it is observed that collective enhancements in energy and power increase for larger dissipation rates, which means that despite of the decrease of the respective performances in both QB versions, the collective one decreases less, i.e. it is more robust under dissipation. Instead, the collective enhancement in charging transfer rate decreases with larger $\kappa$, meaning that the parallel QB is more robust in this regard.

Regarding the ergotropy, its collective enhancement is not shown as the numerator and denominator become (non-simultaneously) exactly zero very often. Except for values of $\kappa \sim 0$, it is obtained $\Gamma_{\bar{\mathcal{E}}} > 1$, meaning that for transducing QBs more energy is available in the collective version. This information is shown in Figure 3.3, specially clear for the Fock case. Figure 3.3 shows the energy distributed in its different available forms, and from here it is concluded that the coherent case is the best. This happens because the coherent case is much more robust than the Fock one against dissipation. Only for $\kappa \approx 0$ and $N \approx 1$ the Fock case is better as seen in the next section. For $\kappa = 0$ and large enough $N$, the coherent case is better because when the initial condition is a coherent state, the amount of energy locked in the charger-holder correlations is minimized as studied in [4].

## 3.2 Comparison between initial conditions

The main differences between the three cases of initial conditions simulated are represented in Figure 3.3. Nonetheless, further details are analyzed in this section. The coherent and thermal cases have been simulated up to $N = 4$ and $N = 6$, respectively, due to the rapid increment in numerical complexity (see appendix F for the specifics). The performances of the dynamical figures of merit (energy, transfer rate, power, and ergotropy) are presented in Figure 3.4. The collective enhancements are presented in Figure 3.5. Simulation results complementary to Figure 3.1 are shown in Figs. 3.6-3.8, showing the Rabi-like oscillations up to near the first energy maximum, for $N = 1, ..., 4$ and $\kappa \in [0, 2\Omega_R]$.

The performances of Figure 3.4 are very similar if we compare them with each other by fixing the dynamical figure of merit and changing the charger initial condition. The most noticeable difference is for $\bar{\Omega}_h^{\#}$, which shows a change of curvature between $\kappa \approx 0$ and $\kappa \approx 0.5$ in the coherent and thermal cases, as opposed to the Fock case. This occurs because, as can be seen in Figure 3.6 by following the dots, the first energy maximum does not move monotonically to the left with the increase of $\kappa$. Additionally, from Figure 3.4, it is noticed that $\bar{\Omega}_h^{\#}$ and $\bar{Q}^{\#}$ are the only quantities whose curves for different $N$ do not quickly converge as $\kappa$ increases. Instead, the curves tend to spread more. In particular, this means that the transfer rate performance increases faster for collective QBs with larger $N$, i.e. $\left.\frac{\partial \bar{\Omega}_h^{\#}}{\partial \kappa}\right|_{N_1} \gtrsim \left.\frac{\partial \bar{\Omega}_h^{\#}}{\partial \kappa}\right|_{N_2}, \forall N_1 > N_2$, where $N_{1,2}$ are values of $N$ from the simulations. This conclusion may appear contradictory with the plots of $\Gamma_{\bar{\Omega}_h}$ in Figure 3.5 showing a decrease as $\kappa$ increases. Nonetheless, this is not the case, because $\frac{\partial \Gamma_{\bar{\Omega}_h}}{\partial \kappa} < 0$ is equivalent to

$$\frac{\frac{\partial \bar{\Omega}_h^{\#}}{\partial \kappa}}{\frac{\partial \bar{\Omega}_h^{\parallel}}{\partial \kappa}} < \frac{\bar{\Omega}_h^{\#}}{\bar{\Omega}_h^{\parallel}} \equiv \Gamma_{\bar{\Omega}_h}. \tag{3.1}$$

Hence, $\frac{\partial \bar{\Omega}_h^{\#}}{\partial \kappa} \gtrsim \frac{\partial \bar{\Omega}_h^{\parallel}}{\partial \kappa}$ is allowed as long as $\Gamma_{\bar{\Omega}_h} \gtrsim 1$, which is always the case in the results.

The collective enhancements of Figure 3.5 are also very similar if we compare them with each other by fixing the figure of merit and changing the charger initial condition, excepting the ergotropy, because of the appearance of zeros in the denominator in the Fock and thermal cases, resulting in non-plotted data. Hence, the ergotropy is better analyzed with Figure

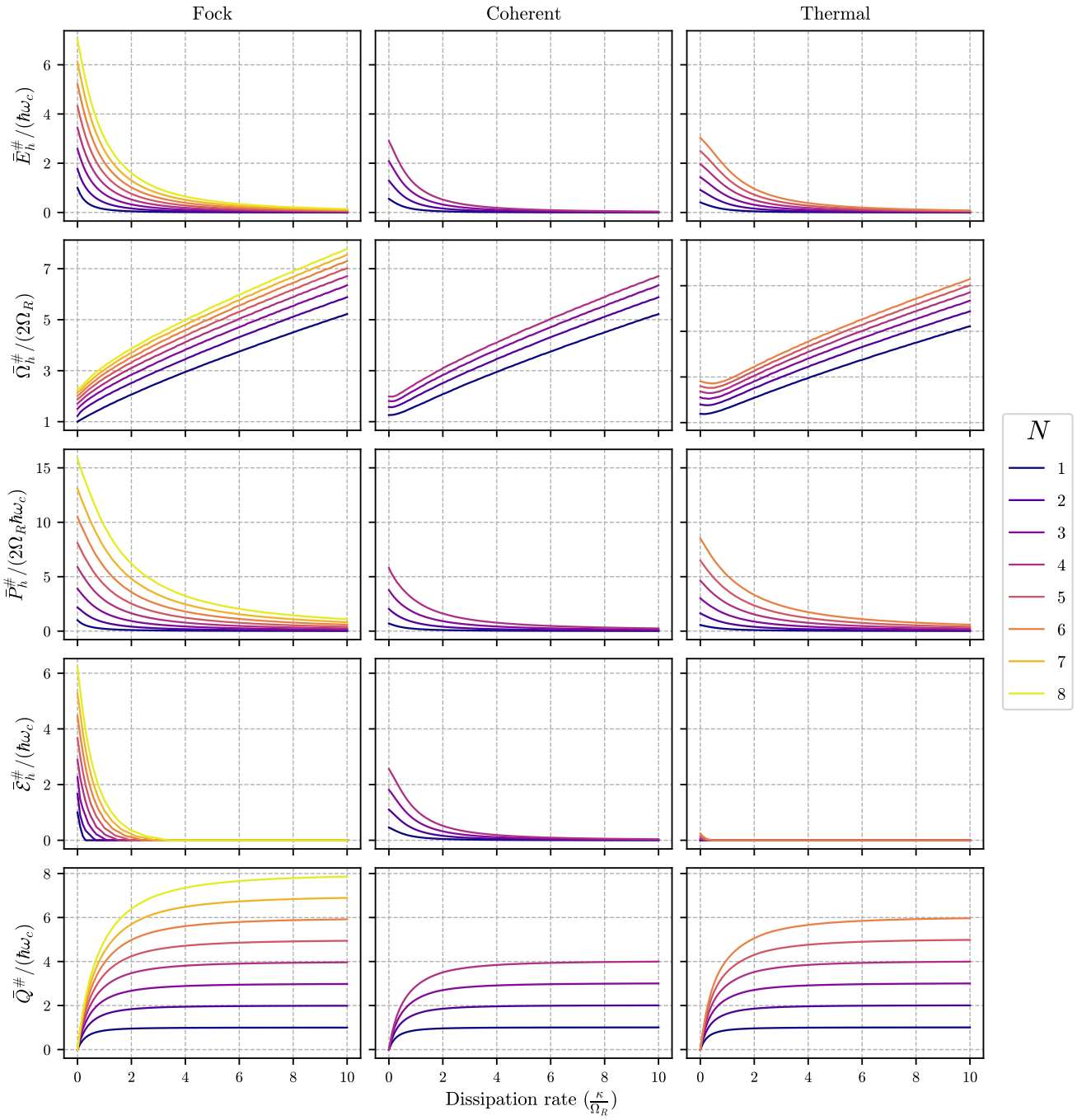


Figure 3.4: Performances of the collective QB for Fock, coherent and thermal states as the charger initial condition. Comparing between these cases of initial condition, there is no significant meaningful difference.

3.7, which clearly shows that the coherent case is the more robust against dissipation, and explains the ergotropy shown in Figure 3.3.

In Figures 3.6, 3.7, and 3.8 the dots mark the value of the quantity studied for the analysis of performances and collective enhancements, i.e. evaluation of the curves at the time of first

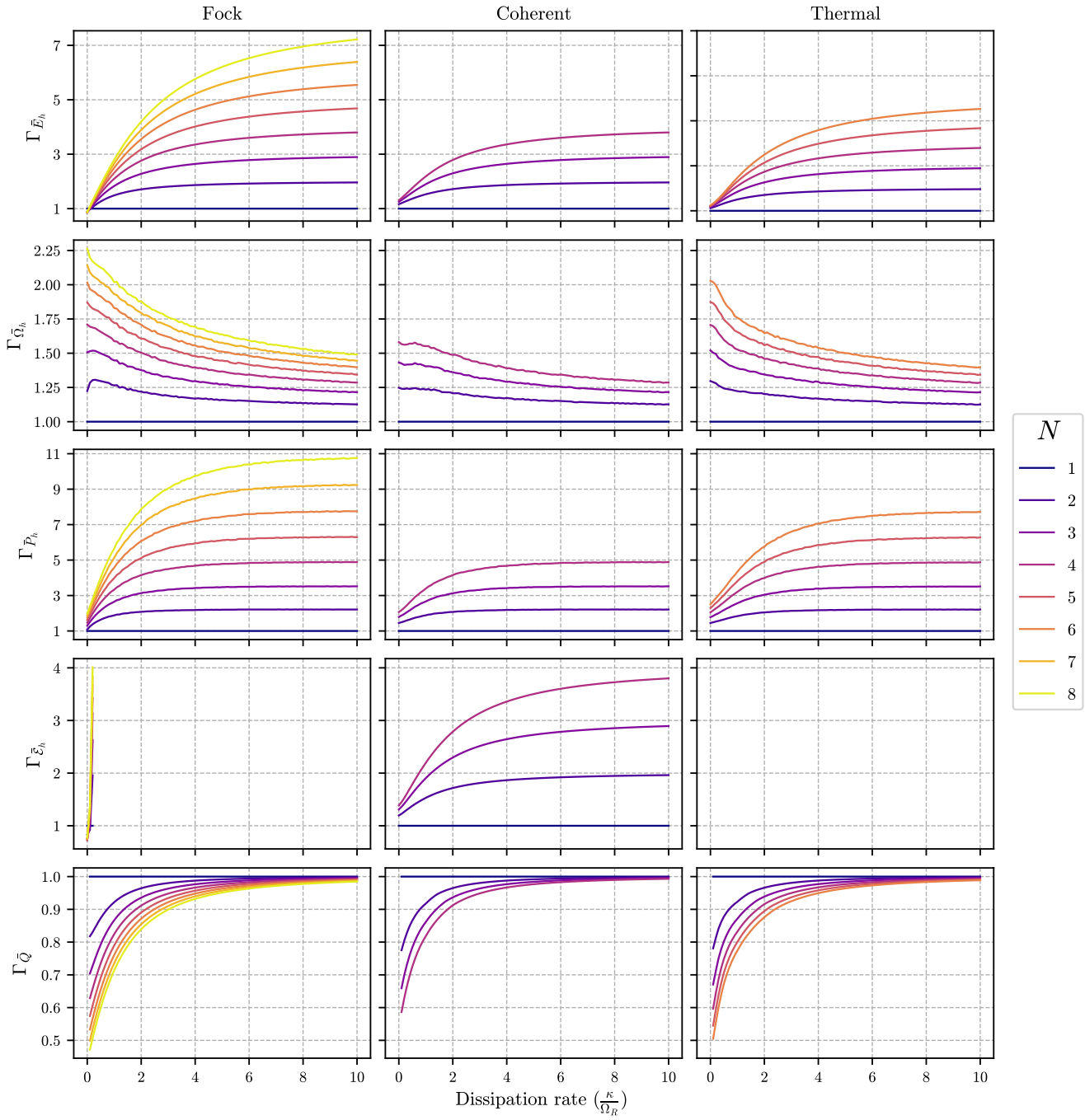


Figure 3.5: Collective enhancements of the relevant figures of merit for Fock, coherent and thermal states as the charger initial condition. Comparing between these cases of initial condition, there is no significant meaningful difference, excepting the ergotropy.

maximum of holder energy. Hence, by tracking the dots it is noticeable that, in general, the maximum of holder energy does not correspond to the maximum of holder ergotropy, nor to the maximum of total excited population $\sum_i p_h^{|e_i\rangle}$. For the latter, this happens because not every eigenstate ponderates the same eigenenergy in the collective quantum system of $N$ qubits. Hence, the energy and population maximums would only coincide if at the time of

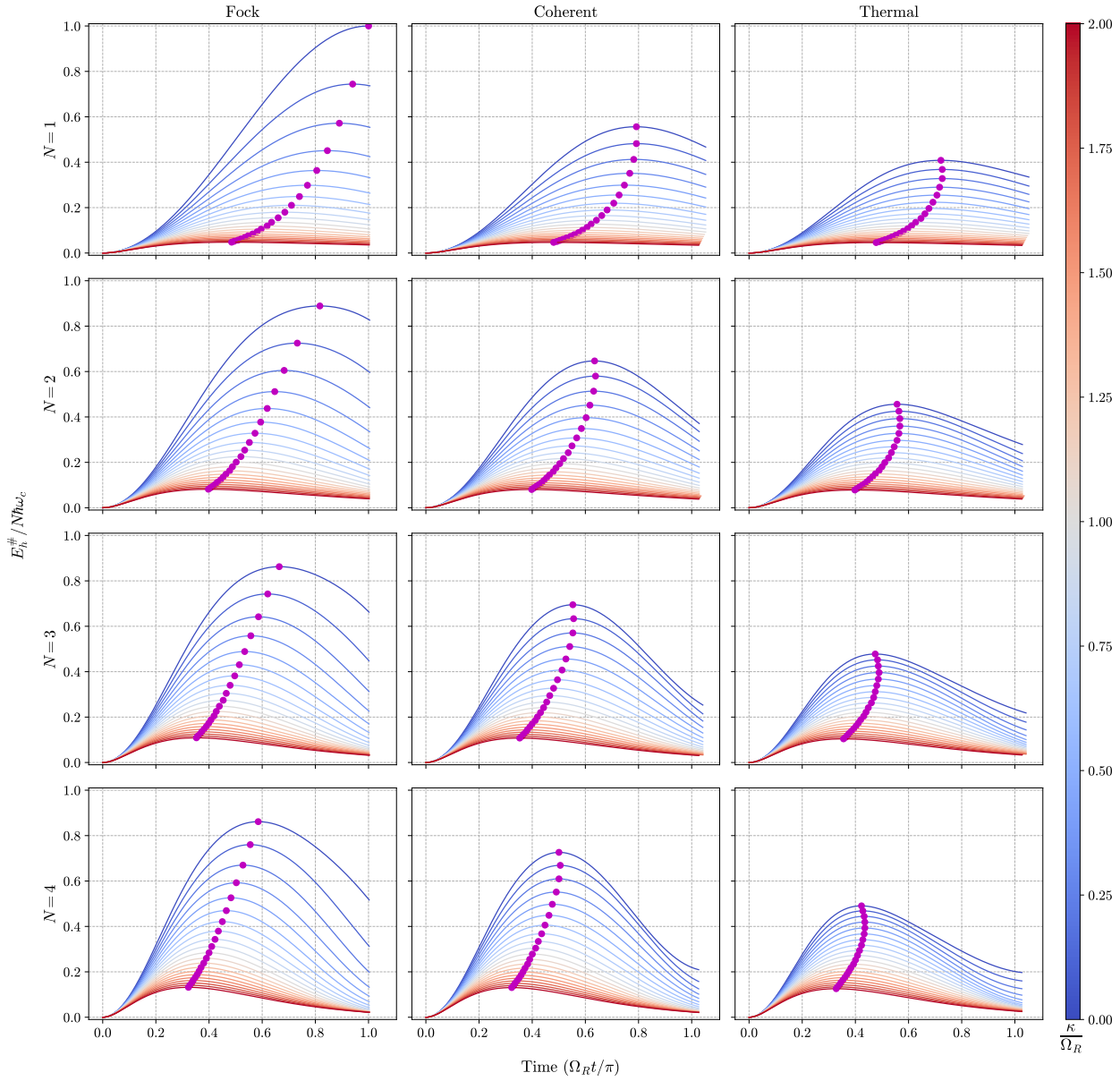


Figure 3.6: Holder energy over time up to near the first maximum for Fock, coherent and thermal states as the charger initial condition. Results of the collective QB version. It it observed that the Fock case reaches a higher first maximum of holder energy $E_h$ than the coherent and thermal cases. Nonetheless, these maximums are obtained in a shorter time in the thermal case. Also, as the dissipation rate growths, the three cases tend to the same curve. The magenta dots show the values used for the performances and collective enhancements.

maximum population, the excited eigenstates correspond to the ones with largest eigenenergies.

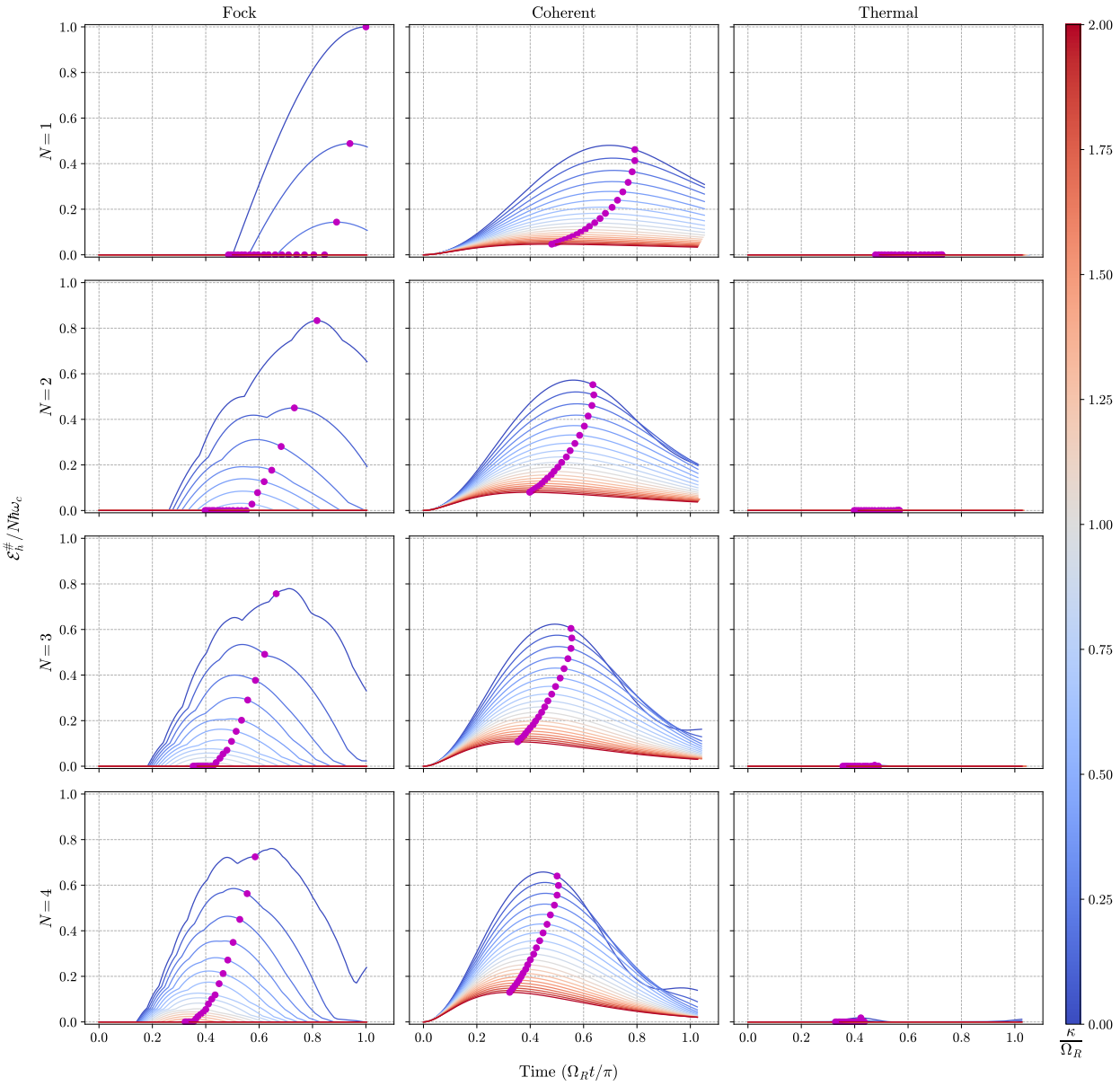


Figure 3.7: Holder ergotropy over time up to near the first holder energy maximum for Fock, coherent and thermal states as the charger initial condition. Results of the collective QB version. The Fock case shows the highest ergotropy for $\kappa \approx 0$, but it rapidly goes to zero as $\kappa$ increases. Instead, the coherent case changes less, which means that its ergotropy performance is more robust under dissipation. The magenta dots show the values used for the performances and collective enhancements.

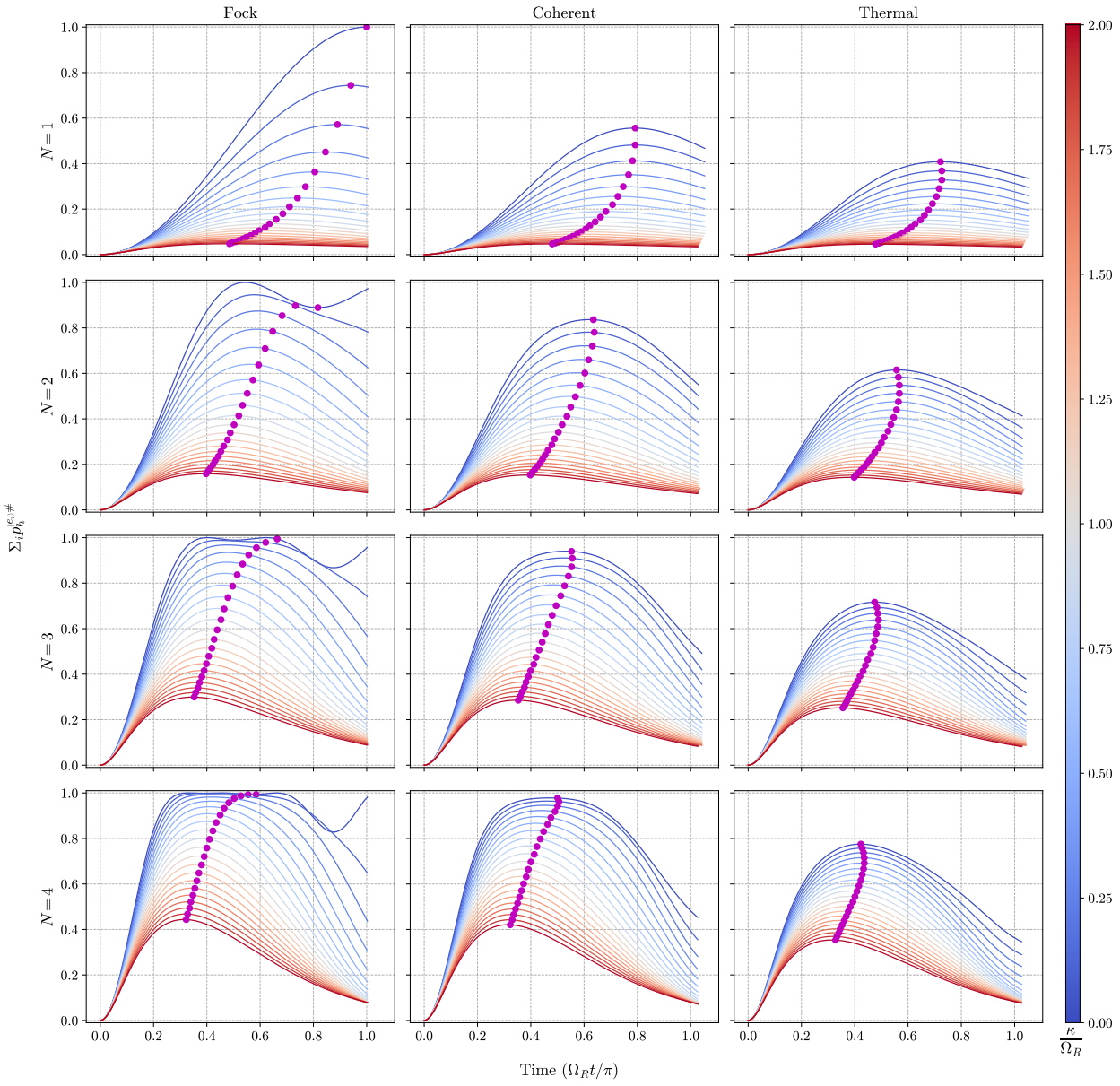


Figure 3.8: Holder population of the excited states over time up to near the first holder energy maximum for Fock, coherent and thermal states as the charger initial condition. Results of the collective QB version. Plots showing how the holder population can be inverted from the ground state into the excited states. The magenta dots show the values used for the performances and collective enhancements.

# Conclusions

In this thesis different types of open QBs have been defined and a study of their collective behavior under dissipation has been done. Three types of charger initial conditions have been considered. For this study, the collective enhancements have been defined as novel figures of merit for the performance of a collective QB over its parallel version. In particular, the work was focused on the case of a QB made of a photonic resonator and an array of qubits to obtain quantitative estimations.

Throughout this work, it has been observed that dissipation, while diminishing the performance in charging energy and power, the corresponding collective enhancements are instead boosted up, because the collective QB version is more robust against dissipation. Regarding the charging transfer rate, the opposite occurs as the parallel version is more robust in this quantity. In addition, it was shown that, a higher collective performance can be achieved by scaling up the QB, i.e. increasing the number of qubits and photonic energy in the same amount, although due to the decrease in energy performance, this effect is only meaningful for $\kappa \lesssim 4g$. Furthermore, this up-scaling increases all collective enhancements. Also, it was shown that initially preparing the resonator light mode in a coherent state produces better results in ergotropy performance than a Fock or thermal state.

This work shows that collective QBs are better than parallel ones in a different way than simple extrapolation from results of isolated QBs ($\kappa = 0$) as was commented for the energy collective enhancement. It also shows that the dissipation rate $\gamma_{c,0} = 2\kappa$ and the scale $N$ of the QB can be seen as degrees of freedom to design a QB with a desired performance, while understanding that collective QBs are more robust under changes in dissipation. This is particularly useful if increasing $N$ is much easier than decreasing $\gamma_{c,0}$ in the specific system to experimentally realize, or if the precision error in obtaining a specific $\gamma_{c,0}$ is important.

An analysis about the feasibility of building charger-based QBs was also realized. A general experimental restriction of the QB protocol was deduced, and it was concluded that it is not possible to fulfill with current technologies if using NV centers as spin qubits conforming the holder. Nonetheless, its potential for building SA-QBs was recognized and it is proposed as future work.

Finally, the collective enhancements and performances introduced here, along the clarification of different types of QBs, will serve for future studies in the field, considering different batteries and their experimental realizations.

# Appendix A

# Quantum Markovian dynamical maps

The map $\mathcal{E}_{(t,t_0)}$ that describes the desired evolution,

$$\mathcal{E}_{(t,t_0)} : \rho_{\mathrm{S}}(0) \mapsto \mathcal{E}_{(t,t_0)}\rho_{\mathrm{S}}(0) \equiv \rho_{\mathrm{S}}(t), \tag{A.1}$$

is very well known for the case of Markovian dynamics, where

$$\mathcal{E}_{(t_2,t_0)} = \mathcal{E}_{(t_2,t_1)}\mathcal{E}_{(t_1,t_0)}, \forall t_2 > t_1 > t_0 \in \mathbb{R} \tag{A.2}$$

is fulfilled. This corresponds to the restricted case where correlations between S and E are negligible during the whole dynamical evolution of $\rho_{\mathrm{U}}$ [36, 37].

The objective is, then, to obtain the most general dynamical map

$$\mathcal{E}_{(t,t_0)} : \rho_{\mathrm{S}}(0) \mapsto \mathcal{E}_{(t,t_0)}\rho_{\mathrm{S}}(0) \equiv \rho_{\mathrm{S}}(t), \tag{A.3}$$

that maintain the properties of the density operator $\rho_{\mathrm{S}}$ to correctly represent a quantum state. These properties are

1. Trace preservation,
2. Complete positivity,

Hence, the super-operator that transforms the open systems' state at the initial time $t_0 = 0$ to the corresponding one at time $t > 0$, i.e. the map

$$\mathcal{E}_t : \rho(0) \mapsto \mathcal{E}_t\rho(0) \equiv \rho(t), \tag{A.4}$$

is the **completely positive trace-preserving (CPTP) contraction one-parameter semigroup** [37]

$$\mathcal{E}_t = \mathrm{e}^{\mathcal{L}t}. \tag{A.5}$$

*CPTP contraction one-parameter semigroup* means that the one-parameter map $\mathcal{E}_t$ has the properties (if it belongs to a finite-dimensional Banach space):

1. Complete positivity: $\mathcal{E}_t \otimes \mathbb{1}$ is a positive operator.
2. Preserves the trace: $\mathrm{Tr}\{\rho(t)\} = 1, \forall t \geq 0$.
3. It is a one-parameter semigroup: $\mathcal{E}_{t_2}\mathcal{E}_{t_1} = \mathcal{E}_{t_2+t_1}, \forall t_1, t_2 \geq 0$, and $\mathcal{E}_0 = \mathbb{1}$.
4. It is a contraction: $\|\mathcal{E}_t\|_1 \leq 1, \forall t \geq 0$.

In the 4th property, $\|\mathcal{E}_t\|_1 \equiv \sup_{\sigma\in\mathcal{H},\sigma\neq 0}\left\{\frac{\|\mathcal{E}_t\sigma\|_1}{\|\sigma\|_1}\right\}$, with $\|\sigma\|_1 \equiv \mathrm{Tr}\left\{\sqrt{\sigma^\dagger\sigma}\right\} = \mathrm{Tr}\{\sigma\}, \forall\sigma \in \mathcal{H}$, where the second equality holds because $\sigma$ is a quantum state ($\sigma^\dagger = \sigma$, $\sigma \geq 0$ and $\mathrm{Tr}\{\sigma\} = 1$), since it belongs to $\mathcal{H}$.

**Allowed transformations to the Lindblad super-operator**

The generator of Lindblad dynamics, i.e. the Lindblad super-operator $\mathcal{L}$ is invariant under the following transformations [36]:

1. Unitary transformations of the set of collapse operators,

$$\sqrt{\gamma_i}L_i \mapsto \sqrt{\gamma_i'}L_i' = \sum_j u_{ij}\sqrt{\gamma_j}A_j, \tag{A.6}$$

   where $u_{ij}$ is a unitary matrix.
2. Inhomogeneous transformations

$$A_i \mapsto A_i' = A_i + a_i, \tag{A.7}$$

$$\mathcal{H} \mapsto \mathcal{H} + \frac{1}{2\mathrm{i}}\sum_j \gamma_j\left(a_j^* A_j - a_j A_j^\dagger\right) + b, \tag{A.8}$$

   where $a_i$ are complex numbers and $b$ is real.

Because of the second invariance property, it is always possible to choose traceless Lindblad operators [36].

# Appendix B

# The Lindblad master equation from a microscopic derivation: the weak coupling limit

The interaction Hamiltonian $\mathcal{H}_{\mathrm{S-E}}$ can always be written as a sum of tensor-product self-adjoint operators[1] $A_a \otimes B_a = A_a^\dagger \otimes B_a^\dagger$,

$$\mathcal{H}_{\mathrm{S-E}} = \sum_a A_a \otimes B_a, \tag{B.1}$$

where $A_a$ and $B_a$ act on $\mathscr{H}_{\mathrm{S}}$ and $\mathscr{H}_{\mathrm{E}}$, respectively.

Within this notation and the weak coupling limit, a **quantum Markovian master equation** that describes the evolution of the reduced state $\rho_{\mathrm{S}}(t)$, in the Schrödinger picture, can be obtained as an extension to the Liouville-von Neumann equation (1.1). In particular, under specific assumptions announced later, the equation obtained is the **Lindblad master equation** [36, 37]

$$\partial_t \rho_{\mathrm{S}} = -\frac{\mathrm{i}}{\hbar}[\mathcal{H}_{\mathrm{L}}, \rho] + \mathfrak{D}(\rho_{\mathrm{S}}), \tag{B.2}$$

[1] To obtain this, it is noticed that, since $\mathcal{H}_{\mathrm{S-E}} = \mathcal{H}_{\mathrm{S-E}}^\dagger$, the most general way to write $\mathcal{H}_{\mathrm{S-E}}$ is: $\mathcal{H}_{\mathrm{S-E}} = \sum_{a=1}^n X_a^\dagger \otimes Y_a + X_a \otimes Y_a^\dagger$, where $X_a, Y_a$ are general operators. But, as any operator $O$ can be written as a sum of its hermitian and anti-hermitian parts: $O = O_{\mathrm{h}} + O_{\mathrm{a-h}} \equiv O_{\mathrm{h}} + \mathrm{i}O'_{\mathrm{h}}$, where $O_{\mathrm{h}} \equiv \frac{(O^\dagger + O)}{2}, O'_{\mathrm{h}} \equiv \frac{\mathrm{i}(O^\dagger - O)}{2}$ are both hermitian; then this property can be applied on $X_a, Y_a$ to obtain equation (B.1) through:

$$\begin{array}{llll} A_a = 2(X_a)_h, & B_a = 2(Y_a)_h, & \text{for} & a = 1, ..., n; \\ A_a = 2(X'_{a-n})_h, & B_a = 2(Y'_{a-n})_h, & \text{for} & a = n+1, ..., 2n. \end{array}$$

where

$$\mathcal{H}_{\mathrm{L}} \equiv \mathcal{H}_{\mathrm{S}} + H_{\mathrm{LS}}, \tag{B.3}$$

$$\mathcal{H}_{\mathrm{LS}} \equiv \sum_{a,b,\omega} S_{a,b}(\omega)\mathcal{A}_a^\dagger(\omega)\mathcal{A}_b(\omega), \tag{B.4}$$

$$S_{a,b}(\omega) \equiv \mathrm{P.V.}\int_{-\omega_{\max}}^{\omega_{\max}} \frac{\mathrm{d}\omega'}{\omega-\omega'}\,\mathrm{Tr}\{\mathcal{B}_a(\omega')B_b\rho_{\mathrm{E}}\} \tag{B.5}$$

$$\mathfrak{D}(\,\cdot\,) \equiv \sum_{a,b}\gamma_{a,b}(\omega)\left[\mathcal{A}_b(\omega)\,\cdot\,\mathcal{A}_a^\dagger(\omega) - \frac{1}{2}\{\mathcal{A}_a^\dagger(\omega)\mathcal{A}_b(\omega),\,\cdot\,\}\right], \tag{B.6}$$

$$\gamma_{a,b}(\omega) \equiv \begin{cases} 2\pi\,\mathrm{Tr}\{\mathcal{B}_a(\omega)B_b\rho_{\mathrm{E}}\}, & \text{if} \quad \omega\in[-\omega_{\max},\omega_{\max}] \\ 0, & \text{if not} \end{cases}, \tag{B.7}$$

$$\mathcal{A}_a(\omega) = \sum_{\epsilon,\epsilon':\ \epsilon'-\epsilon=\hbar\omega} |\epsilon\rangle\langle\epsilon|\,A_a\,|\epsilon'\rangle\langle\epsilon'|\,, \tag{B.8}$$

$$\mathcal{B}_a(\omega) = \int_{\varepsilon'-\varepsilon=\hbar\omega} \mathrm{d}\varepsilon\,\mathrm{d}\varepsilon'\ |\varepsilon\rangle\langle\varepsilon|\,B_a\,|\varepsilon'\rangle\langle\varepsilon'|\,, \tag{B.9}$$

with $\mathcal{H}_{\mathrm{U}} \equiv \mathcal{H}_{\mathrm{S}} + \mathcal{H}_{\mathrm{E}} + \mathcal{H}_{\mathrm{S-E}}$ **independent of time** (although, still valid for certain time-dependent situtions, as in driven cavity photonic fields considered in this thesis [42])

In the above, $t \geq 0$ is the time variable (evolution parameter), $\mathcal{H}_{\mathrm{L}}$ is what is called **Lindblad hamiltonian** in this thesis, $H_{\mathrm{LS}}$ is the **Lamb-Shift hamiltonian**, $\mathfrak{D}(\cdot)$ is the **dissipator** (super-)operator, $\mathrm{Tr}\{\mathcal{B}_a(\omega)B_b\rho_{\mathrm{B}}\}$ are called **environmental correlation functions**, and $[-\omega_{\max},\omega_{\max}]$ is the range of frequencies (energies) where the interaction is allowed (i.e. **the interaction is bounded**, which is a requisite for the Lindblad equation to be well defined in the WCL).

Also, $\mathcal{A}_a(\omega), \mathcal{B}_a(\omega)$ are the eigenoperators of the super-operators $\mathrm{i}[\mathcal{H}_{\mathrm{S}},\cdot]$ and $\mathrm{i}[\mathcal{H}_{\mathrm{E}},\cdot]$, respectively (with eigenvalues $-\mathrm{i}\omega$):

$$\mathcal{A}_a(\omega) = \sum_{\epsilon,\epsilon':\ \epsilon'-\epsilon=\omega} |\epsilon\rangle\langle\epsilon|\,A_a\,|\epsilon'\rangle\langle\epsilon'|\,,$$

$$\mathcal{B}_a(\omega) = \int_{\varepsilon'-\varepsilon=\omega} \mathrm{d}\varepsilon\,\mathrm{d}\varepsilon'\ |\varepsilon\rangle\langle\varepsilon|\,B_a\,|\varepsilon'\rangle\langle\varepsilon'|\,,$$

where $|\epsilon\rangle\,, |\varepsilon\rangle$ are the eigenvector-states associated with the eigenvalues $\epsilon, \varepsilon$ of $\mathcal{H}_{\mathrm{S}}$ and $\mathcal{H}_{\mathrm{E}}$, respectively. For equation (B.9), an integral is used instead of a sum, because **the spectrum of $\mathcal{H}_{\mathrm{E}}$ must be continuous** for the Lindblad equation to be well defined in the WCL (avoiding divergencies).

By defining the super-operator

$$\mathcal{L}\cdot \equiv -\mathrm{i}[H_L,\cdot] + \mathfrak{D}(\cdot), \tag{B.10}$$

then the Lindblad equation can be rewritten as

$$\partial_t\rho_{\mathrm{S}} = \mathcal{L}\rho_{\mathrm{S}}. \tag{B.11}$$

Thus, the solution to the Lindblad equation is given by

$$\rho_{\mathrm{S}}(t) = \mathrm{e}^{\mathcal{L}t}\rho_{\mathrm{S}}(0), \tag{B.12}$$

which is well defined (by the series expansion) in the WCL with $H_{\mathrm{U}}$ independent of time. Therefore, $\mathcal{L}$ is called the **generator of the evolution** of the state $\rho_{\mathrm{S}}$.

All of the above (of this appendix) is valid only if the initial condition of the universe-system is

$$\rho_{\mathrm{U}}(0) = \rho_{\mathrm{S}}(0) \otimes \rho_{\mathrm{E}}(0), \tag{B.13}$$

i.e. the initial state of the universe-system is **completely separated** [36, 37].

# Appendix C

# Gauge invariance of the radiation field

Within Coulomb's gauge, the electromagnetic fields of radiation are related to $\mathbf{A}$ by

$$\mathbf{B} \equiv \boldsymbol{\nabla} \times \mathbf{A}, \tag{C.1}$$

$$\mathbf{E}_{\perp} = -\frac{\partial}{\partial t}\mathbf{A}, \tag{C.2}$$

$$\mathbf{E}_{\parallel} = -\boldsymbol{\nabla} U, \tag{C.3}$$

where $\mathbf{E}_{\perp} \equiv [\mathbf{E} \cdot \hat{\mathbf{e}}_1]\,\hat{\mathbf{e}}_1 + [\mathbf{E} \cdot \hat{\mathbf{e}}_2]\,\hat{\mathbf{e}}_2$, and the static electric field is $\mathbf{E}_{\parallel} \equiv [\mathbf{E} \cdot \hat{\mathbf{k}}]\hat{\mathbf{k}}$.

Now, the general admitted gauge transformations that leave Maxwell's equations invariant, are

$$\mathbf{A} \mapsto \mathbf{A}' = \mathbf{A} + \boldsymbol{\nabla}\phi, \tag{C.4}$$

$$U \mapsto U' = U - \frac{\partial \phi}{\partial t}, \tag{C.5}$$

where $\phi$ is a function of class $C^2$ (i.e. doubly differentiable with continuous second derivative). But, $\boldsymbol{\nabla}\phi \cdot \hat{\mathbf{e}}_1 = \boldsymbol{\nabla}\phi \cdot \hat{\mathbf{e}}_2 = 0$, since in spatial Fourier space $\boldsymbol{\nabla}\phi$ becomes $\mathrm{i}\mathbf{k}\tilde{\phi} \parallel \mathbf{E}_{\parallel}$. Hence, projecting in the $\hat{\mathbf{e}}_1, \hat{\mathbf{e}}_2$ directions, returns back to equation (C.2) as if no change had been performed, i.e. both $\mathbf{E}_{\perp}$ and $\mathbf{A}$ were kept invariant under the gauge transformation.

■

# Appendix D

# Relation between interaction hamiltonians in the Tavis-Cummings model

Let's change $g \longrightarrow \hbar g$, or equivalently, set $\hbar = 1$ for the calculations of this section. Given the interaction Hamiltonians

$$\mathcal{H}_s = \mathrm{i}g(aJ_+ - a^\dagger J_-), \tag{D.1}$$

$$\mathcal{H}_e = g(aJ_+ + a^\dagger J_-), \tag{D.2}$$

of the Tavis-Cummings model, corresponding to different polarizations of the electromagnetic field; it is desired to find a unitary transformation $\tilde{U}$ relating the two as

$$\mathcal{H}_e = \tilde{U}^\dagger \mathcal{H}_s \tilde{U}. \tag{D.3}$$

Since $\tilde{U}$ is unitary, it must have an exponential form $\tilde{U} = \mathrm{e}^{-\mathrm{i}\alpha A}$, where $A$ is an operator. Hence, setting $B = \mathrm{i}\alpha^* A^\dagger$, and imposing (*ansatz* to be able to use the Baker-Campbell-Hausdorff, or BCH, lemma [55]) $B^\dagger = -B$, it is obtained

$$\mathcal{H}_e = \mathrm{e}^B \mathcal{H}_s \mathrm{e}^{-B} \tag{D.4}$$

$$= \mathrm{i}g\left(\mathrm{e}^B a J_+ \mathrm{e}^{-B} - \mathrm{e}^B a^\dagger J_- \mathrm{e}^{-B}\right), \tag{D.5}$$

which can only be true if equations

$$\mathrm{e}^B a^\dagger J_- \mathrm{e}^{-B} = \mathrm{i}a^\dagger J_-, \tag{D.6}$$

$$\mathrm{e}^B a J_+ \mathrm{e}^{-B} = -\mathrm{i}a J_+, \tag{D.7}$$

are fulfilled.

These conditions can be summarized as

$$\mathrm{e}^B C_\pm \mathrm{e}^{-B} = \pm\mathrm{i}C_\pm = C_\pm \mathrm{e}^{\pm\mathrm{i}\pi/2} \tag{D.8}$$

$$= C_\pm \sum_k \frac{1}{k!}\left(\pm\mathrm{i}\frac{\pi}{2}\right)^k, \tag{D.9}$$

which, applying the BCH lemma, is equivalent to fulfill

$$[B,[B,\cdots,[B,C_\pm]\cdots] = \left(\pm \mathrm{i}\frac{\pi}{2}\right)^k C_\pm,\ \forall k \in \mathbb{N}, \tag{D.10}$$

where the left-hand-side is a $k$-times nested commutator.

Now, as a natural *ansatz* for $B$, is chosen

$$B = \beta_1 a a^\dagger + 2\beta_2 J_z, \tag{D.11}$$

with $\beta_{1,2}^* = -\beta_{1,2}$ in order to fulfill $B^\dagger = -B$. Hence, $\mathrm{Re}\{\beta_{1,2}\} = 0$.

From here, it is enough to know the commutation relations $[J_z, J_\pm] = \pm J_\pm/2$ and $[a, a^\dagger] = 1$ to calculate the first terms of the BCH formula for both $C_\pm$, and recognize the pattern obtained as

$$[B,[B,\cdots,[B,C_\pm]\cdots] = (\pm\beta)^k C_\pm, \tag{D.12}$$

where $\beta \equiv \beta_1 - \beta_2$, so $\mathrm{Re}\{\beta\} = 0$.

Then, choosing $\beta = \mathrm{i}\pi/2$ all the restrictions are fulfilled. Therefore,

$$\tilde{U} = \mathrm{e}^{-(\beta_1 a^\dagger a + 2\beta_2 J_z)}, \forall \beta_{1,2} \in \mathrm{i}\mathbb{R} : (\beta_1 - \beta_2) = \mathrm{i}\frac{\pi}{2}; \tag{D.13}$$

represents a family of unitary transformations that transform between the two versions of the Tavis-Cummings model. Hence, either can be used without loss of generality to represent either case.

■

# Appendix E

# Qubit ergotropy in the Jaynes-Cummings model

If the state $\rho$ and (non-degenerate) Hamiltonian $\mathcal{H}$ of a system are written orderly as

$$\rho = \sum_k r_k \left|r_k\right\rangle\!\left\langle r_k\right|, \ r_k \geq r_{k+1}, \tag{E.1}$$

$$\mathcal{H} = \sum_k \epsilon_k \left|\epsilon_k\right\rangle\!\left\langle \epsilon_k\right|, \ \epsilon_k < \epsilon_{k+1}, \tag{E.2}$$

where $r_k, \epsilon_k$ are the eigenvalues and $\left|r_k\right\rangle, \left|\epsilon_k\right\rangle$ the eigenkets of the state and Hamiltonian, respectively; then the ergotropy of $\rho$ can be calculated by [52]

$$\mathcal{E}[\rho] = \sum_{jk} r_j \epsilon_k (|\langle r_j|\epsilon_k\rangle|^2 - \delta_{jk}), \tag{E.3}$$

where $\delta_{jk}$ is the Kronecker delta. Thus, for the case of the Jaynes-Cummings model ($N = 1$) with a Fock state as the charger initial condition, focusing on the qubit sub-system (tracing over the resonator), it is easy to obtain the state of the qubit

$$\rho = \sin^2(gt) \left|e\right\rangle\!\left\langle e\right| + \cos^2(gt) \left|g\right\rangle\!\left\langle g\right|, \tag{E.4}$$

which is diagonal in the energy basis with eigenvalues $\lambda_1(t) = \sin^2(gt)$ and $\lambda_2(t) = \cos^2(gt)$ corresponding to the eigenkets $|e\rangle$ and $|g\rangle$, respectively.

It can be seen that if

$$\lambda_1(t) \geq \lambda_2(t) \iff \cos(2gt) \leq 0 \tag{E.5}$$

$$\iff gt \in \left[\frac{\pi}{4}, \frac{3\pi}{4}\right] \pm k\pi, k \in \mathbb{N}. \tag{E.6}$$

Therefore, outside of these intervals, the ordering of the eigenvalues is inverted.

Now, in units of $\hbar\omega_c$, $\mathcal{H} = \sigma_z/2$ with eigenvalues $\epsilon_1 = -1/2$, $\epsilon_2 = 1/2$ and eigenkets $|\epsilon_1\rangle = |g\rangle$, $|\epsilon_2\rangle = |e\rangle$.

Finally, by simply applying the formula (E.1), the ergotropy is obtained as

$$\mathcal{E}(t) = \begin{cases} 1 - 2\cos^2(gt), & gt \in \left[\frac{\pi}{4}, \frac{3\pi}{4}\right] \pm k\pi \\ 0 & gt \notin \left[\frac{\pi}{4}, \frac{3\pi}{4}\right] \pm k\pi \end{cases}, \tag{E.7}$$

which corresponds to $\mathcal{E}_h/(\hbar\omega_c)$, and clearly has the first maximum at $t = 2\pi/4g \equiv \pi/\Omega_R$ (used as timescale for all plots) with a value $\bar{\mathcal{E}}_h = \hbar\omega_c$, after recovering the original units in energy.

For the Tavis-Cummings model ($N \geq 1$), the equivalent numerical procedure is done to calculate the ergotropy.

# Appendix F

# Complementary plots and simulation's details

Simulation results that are complementary to the plots shown in chapter 3, are displayed in Figures F.1-F.5. Indeed, if the resonator energy, $E_c^{\#}$, and the heat from the QB, $Q^{\#}$, are added to the holder energy, $E_h^{\#}$, the total energy is conserved constant over time and equal to $N\hbar\omega_c$, as it should. In other words, adding the corresponding plots of Figures F.3, F.4, and 3.6, it always gives 1, as the energy is normalized in units of $N\hbar\omega_c$ in these plots. The same can be done with the populations of Figures F.5 and 3.8. This serves as a first validity check of the numerical results.

Although, a more important validity check was done in all simulations: *checking that the Hilbert space of the electromagnetic field was correctly truncated.* This was achieved by setting an error tolerance of 4 decimals for the calculation of $E_c^{\#}$. If the tolerance was surpassed, the simulation was automatically redone with a larger Hilbert space until the tolerance is no longer surpassed. This is very important to keep good calculations of the ergotropy and heat, that require information of the whole density matrix $\rho$. When choosing thermal and coherent states as the charger's initial condition, it was very difficult to fulfill the error tolerance restriction, which is the main reason to present less data for those simulations.

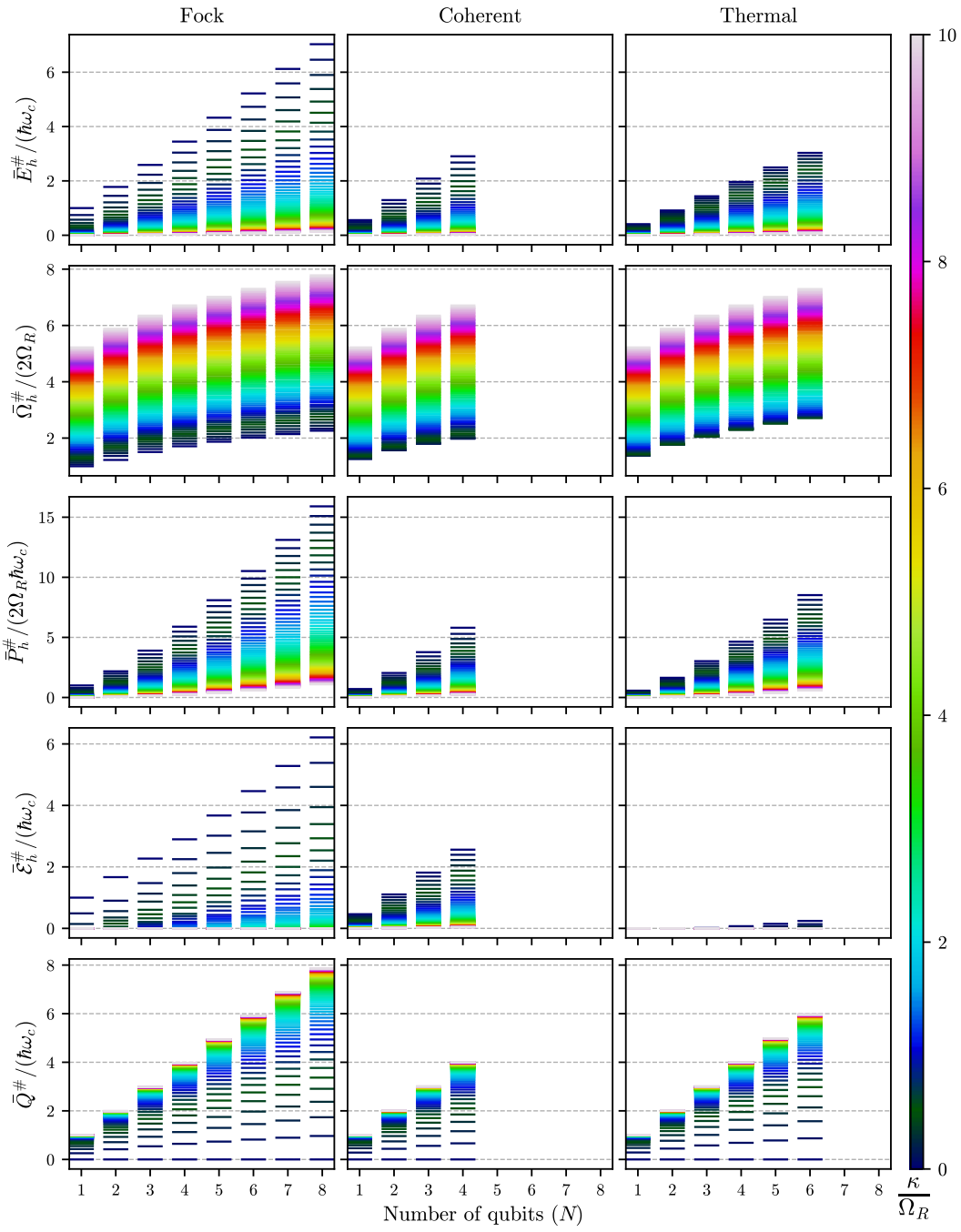


Figure F.1: Performances of the collective QB for Fock, coherent and thermal states as the charger initial condition. Same data of Fig. 3.4, interchanging the way of visualizing $N$ and $\kappa$.

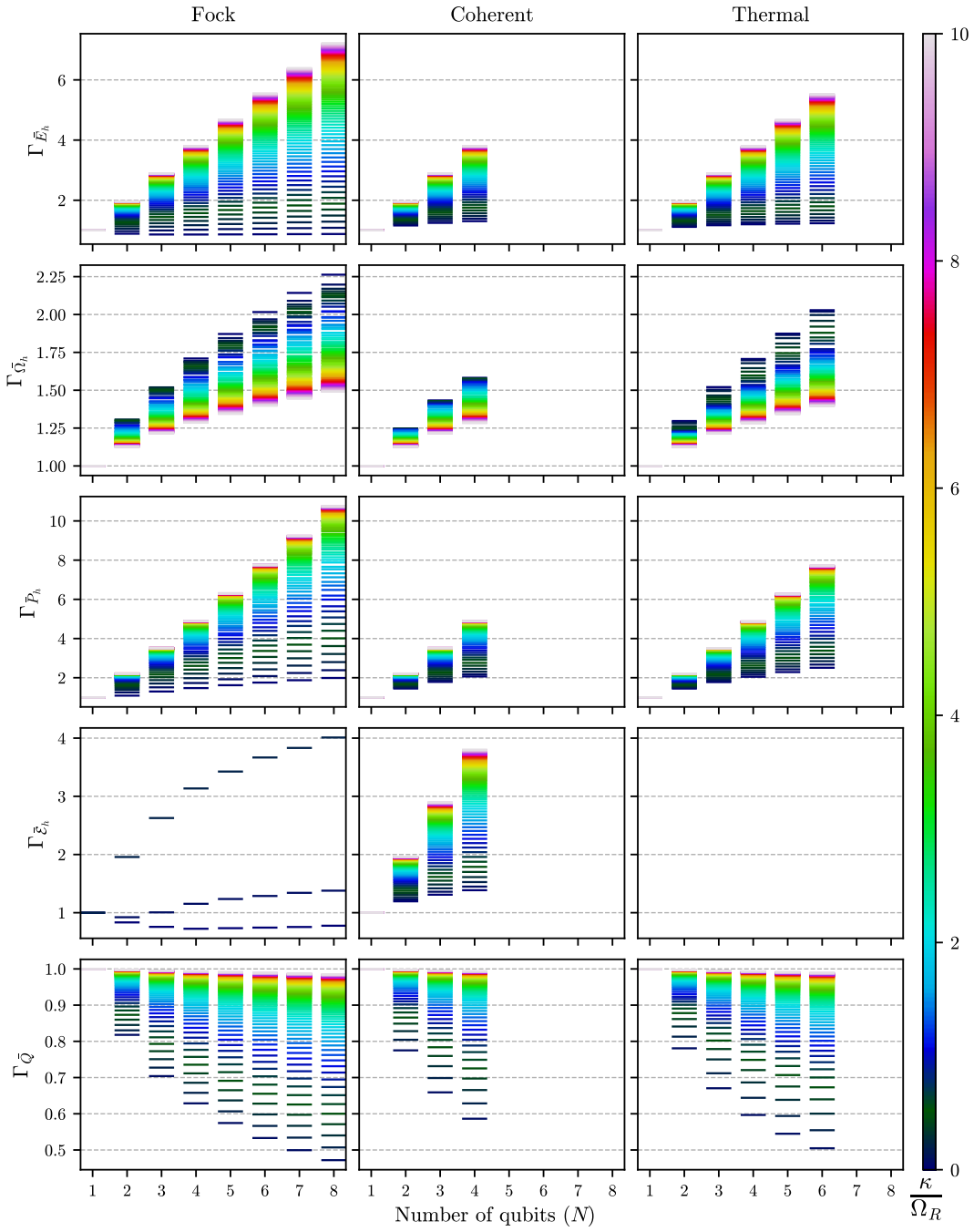


Figure F.2: Collective enhancements of the relevant figures of merit for Fock, coherent and thermal states as the charger initial condition. Same data of Fig. 3.5, interchanging the way of visualizing $N$ and $\kappa$.

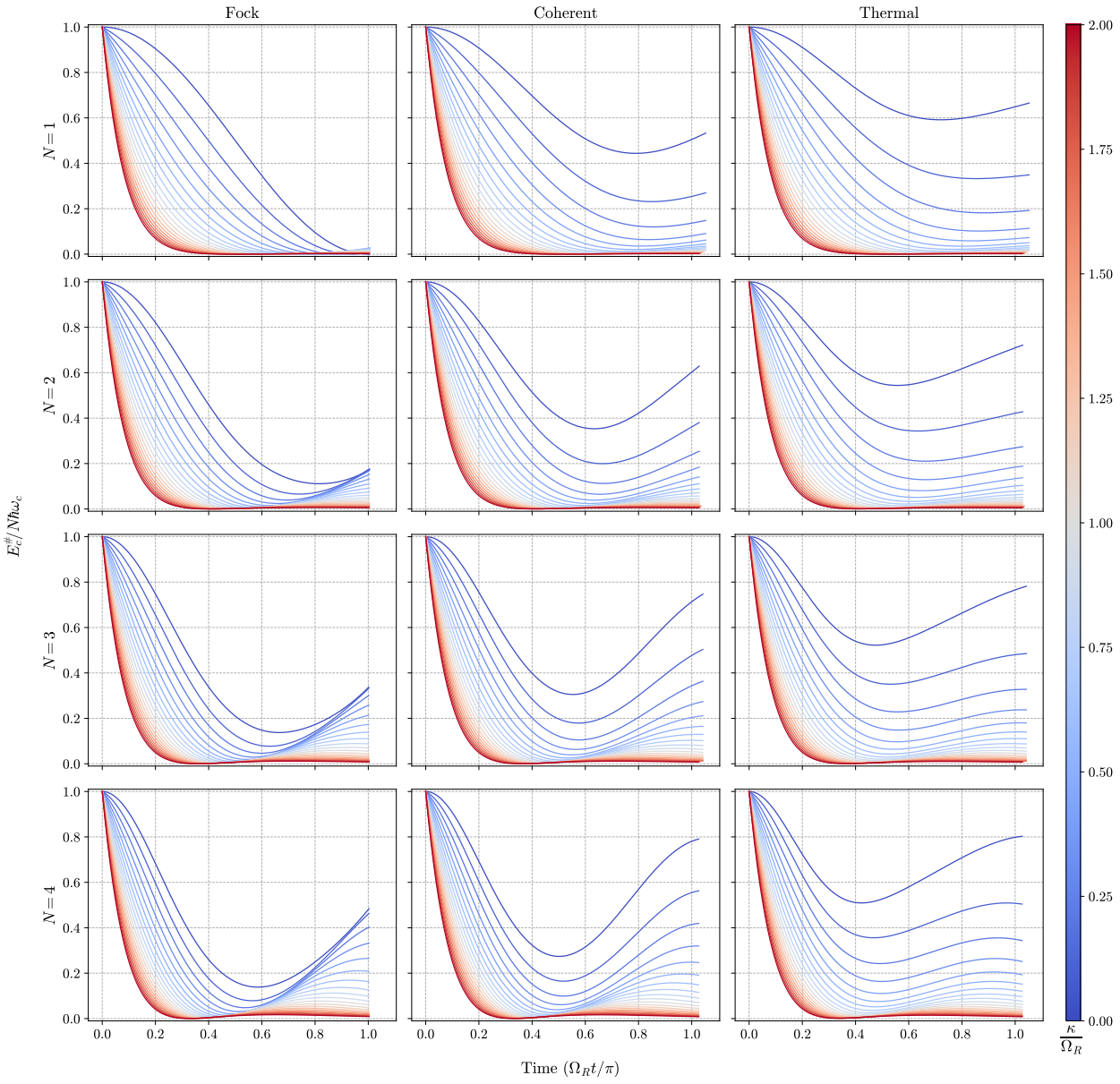


Figure F.3: Resonator energy over time up to near the first holder energy maximum for Fock, coherent and thermal states as the charger initial condition. Results of the collective QB version. These plots can be seen as the complement of Fig. 3.6, since it shows how the resonator energy $E_c$ is reduced while it is been transferred to the holder as $E_h$. Although, $E_c + E_h$ is not a constant because some energy is lost in form of heat $Q$, shown in Fig. F.4.

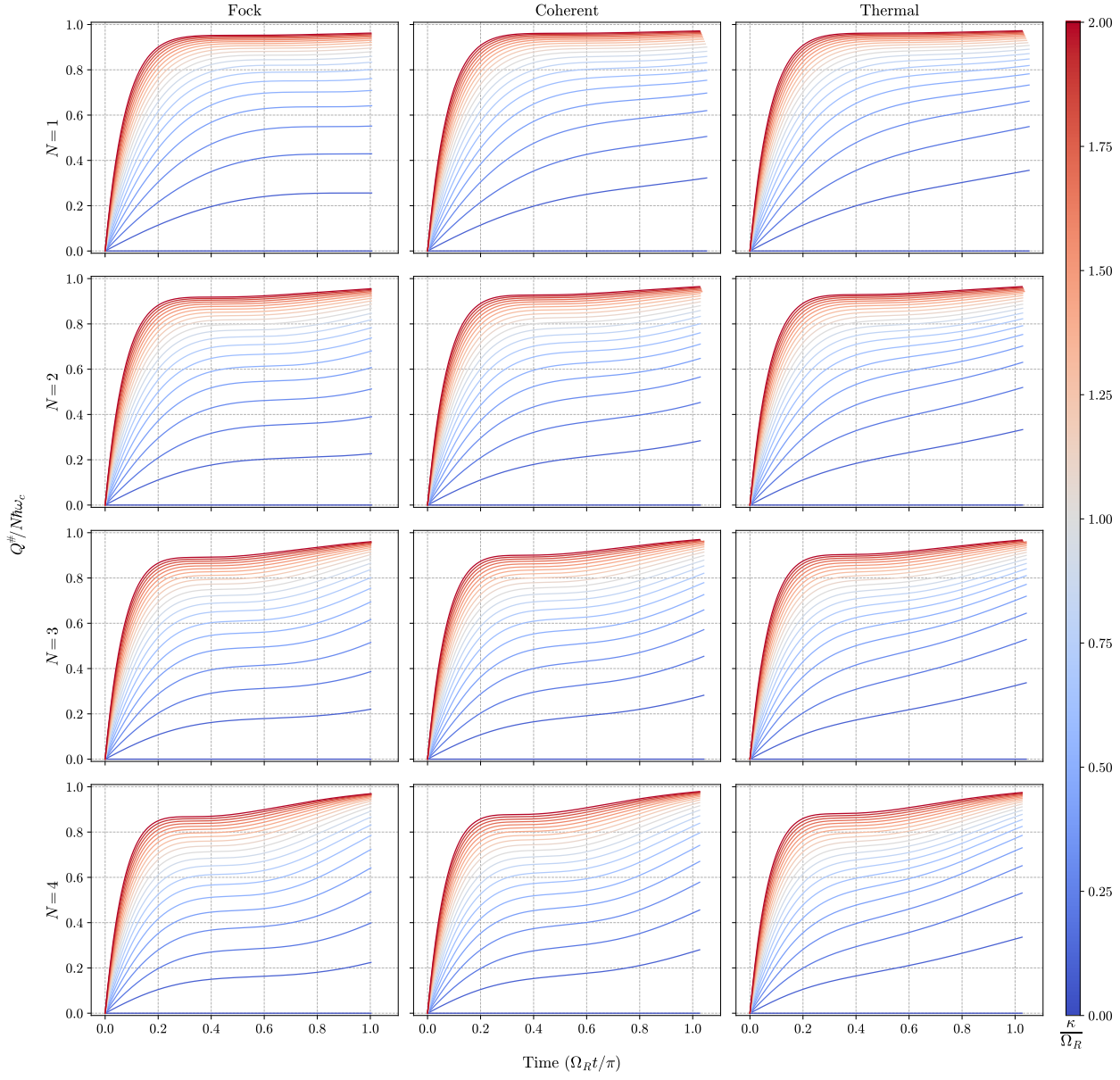


Figure F.4: Heat from the QB over time up to near the first holder energy maximum for Fock, coherent and thermal states as the charger initial condition. Results of the collective QB version. These plots are very similar between the three cases of initial condition, with small differences only appreciable for $\kappa \approx 0$.

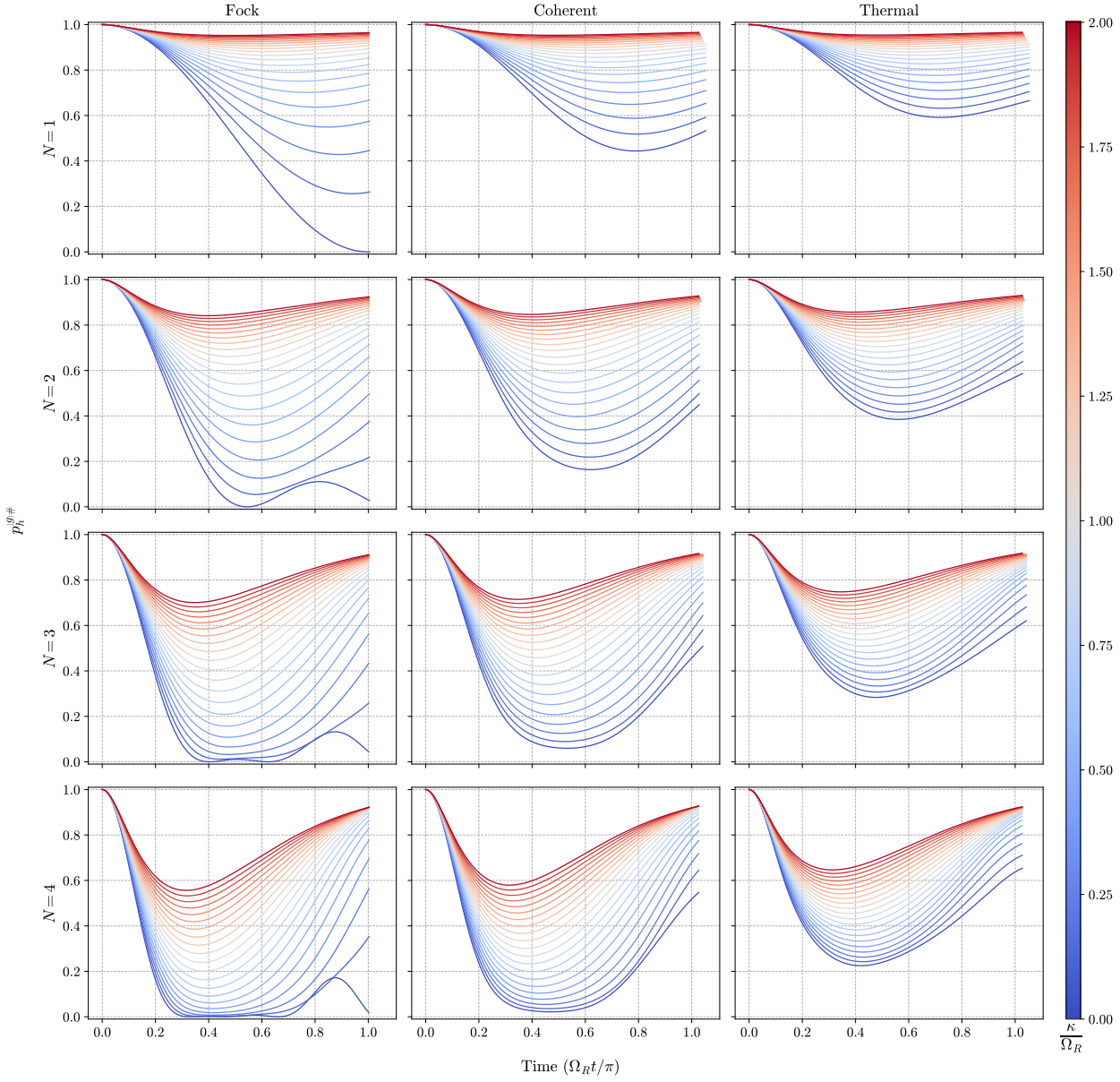


Figure F.5: Holder population of the ground state over time up to near the first holder energy maximum for Fock, coherent and thermal states as the charger initial condition. Results of the collective QB version. These plots show that inverting the holder population is better done in the Fock case, but as $\kappa$ increases the differences tend to be negligible.

# Bibliography


[1] Francesco Campaioli et al. Quantum batteries. *arXiv:1805.05507 [quant-ph]*, 2018.

[2] Ivan Henao and Roberto M. Serra. Role of quantum coherence in the thermodynamics of energy transfer. *Phys. Rev. E*, 97:062105, Jun 2018.

[3] Gian Marcello Andolina, Maximilian Keck, Andrea Mari, Vittorio Giovannetti, and Marco Polini. Quantum versus classical many-body batteries. *Phys. Rev. B*, 99:205437, May 2019.

[4] Gian Marcello Andolina, Maximilian Keck, Andrea Mari, Michele Campisi, Vittorio Giovannetti, and Marco Polini. Extractable work, the role of correlations, and asymptotic freedom in quantum batteries. *Phys. Rev. Lett.*, 122:047702, Feb 2019.

[5] Alan C. Santos, Barı ş Çakmak, Steve Campbell, and Nikolaj T. Zinner. Stable adiabatic quantum batteries. *Phys. Rev. E*, 100:032107, Sep 2019.

[6] Alan C. Santos, Andreia Saguia, and Marcelo S. Sarandy. Stable and charge-switchable quantum batteries. *Phys. Rev. E*, 101:062114, Jun 2020.

[7] Sebastian Deffner and Steve Campbell. Quantum speed limits: from heisenberg's uncertainty principle to optimal quantum control. *Journal of Physics A: Mathematical and Theoretical*, 50(45):453001, oct 2017.

[8] V Giovannetti, S Lloyd, and L Maccone. The role of entanglement in dynamical evolution. *Europhysics Letters (EPL)*, 62(5):615–621, jun 2003.

[9] Dario Ferraro et al. High-power collective charging of a solid-state quantum battery. *Phys. Rev. Lett.*, 120(117702), 2018. doi: 10.1103/PhysRevLett.120.117702.

[10] Romana Schirhagl et al. Nitrogen-vacancy centers in diamond: Nanoscale sensors for physics and biology. *Annu. Rev. Phys. Chem.*, 65:83—-105, 2014. doi: 10.1146/annurev-physchem-040513-103659.

[11] Marcus W. Doherty et al. The nitrogen-vacancy colour centre in diamond. *Physics Reports*, 2013. doi: 10.1016/j.physrep.2013.02.001.

[12] Robert Alicki and Mark Fannes. Entanglement boost for extractable work from ensembles of quantum batteries. *Phys. Rev. E*, 87:042123, Apr 2013.

[13] Karen V. Hovhannisyan, Martí Perarnau-Llobet, Marcus Huber, and Antonio Acín. Entanglement generation is not necessary for optimal work extraction. *Phys. Rev. Lett.*, 111:240401, Dec 2013.

[14] Felix C Binder, Sai Vinjanampathy, Kavan Modi, and John Goold. Quantacell: powerful charging of quantum batteries. *New J. Phys*, 17(7):075015, jul 2015.

[15] Francesco Campaioli, Felix A. Pollock, Felix C. Binder, Lucas Céleri, John Goold, Sai Vinjanampathy, and Kavan Modi. Enhancing the charging power of quantum batteries. *Phys. Rev. Lett.*, 118:150601, Apr 2017.

[16] Thao P. Le, Jesper Levinsen, Kavan Modi, Meera M. Parish, and Felix A. Pollock. Spin-chain model of a many-body quantum battery. *Phys. Rev. A*, 97:022106, Feb 2018.

[17] Gian Marcello Andolina, Donato Farina, Andrea Mari, Vittorio Pellegrini, Vittorio Giovannetti, and Marco Polini. Charger-mediated energy transfer in exactly solvable models for quantum batteries. *Phys. Rev. B*, 98:205423, Nov 2018.

[18] Yu-Yu Zhang, Tian-Ran Yang, Libin Fu, and Xiaoguang Wang. Powerful harmonic charging in a quantum battery. *Phys. Rev. E*, 99:052106, May 2019.

[19] Alba Crescente, Matteo Carrega, Maura Sassetti, and Dario Ferraro. Ultrafast charging in a two-photon dicke quantum battery. *Phys. Rev. B*, 102:245407, Dec 2020.

[20] Anna Delmonte, Alba Crescente, Matteo Carrega, Dario Ferraro, and Maura Sassetti. Characterization of a two-photon quantum battery: Initial conditions, stability and work extraction. *Entropy*, 23(5), 2021.

[21] Y. Yao and X. Q. Shao. Stable charging of a rydberg quantum battery in an open system. *Phys. Rev. E*, 104:044116, Oct 2021.

[22] Donato Farina, Gian Marcello Andolina, Andrea Mari, Marco Polini, and Vittorio Giovannetti. Charger-mediated energy transfer for quantum batteries: An open-system approach. *Phys. Rev. B*, 99:035421, Jan 2019.

[23] Felipe Barra. Dissipative charging of a quantum battery. *Phys. Rev. Lett.*, 122:210601, May 2019.

[24] Faezeh Pirmoradian and Klaus Mølmer. Aging of a quantum battery. *Phys. Rev. A*, 100:043833, Oct 2019.

[25] Junjie Liu, Dvira Segal, and Gabriel Hanna. Loss-free excitonic quantum battery. *The Journal of Physical Chemistry C*, 123(30):18303–18314, 2019.

[26] M Carrega, A Crescente, D Ferraro, and M Sassetti. Dissipative dynamics of an open quantum battery. *New J. Phys*, 22(8):083085, sep 2020.

[27] Stefano Gherardini, Francesco Campaioli, Filippo Caruso, and Felix C. Binder. Stabilizing open quantum batteries by sequential measurements. *Phys. Rev. Research*, 2:013095,

Jan 2020.

[28] Srijon Ghosh, Titas Chanda, Shiladitya Mal, and Aditi Sen(De). Fast charging of a quantum battery assisted by noise. *Phys. Rev. A*, 104:032207, Sep 2021.

[29] Michael Tavis and Frederick W. Cummings. Exact solution for an $n$-molecule—radiation-field hamiltonian. *Phys. Rev.*, 170:379–384, Jun 1968.

[30] Michael Tavis and Frederick W. Cummings. Approximate solutions for an $n$-molecule-radiation-field hamiltonian. *Phys. Rev.*, 188:692–695, Dec 1969.

[31] J. M. Fink, R. Bianchetti, M. Baur, M. Göppl, L. Steffen, S. Filipp, P. J. Leek, A. Blais, and A. Wallraff. Dressed collective qubit states and the tavis-cummings model in circuit qed. *Phys. Rev. Lett.*, 103:083601, Aug 2009.

[32] P. J. Leek, S. Filipp, P. Maurer, M. Baur, R. Bianchetti, J. M. Fink, M. Göppl, L. Steffen, and A. Wallraff. Using sideband transitions for two-qubit operations in superconducting circuits. *Phys. Rev. B*, 79:180511, May 2009.

[33] Jared Lolli, Alexandre Baksic, David Nagy, Vladimir E. Manucharyan, and Cristiano Ciuti. Ancillary qubit spectroscopy of vacua in cavity and circuit quantum electrodynamics. *Phys. Rev. Lett.*, 114:183601, May 2015.

[34] Ping Yang, Jan David Brehm, Juha Leppäkangas, Lingzhen Guo, Michael Marthaler, Isabella Boventer, Alexander Stehli, Tim Wolz, Alexey V. Ustinov, and Martin Weides. Probing the tavis-cummings level splitting with intermediate-scale superconducting circuits, 2018.

[35] Javier Carrasco, Jerónimo R. Maze, Carla Hermann-Avigliano, and Felipe Barra. Collective enhancement in dissipative quantum batteries. *arXiv:2110.15490 [quant-ph]*, 2021.

[36] H.P. Breuer, F. Petruccione, and S.P.A.P.F. Petruccione. *The Theory of Open Quantum Systems*. Oxford University Press, 2002.

[37] Á. Rivas and S.F. Huelga. *Open Quantum Systems: An Introduction*. SpringerBriefs in Physics. Springer Berlin Heidelberg, 2011.

[38] Claude Cohen-Tannoudji, Jacques Dupont-Roc, and Gilbert Grynberg. *Lagrangian and Hamiltonian Approach to Electrodynamics, The Standard Lagrangian and the Coulomb Gauge*, chapter 2, pages 79–168. John Wiley & Sons, Ltd, 1997.

[39] Stefan Putz. *Spins in the Cavity—Cavity QED*, pages 25–49. Springer International Publishing, Cham, 2017.

[40] Marlan O. Scully and M. Suhail Zubairy. *Quantum Optics*. Cambridge University Press, 1997.

[41] Christopher Gerry and Peter Knight. *Introductory Quantum Optics*. Cambridge University Press, 2004.

[42] H.J. Carmichael. *Statistical Methods in Quantum Optics 1: Master Equations and Fokker-Planck Equations*. Theoretical and Mathematical Physics. Springer Berlin Heidelberg, 2002.

[43] A.B. Klimov and S.M. Chumakov. *A Group-Theoretical Approach to Quantum Optics: Models of Atom-Field Interactions*. Wiley, 2009.

[44] Peter Kirton, Mor M. Roses, Jonathan Keeling, and Emanuele G. Dalla Torre. Introduction to the dicke model: From equilibrium to nonequilibrium, and vice versa (adv. quantum technol. 1-2/2019). *Advanced Quantum Technologies*, 2(1-2):1970013, 2019.

[45] Norbert Kalb. *Diamond-based quantum networks with multi-qubit nodes*. Ph.D. thesis, Delft University of Technology, 2018. doi: 10.4233/uuid:249753ae-9000-446a-9375-63c1e1165cc1.

[46] Toreno van der Saar. *Quantum control of single spins and single photons in diamond*. Ph.D. thesis, Delft University of Technology, 2012. ISBN: 978-94-6191-217-6.

[47] D. Awschalom et al. Quantum technologies with optically interfaced solid-state spins. *Nature Photonics*, 12:516—-527, 2018. doi: 10.1038/s41566-018-0232-2.

[48] Chong Zu. *Experimental quantum information processing with entangled photons and solid-state spins*. Ph.D. thesis, Tsinghua University, 2016.

[49] Sorawis Sangtawesin. *Quantum Control of Nuclear Spins Coupled to Nitrogen-Vacancy Centers in Diamond*. Ph.D. thesis, Princeton University, 2016.

[50] M. Mrózek et al. Longitudinal spin relaxation in nitrogen-vacancy ensembles in diamond. *EPJ Quantum Technology*, 2(1):22, Oct 2015.

[51] J. Gugler et al. Ab initio calculation of the spin lattice relaxation time t1 for nitrogen-vacancy centers in diamond. *arXiv:1801.09529v2 [cond-mat.mes-hall]*, 2018.

[52] A. E Allahverdyan, R Balian, and Th. M Nieuwenhuizen. Maximal work extraction from finite quantum systems. *Europhysics Letters (EPL)*, 67(4):565–571, aug 2004.

[53] J.R. Johansson, P.D. Nation, and Franco Nori. Qutip 2: A python framework for the dynamics of open quantum systems. *Computer Physics Communications*, 184(4):1234 – 1240, 2013.

[54] S. Haroche and J.M. Raimond. *Exploring the Quantum: Atoms, Cavities, and Photons*. Oxford Graduate Texts. OUP Oxford, 2006.

[55] J.J. Sakurai and J. Napolitano. *Modern Quantum Mechanics*. Addison-Wesley, 2011.